SOLUBLE ORGANIC-FE(III) COMPLEXES: RETHINKING IRON SOLUBILITY AND BIOAVAILABILITY

A Thesis
Presented to
The Academic Faculty

by

Morris Edward Jones

In Partial Fulfillment
of the Requirements for the Degree
Doctor of Philosophy in the
School of Earth and Atmospheric Sciences

Georgia Institute of Technology
December 2011

SOLUBLE ORGANIC-FE(III) COMPLEXES: RETHINKING IRON SOLUBILITY AND BIOAVAILABILITY

Approved by:

Dr. Martial Taillefert, Advisor
School of Earth and Atmospheric Sciences
Georgia Institute of Technology

Dr. Joel E. Kostka
School of Biology
Georgia Institute of Technology

Dr. Thomas J. DiChristina
School of Biology
Georgia Institute of Technology

Dr. Philippe Van Capplen
Department of Earth and Environmental Sciences
University of Waterloo

Dr. E. Michael Perdue
School of Earth and Atmospheric Sciences
Georgia Institute of Technology

Date Approved: November 21, 2011

ACKNOWLEDGEMENTS

I wish to thank Dr. Martial Taillefert for being an excellent graduate advisor teaching me what I needed and giving me the opportunity to explore my ideas. I wish to thank my committee members Dr. Thomas J. DiChristina, Dr. E. Michael Perdue, Dr. Joel E. Kostka, and Dr. Philippe Van Cappllen. Thank you to Dr. George W. Luther for providing the opportunity to dive in the *Alvin* and study hydrothermal vents.

Thank you to all of the Taillefert lab group past (Stephanie, Melanie, Deidre) and present (Jordon, Lin, Kate, Anna, Keaton, Colin) you guys have been great. Also, I would like to thank the DiChristina lab group for their biological help and friendship (Justin, Christine, Nadia, Seng).

I wish to thank my mother and father, the most inspiring "teachers" I ever had. You showed me the world in all its wonder and what I could be in it. I am eternally grateful.

TABLE OF CONTENTS

LIST OF TABLES

LIST OF FIGURES

Page

LIST OF SYMBOLS AND ABBREVIATIONS

ATP	adenosine triphosphate
ACS	American Chemical Society
AQDS	anthraquinone-2,6-disulfonate
CAS	Chrome Azurol S
CCM	*c*-type cytochrome maturation
CLE-ACSV	Competitive Ligand Equilibration Adsorptive Cathodic Stripping Voltammetry
DOC	dissolved organic carbon
DOM	Dissolved Organic Matter
EDTA	ethylenediaminetetraacetic acid
EMS	ethyl methanesulfonate
EPR	East Pacific Rise
EPS	Extracellular Polymeric Substances
DIR	Dissimilatory Iron Reduction
DIRB	Dissimilatory Iron Reducing Bacteria
DMSO	dimethylsulfoxide
HNLC	High Nutrient Low Chlorophyll
HDTMA	hexadecyltrimethyl amine
IC	ion chromatography
ICP-MS	Inductively Coupled Plasma Mass Spectrometry
MESA	Microelectrode Screening Array
NN or 1N2N	1-nitroso-2-napthol

PEEK	Polyether ether ketone
PIPES	piperazine-1,4-bis(2-ethanesulfonic acid
TEA	Terminal Electron Acceptor
TMAO	trimethylamine-*N*-oxide
UV	ultraviolet

SUMMARY

The bioavailability of iron is limited by the solubility of Fe(III) at circumneutral pH. In the High Nutrient-Low Chlorophyll (HNLC) zones of the ocean, the natural or anthropogenic addition of iron stimulates primary productivity and consumes carbon dioxide. As a result, iron fertilization has been proposed to mitigate anthropogenic carbon emissions and lower global temperatures. The natural sources of iron to the ocean are not fully constrained and include eolian depositions as well as inputs from continental shelf sediments, rivers, hydrothermal vents, and icebergs. Regardless of their source, the effectiveness of iron additions in promoting carbon fixation depends on the presence of organic ligands either natural or produced by microorganisms that stabilize or solubilize Fe(III) at neutral pH. For example, siderophores are well known to be expressed extracellularly by prokaryotes in the photic zones of the oceans to increase the bioavailability of iron. In this dissertation, the production of iron nanoparticles is demonstrated in vent fluids from the 9^0 North hydrothermal system. These iron nanoparticles may either catalyze the oxidation of sulfide to thiosulfate and produce a potential electron acceptor for microbial respiration or provide a source of iron that stimulates primary production at great distances from the hydrothermal vents. In addition, dissolved iron under the form of soluble organic-Fe(III) complexes is demonstrated to constitute a significant source of iron in estuarine sediments that receive large amounts of particulate iron from flocculation and precipitation at the salinity transition of this estuary. A novel competitive ligand equilibration absorptive cathodic stripping voltammetry (CLE-ACSV) technique reveals that the speciation of iron changes from largely colloidal or particulate in the upper estuary to truly dissolved organic-Fe(III)

in the lower estuary. It is also demonstrated that organic-Fe(III) complexes are produced far below the sediment-water interface, suggesting that dissimilatory iron-reducing bacteria may play an important role in their production. These complexes then diffuse across the sediment-water interface and provide a significant source of iron to the continental shelf.

The mechanism of reduction of iron oxides by iron-reducing bacteria is not fully understood and presents a unique physiological problem for the organism, as the terminal reductase has to transfer electrons to a solid electron acceptor. In this dissertation, it is demonstrated for the first time using random mutagenesis that the respiration of solid Fe(III) oxides by *Shewanella oneidensis*, a model iron-reducing prokaryote, first proceeds through a non-reductive dissolution step involving organic ligands that are released extracellularly by the cells. These soluble complexes are then reduced by the organism to produce Fe(II) and recycle the ligand for additional solubilization. Incubations with deletion mutants of the proteins involved in the respiration of Fe(III) revealed that the type-II secretion system, which translocates proteins on the outer membrane of gram-negative bacteria, is involved in the production of organic-Fe(III) complexes by secreting an endogenous iron-solubilizing ligand or a protein involved in the biosynthesis of this ligand on the outer membrane. In addition, periplasmic decaheme cytochromes produced by *Shewanella* appear to be involved in the mechanism of production of the endogenous organic ligand either directly or through a sensing mechanism that controls its production. In turn, two decaheme cytochromes positioned on the outer-membrane and hypothesized to be involved in the electron transfer to the mineral surface do not appear to be involved in the solubilization mechanism, suggesting either that the cells regulate

the ligand production via periplasmic sensing systems or that these cytochromes are not involved in the solubilization mechanism.

Altogether this research shows the production of organic-Fe(III) complexes in sediments generates a significant flux of dissolved iron to support primary production in continental shelf waters and that these complexes may be partly produced by iron-reducing bacteria. Indeed, experiments with a model organism demonstrate dissimilatory iron reducing bacteria produce endogenous organic ligands with high iron-binding constants to non-reductively solubilize iron oxides during the anaerobic respiration of iron oxides. The organic ligand is apparently recycled several times to minimize the energy cost associated with its biosynthesis. These findings demonstrate that the solubilization of iron oxides by organic ligands may be an important, yet underappreciated process in aquatic systems.

CHAPTER 1

INTRODUCTION

1.1 Iron Chemistry and Solubility

Iron is the fourth most abundant metal in the earth's crust yet its bioavailability is severely limited by the low solubility of Fe(III) at circumneutral pH. The primary oxidation states of iron are the ferrous (Fe(II)) and ferric (Fe(III)) states. Ferrous iron displays high solubility over a large range of pH and ionic strength values. At circumneutral pH, Fe(II) is rapidly oxidized to Fe(III) by dissolved oxygen with a half-life of Fe(II) in fully oxygenated waters on the order of 5 minutes (Davison 1993; Millero et al. 1995) (Fig. 1.1 A). Ferric iron is soluble at high and low pHs but is highly insoluble in the middle pH range (6-8) and forms solid phase ferric (hydr)oxides (Fig. 1.1 B). The concentration of iron in oxic environments at circumneutral pH is very low at around 11 pM in seawater (Liu and Millero 2002). This creates a unique physiological problem for organisms that require the use of iron for either assimilation or for dissimilatory purposes. Besides the oxidation of Fe(II) by dissolved oxygen, the redox reactions that influence the biogeochemical cycling of iron include the oxidation of ferrous iron by manganese oxides (Postma 1985) and the reduction of solid iron oxides and soluble Fe(III) complexes by ferrous iron (Wehrli et al. 1989) or sulfides (Pyzik and Sommer 1981; Luther et al. 1992; Taillefert et al. 2000). The latter forms elemental sulfur as main sulfur oxidation product, though thiosulfate has been reported in various concentrations depending on the pH (Pyzik and Sommer 1981). Iron oxides are strong adsorbents of heavy metals (Tessier et al. 1985) and the dissolution of iron oxides may mobilize these metals into the aqueous phase (Graybeal and Heath 1984).

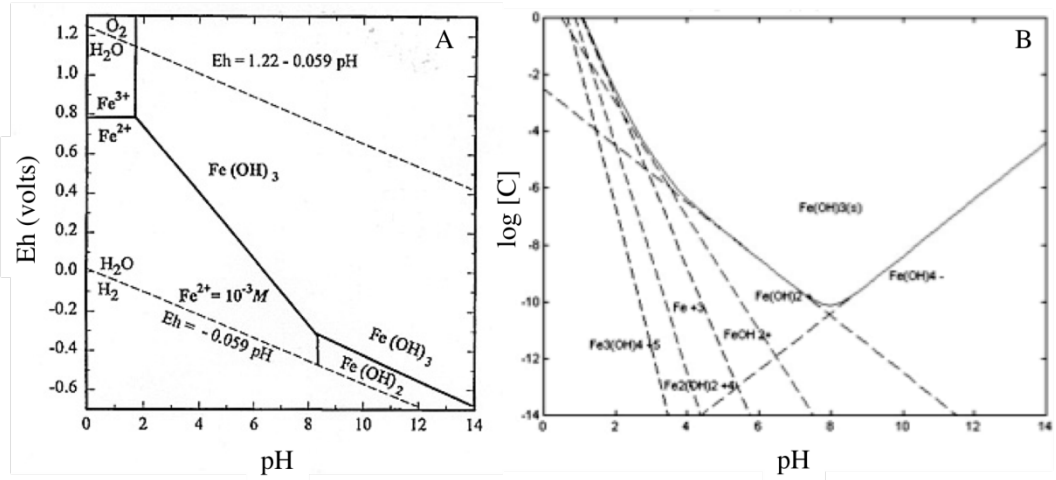

Figure 1.1 – Thermodynamic characteristics of iron in pure water. (A) Eh-pH diagram of the redox properties of iron. (B) pC-pH diagram showing the solubility of ferric iron in pure water. (Eh-pH diagram obtained from the Federation of American Scientist (www.fas.org/irp/imint/docs); pC-pH diagram calculated for the aqueous Fe(III) hydroxide species and $Fe(OH)_3(s)$.)

1.2 Iron limitation in the Oceans

The availability of iron limits primary production in the surface waters of large portions of the ocean. Areas with abundant macronutrients (nitrate, phosphate, and silica) are sometimes characterized by low phytoplankton activity. These high-nutrient low chlorophyll (HNLC) zones are suspected to be the result of iron limitation (Martin et al. 1990). Iron fertilization has been proposed to mitigate the vast amounts of carbon dioxide produced during the combustion of fossil fuels. Iron additions to HNLC zones have been shown to stimulate phytoplankton blooms, through, the long-term sequestration of the organic carbon produced from these blooms is still a matter of debate (Strong et al. 2009). Iron is required for photosynthesis, cytochrome production, nitrogen fixation, and ATP synthase (Link et al. 1999). To maintain physiological demands, most organisms under iron limitation produce siderophores, iron binding organic molecules, to increase the solubility of iron (Vraspir and Butler 2009). Additionally, the limited solubility of Fe(III) is enhanced by the presence of organic ligands, including fulvic and

humic acids (Laglera et al. 2009), extracellular polymeric substances (EPS), and cell lysis products (Hutchins et al. 1999; Hassler and Schoemann 2009). Together, these organic ligands increase the bioavailability of iron in the open ocean by increasing its half-life in surface waters and preventing its scavenging on sinking particles (Rue and Bruland 1997). While iron limitation in the open ocean is well documented, the sources of iron to surface waters and their relative contributions are not fully resolved (Moore et al. 2008, Tagliabue et al. 2009). Sources of iron to the ocean include eolian particles (Duce and Tindell 1991; Fung et al. 2000), continental shelf sediments (Elrod et al. 2004, Lam et al. 2008), riverine dissolved and particulate material (Buck et al. 2007; Gerringa et al. 2007; Krachler et al. 2010), hydrothermal vents (Bennett et al. 2008; Tagliabue et al. 2010), and icebergs (Raiswell et al. 2006; Statham et al. 2008). Each source plays an important role in delivering iron to the surface ocean, however, the half-life of iron may be extended significantly depending on the concentration and composition of organic ligands present (Millero et al. 1995). In addition, it has been shown that nanoparticles of iron sulfide species may increase the half-life of iron in a variety of environmental settings, including rivers (Rozan et al. 2000) and, more recently, hydrothermal systems (Yucel et al. 2011). Thus, environments that also provide sulfidic or organic ligands may represent proportionally a more important source of stable dissolved iron complexes that could be transported over large distances including to the photic zones of the oceans. Organic ligands have been shown to stabilize iron fluxing from hydrothermal sources (Bennett et al. 2008; Toner et al. 2009) and recently proposed to account for 10% of the flux of iron in deep waters (Sander and Kochinsky, 2011). Additionally, pyrite nanoparticles have been shown to oxidize more slowly than than aqueous Fe(II) and FeS and are thus

expected to sink more slowly than larger particles, facilitating their delivery to greater distances (Yucel et al. 2011). Nanoparticulate pyrite is suspected to form within the vent prior to interation with seawater by the reaction of FeS with sulfide (Yucel et al. 2001). Organic-rich rivers draining peatlands and anaerobic sediments may also provide sources of both iron and organic ligands and increase the half-life of iron in surface waters (Krachler et al. 2010). The flux of ferrous from sediments is often accompanied by organic ligands that are able to stabilize ferric iron as organic-Fe(III) complexes after oxidation (Bruland et al. 2001; Buck et al. 2007; Gerringa et al. 2008). Alternatively, organic-Fe(III) complexes maybe formed within shelf sediments by the non-reductive dissolution of iron oxides by organic ligands (Biber et al. 1994) or the oxidation of Fe(II) by manganese or iron oxides in the presence of organic ligands (Luther et al. 1992; Taillefert et al. 2000). The importance of hydrothermal fluids and riverine sediments as source of iron to the oceans remains, however, poorly quantified.

1.3 Iron Assimilation

Iron-containing metalloproteins are required for a variety of physiological processes including photosynthesis, respiration, and nitrogen fixation (Vraspir and Bulter 2009). The majority of Fe required by prokaryotes (~95%) is used in the Rieske proteins NADH-Q reductase, succinate-Q reductase, cytochrome b_1, and cytochrome oxidase of the electron transport chain (Tortell et al. 1999). The 2Fe-2S iron clusters of the Rieske type metalloproteins are coordinated by two cysteine residues and two histidine residues and can be poised over a broad range of reduction potentials from -155 to +375 mV (Link 1999). Many organisms produce siderophores for the purpose of increasing the solubility of Fe(III) in their local environment. Ferric iron is commonly bound by three

hydroxamate or catecholate functional groups along an organic carbon backbone, occasionally forming macrocyclic ring structures (Crosa and Walsh 2002). In addition to producing siderophores, outer membrane siderophore receptors are produced that recognize the Fe(III)-siderophore complex (Vraspir and Butler 2009). Iron is translocated across the outer membrane, a process that hydrolyzes ATP, then is transported to the cytoplasm where ligand hydrolysis or a Fe(III)-siderophore reductase weakens the complex to dissociate iron for incorporation in the cell (Caldwell and Crumbliss 1998; Martinez and Butler 2007).

1.4 Dissimilatory iron reduction

Microbial respiration involves the oxidation of small organic acids or hydrogen coupled to the reduction of a terminal electron acceptor (TEA). In standard conditions (1 M, pH 7), the reduction potential of TEA decreases in the order of O_2, NO_3^- Mn and Fe oxides, SO_4^{2-} and CO_2 (Froelich et al. 1979). Electrons are taken from the donor, moved through the electron transport chain and deposited on the TEA. The movement of electrons through the electron transport chain generates proton motive force (PMF) (Mitchell 1961), which is used to generate adenosine 5'-triphosphate (ATP) for energy storage. The proton pumping redox reactions of cytochromes, flavoproteins, and the quinone pool at the inner membrane increase PMF, while additional PMF is generated by the consumption of protons within the cytoplasm during redox reactions (Fig. 1.2). PMF together with substrate level phosphorylation are the sources of energy conservation during aerobic or anaerobic respiration (Mitchell 1961). The TEA is then reduced by a terminal reductase at the end of the electron transport chain. Known reductases exist on the inner membrane for the respiration of molecular oxygen (Ingledew and Poole 1984)

and within the periplasmic space for the reduction of nitrate, sulfate, and fumarate (Brittain et al. 1992; Peck et al. 1982; Leys et al. 1999). The amount and rate of energy gained by the redox couple represents the difference between the oxidation potential of the donor and the reduction potential of the acceptor minus the amount energy required for cellular processes (Jin and Bethke 2002).

Dissimilatory iron reduction is a deeply rooted process in both Archaea and Bacteria suggesting use of iron, as electron acceptor, may have been one of the first respiratory processes to evolve on Early Earth (Vargas et al. 1998; Schultze-Makuch et al. 2005). Diverse and abundant populations of iron reducing bacteria are present in redox stratified sediment and affect the cycling of carbon (Thamdrup, 2000; Kostka et al. 2002; Koretsky et al. 2003), the stability of iron oxides (Lovley 1991), and the transport of contaminants (Lovley et al. 1991; DiChristina et al. 2005). At circumneutral pH, Fe(III) is sparingly soluble and is typically found in the form of crystalline or amorphous oxyhydroxides (Zinder et al. 1986). Consequently, respiration of a solid TEA cannot be explained with the known pathways used by neutrophilic gram-negative bacteria. While several proteins involved in dissimilatory iron reduction have been isolated, a terminal reductase of iron-reducing bacteria has yet to be positively identified (DiChristina et al. 2005). Knowing the terminal reductase involved in dissimilatory iron reduction would be beneficial to understand the mechanism of iron reduction and the genes encoding the reductase could be used to trace DIR through the environment in a similar fashion to the use of the *dsr* gene as a probe for the activity of sulfate reduction (Wagner et al. 2005). In addition, discrepancies in the carbon budget of continental margins make estimations of carbon fluxes to the open ocean difficult to quantify (Hedges et al. 1997). Better

constraints on the microbial respiration processes coupled to carbon remineralization may help clarify the role of continental margins as sources or sinks of carbon. As the reduction of sulfate to sulfide involves the transfer of eight electrons and oxidizes two moles of carbon (Z_C=0) per mole of sulfide produced, sulfate reduction is generally thought to be the dominant anaerobic respiratory process in coastal marine sediments (Howarth and Teal 1979; Hines et al. 1989, Kostka et al. 2002). In contrast, dissimilatory iron reduction, which involves only one electron transfer and thus requires four moles of iron to oxidize one mole of carbon (Z_C=0), is often neglected as an important process in the cycling of carbon within marine environments (Canfield et al. 2005). Even though one electron is transferred to carbon per mole of iron, the rapid reoxidation of ferrous iron at oxic-anoxic transitions may recycle iron oxides rapidly and allow iron reduction to outcompete sulfate reduction (Taillefert et al. 2007). Additionally, sulfate reduction first requires the activation of the sulfate to adenosine 5'-phosophosulfate (APS) consuming one ATP. The subsequent reduction of APS forms sulfite, which is further reduced to sulfide and adenosine monophosphate (AMP). The conversion of AMP to adenosine diphosphate consumes an additional ATP. Altogether the respiration of sulfate consumes two ATP and produces 3 ATP for a net production of 1 ATP (Badziong and Thauer, 1978). Indeed in the past 15 years, DIR has increasingly been recognized as an important carbon remineralization process in coastal sediments (Thamdrup 2000; Kostka et al. 2002; Koretsky et al. 2003; Carey and Taillefert 2005). Identifying a molecular tool to quantify the activity of iron-reducing bacteria in marine environments therefore relies on characterizing the genetic components unique to iron-reducing bacteria. Such efforts can only be realized by characterizing the molecular pathways of dissimilatory iron reduction.

Three pathways have been proposed to overcome the physiological problem associated with the respiration on a solid TEA. In a direct contact pathway, the terminal reductase responsible for iron reduction is localized on the outer membrane and is in contact with the mineral surface to transfer electrons to the Fe(III) centers in the mineral crystal lattice (Myers and Myers 1992). The expression of proteins on the outer membrane, required for metal reduction, is facilitated by the translocation of proteins by the type-II secretion apparatus. The type-II secretion apparatus appears to be required for DIR (Fig. 1.2), as deletion of the GspD multimeric channel protein inhibits reduction of Fe(III) and Mn(IV) presumably due to the inability to secrete components of the terminal reductase to the outer membrane (DiChristina et al. 2002). Second, a MtrABC trans outer-membrane protein complex has been identified and proposed to deliver electrons from the periplasm to the mineral surface (Fig. 1.2). In this complex, MtrB is a β-barrel porin spanning across the outer membrane (Ross et al. 2007; Hartshorne et al. 2009). The decaheme cytochrome MtrA is associated with MtrB on the periplasmic side of the outer membrane (Ross et al. 2007; Hartshorne et al. 2009), while the decaheme cytochrome MtrC, located on the outside of the outer membrane, has been theorized to be the terminal reductase in dissimilatory iron reduction (Myers and Myers 1992). Finally, the outer membrane decaheme OmcA is a homolog of MtrC that may

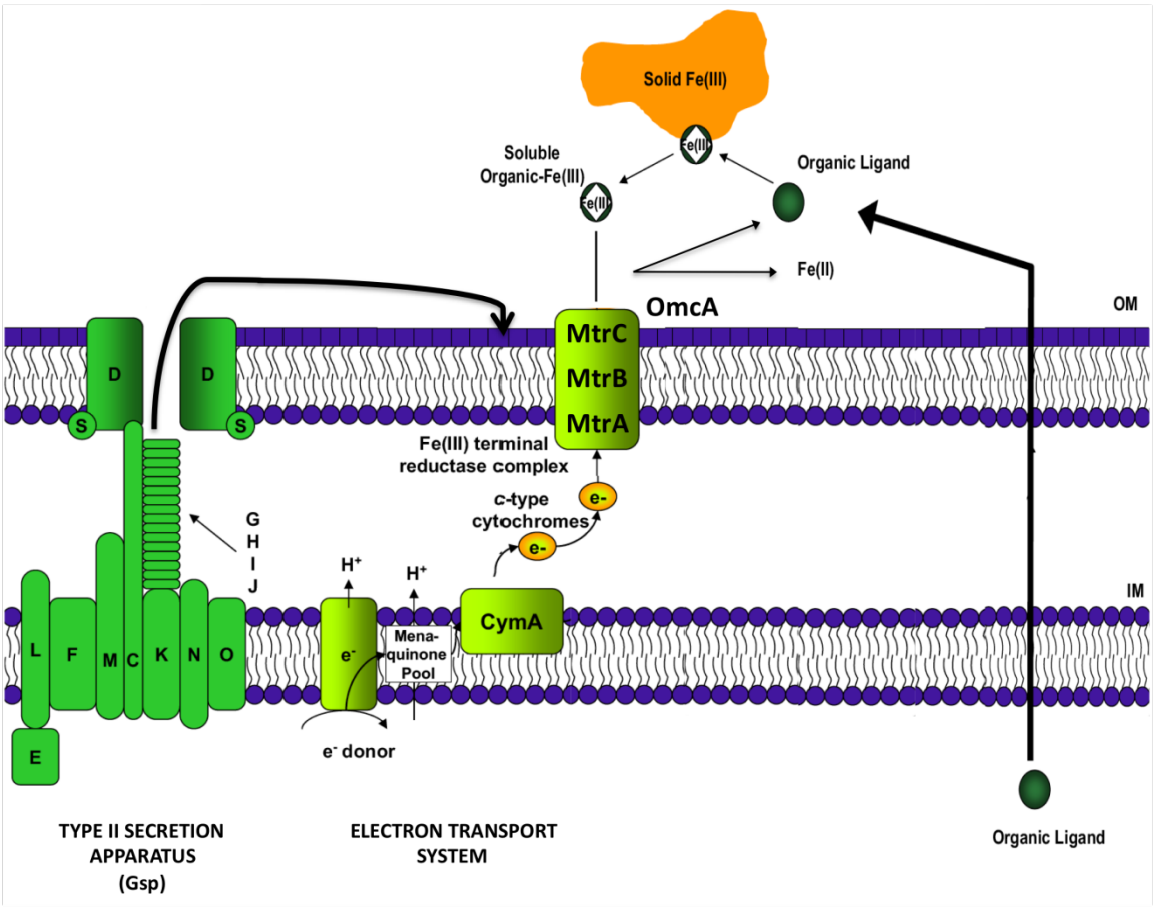

Figure 1.2 – Proposed chelation pathway for DIR by *S. oneidensis* for the non-reductive dissolution of iron oxides by endogenous ligands of *S. oneidensis*. Organic ligands, secreted by the cell, non-reductively dissolve the iron oxide producing a soluble organic-Fe(III) complex where the outer membrane complex MtrABC may reduce this complex. The decaheme c-type cytochromes MtrC and OmcA are translocated to the outer membrane by the type-II secretion apparatus, which is required for DIR (Figure modified from DiChristina et al. 2005).

be able to accept electrons from the MtrABC complex (Shi et al. 2006). Deletion of these proteins has been demonstrated to disrupt DIR, however, the terminal reductase has yet to be isolated. Additionally, conductive 'nanowires' may be deployed by DIRB to reach iron oxide electron acceptors at distance (Gorby et al. 2006; El-naggar et al. 2010), and it was shown that the outer-membrane cytochromes MtrC and OmcA, and the type II

secretion apparatus are required for the expression of electro-conductive nanowires (Gorby et al. 2006, El-Naggar et al. 2010).

Alternately, a two-step electron shuttling mechanism using either endogenous or exogenous electron shuttles is used to transfer electron to the mineral surface (Lovley and Woodward 1996). Proposed electron shuttles include AQDS (Lies et al. 2005; Bond and Lovley 2005), humic acids (Coates et al. 1998; Kappler et al. 2004), flavins (Marsilli et al. 2008; Covington et al. 2010), and organic sulfur compounds (Doong and Schink 2002; Kaden et al. 2002). In this case, a terminal reductase, either in the periplasm or on the outer membrane, reduces an electron shuttling molecule. The reduced shuttles are released to nonspecifically reduce solid iron oxides or any other reducible material in the surrounding media (Hernandez and Newman 2001; Rosso et al. 2003). It is assumed that some level of recycling of the shuttling molecules occurs to offset the biosynthetic cost of shuttle production (Schink 1997). It has also been shown that the rapid cycling of iron using electron shuttles may play a significant role in the cycling of iron (Doong and Schink 2002; Roden et al. 2004) and syntrophic systems of reducers and oxidizers can share electron shuttle processes (Kaden et al. 2002).

Finally, in the chelation pathway, small endogenous molecules secreted to the surrounding environment form soluble organic-Fe(III) complexes during the non-reductive dissolution of Fe(III) from iron bearing minerals (Taillefert et al., 2007). These soluble Fe(III) complexes are reduced on the cell surface or taken into the periplasmic space, where known terminal reductases apparently reduce soluble Fe(III). Upon reduction the complex can be released to continue the cycle of non-reductive dissolution of iron oxides followed by the microbial reduction of soluble Fe(III). As for the

endogenous electron shuttles, the biosynthetic energy cost for ligand production must be recoverable during reduction of soluble Fe(III). The non-reductive dissolution of Fe(III) by organic ligands prior to DIR may provide several advantages over other pathways: it may increase the reduction potential of Fe(III) (Zinder et al. 1986; Taillefert et al. 2007); it may lower the activation energy required to reduce Fe(III) and thus increase reduction rates (Taillefert et al. 2007; Wang et al. 2008); and it may help prevent mineral passivation by binding the Fe(II) reduction product to organic ligands (Royer et al. 2004; Roden 2006). Reduction rates of soluble Fe(III) substrates are up to 50 times greater than the rates of reduction with solid Fe(III) oxides, suggesting the chelation pathway is energetically more favorable to direct contact (Arnold et al. 1988). The large number of studies investigating these processes suggests that multiple pathways may be in use at the same time, and cells adjacent to the mineral surface may prefer to use the direct contact mechanism while cells at a distance may rely on the shuttling or chelation pathways. Until the key components of the genetic machinery involved in each of these pathways are identified, these mechanisms will remain theoretical.

1.5 Research Scope and Objectives

Iron is an essential element in a wide variety of biological reactions and simultaneously regulates the distribution of toxic contaminants in aquatic systems. The solubility of Fe(III) directly controls the bioavailability of iron for both nutrient assimilation and dissimilatory use, but the mechanisms responsible for the formation of soluble Fe(III) remain poorly understood. In addition, the role of some environments in supplying this limiting nutrient to the surface waters of the oceans remains poorly quantified. In this thesis, both field and laboratory approaches are adopted to elucidate

the role of soluble organic-Fe(III) complexes in dissimilatory iron reduction and the use of these complexes as sources of iron to the surface ocean. Two main hypotheses were tested in this dissertation:

1. **Hydrothermal vents and estuarine sediments provide a significant source of dissolved iron to the ocean that may be transported in the photic zone under the form of stable organic-Fe(III) complexes.**
2. **Iron-reducing bacteria may be partly responsible for the production of organic-Fe(III) complexes as these bacteria extracellularly produce organic ligands to non-reductive solubilize iron oxides during dissimilatory iron reduction.**

Chapter II of this thesis outlines the analytical techniques used and developed to measure organic-Fe(III) complexes and investigate the speciation of Fe in marine waters and during microbial incubations. Conventional techniques employed in this work are described, including colorimetric techniques (Fe(II), total Fe, and nitrite), voltammetric microelectrode measurements (dissolved oxygen, organic-Fe(III), Fe(II), Mn(II), $FeS_{(aq)}$, and ΣH_2S), chromatographic measurement of anions (Cl^-, SO_4^{2-}) and polysulfides ($S_2O_3^{2-}$, $S_3O_4^{2-}$), and inductively coupled plasma mass spectrometry (ICP-MS) for the determination of metals including iron. Novel applications of competitive ligand equilibration-adsorptive cathodic stripping voltammetry (CLE-ACSV) were developed to probe the speciation of soluble Fe(III) complexes in sediments of the Satilla River Estuary and in pure cultures of DIRB. Additionally a microelectrode screening array (MESA) was developed to identify mutant strains of the model DIRB *Shewanella*

oneidensis. This technique is used to screen large numbers of these mutant strains in a short period of time and identify genes responsible for the production of organic-Fe(III) complexes during dissimilatory iron reduction.

Hydrothermal vent fluid is metal rich and highly reduced (Von Damm 1990) and possibly provides a source of iron to the surface ocean (Tagliabue et al 2010). Chapter III investigates the chemistry of hydrothermal vent fluid at 9° North on the East Pacific Rise. The 9° North hydrothermal vents support a unique biological community including tube worms (*Alvinella pompejana, Alvinella caudate,* and *Riftia pachyptila*), mussels (*Bathymodiolus thermophilis* and *Calyptogena magnifica*), and crabs (*Munidopsis* and *Bythograea*). These megafauna are in a symbiotic relationship with the chemautotrophic bacteria which depend on sulfide from vent fluids as electron donor. In this chapter the speciation of the polythionate sulfide oxidation products was investigated in hydrothermal vent fluids. Metal concentrations and seawater mixing were used to determine the percentage of fresh seawater mixed with the vent fluid (Von Damm 1990). The objectives of this study were to characterize the chemistry of hydrothermal vent fluids at 9° North based on the age and subsurface interactions with the basalt, determine the size distribution of iron particles to ascertain the role of hydrothermal vents as sources of iron as nutrient to the pelagic ocean, and ascertain the oxidation products of vent sulfide and their role in the cycling of iron.

Iron is a limiting nutrient in many parts of the photic zone of the upper ocean and indirectly controls parts of the global carbon cycle (Martin et al. 1990). Describing the processes that regulate the distribution of iron in the oceans is therefore of utmost importance. The bioavailability of iron in seawater is largely controlled by organic

ligands that increase the half-life of soluble iron in the surface oceans (Rue and Bruland 1997). Recently, iron fluxing from sediments has been investigated as a viable source of iron to the ocean (Elrod et al. 2004; Lam et al 2008). The microbial reduction of iron(III) in anaerobic sediments produces soluble Fe(II) that may diffuse across the sediment water interface and provide a source of iron to surface waters during upwelling (Berelson et al. 2003; Elrod et al. 2004). This process requires a source of Fe(III) to sediments and sufficient organic carbon to support microbial reduction. In estuaries the majority of river borne iron and dissolved organic matter (DOM) flocculates and precipitates as fresh water mixes with seawater (Boyle et al. 1977). Typically, more than 90% of the iron entering estuaries is lost to the sediment prior to reaching the mouth of the estuary (Moore et al. 1979). Chapter IV investigates the speciation of Fe(III) through an estuary off the coast of Georgia, determines the role of iron reduction in estuarine sediments as a source of iron to the surface waters, and characterizes the flux of organic-Fe(III) complexes to the overlying waters and the continental margin.

As the production of soluble Fe(III) complexes in marine sediments may involve intermediates formed during microbial iron reduction, the rest of this thesis investigates the mechanism of the production of these complexes by a model iron reducing microorganism. Organic-Fe(III) complexes, similar to those observed in marine sediments, have been detected with mercury amalgam microelectrodes during iron reduction by *Shewanella putrefaciens* (Taillefert et al. 2007). Chapter V sought to identify random mutants of *Shewanella oneidensis* strain MR-1 for their inability to produce organic-Fe(III) complexes during dissimilatory iron reduction. The objectives of this work were to determine if *Shewanella oneidensis* was capable of producing soluble

organic-Fe(III) complexes during DIR and to develop a voltammetric-based, screening technique for the identification of random *S. oneidensis* mutants unable to produce soluble organic-Fe(III) complexes. Siderophores were investigated as a source of organic ligands for iron complexation during DIR. Additionally, the production of organic-Fe(III) was investigated over a range of reduction potentials using iron oxides and alternate electron acceptors.

Organic-Fe(III) complexes have been shown to be produced by some DIRB (Taillefert et al. 2007; Fennessey et al. 2010). The ligands, however, have yet to be identified. Quantifying the concentrations and conditional stability constants of the Fe(III)-ligand complexes is necessary to determine to role of these organic-Fe(III) complexes as intermediates during iron reduction. Competitive ligand equilibration – adsorptive cathodic stripping voltammetry (CLE-ACSV) has been recently applied to determine the concentration of organic-Fe(III) complexes in estuarine sediments associated with zones of iron reduction (Chapter IV). Additionally CLE-ACSV has been used to determine the complexation capacity of culture media supplemented with cadmium (Ceretti et al. 2010). The speciation of organic-Fe(III) complexes produced during dissimilatory iron reduction are investigated in Chapter VI. The objectives of this work were to determine the ligand concentration and conditional stability constant of the organic-Fe(III) complex production during iron reduction and determine the effects of growth media and iron oxide type on the production of organic-Fe(III) complexes.

Finally, Chapter VII synthesizes the findings of this research, discusses the role of organic-Fe(III) complexes in the solubility and bioavailability of iron, introduces new

questions identified by these studies, and presents recommendations for future work on organic-Fe(III) complexes.

CHAPTER 2

ANALYTICAL TECHNIQUES

2.1 Colorimetry

2.1.1 Iron

Total dissolved iron in estuarine and pore waters, including soluble species and colloids smaller than 0.2 μm, was determined by the ferrozine method after reduction by hydroxylamine (0.2 mol L^{-1} at pH 1) (Stookey 1970). Detection limits for total iron by this method were 0.24 ± 0.03 μmol L^{-1}. Dissolved ferrous iron in pore waters was measured by the ferrozine method without the addition of hydroxylamine. Dissolved ferric iron in pore waters was determined by difference between the total dissolved and ferrous iron concentrations.

Total ferrous iron concentration in microbial incubations was determined by the ferrozine method after acid extraction. In an oxygen free atmosphere, an aliquot (200 μL) of well mixed incubation medium including solid iron particles was added to 1 mL of 3 M HCl to release any Fe^{2+} adsorbed on to iron oxides and dissolve any secondary Fe(II) mineral products (Lovley and Phillips 1986). Samples were analyzed for total Fe^{2+} by the Ferrozine colorimetric method (Stookey 1970). For some incubations, total dissolved and dissolved ferrous iron were determined after filtration (0.2 micron PE syringe filters, minimum 5 mL) in an oxygen free atmosphere. The dissolved iron species were maintained in 0.5 M HCl until analysis by the ferrozine method as described above.

2.1.2 Nitrite

Nitrite (NO_2^-) concentrations in nitrate-grown cultures, were determined by 250-fold dilution in a solution consisting of 9.6 mM sulfanilic acid, 96 mM $KHSO_4$, and 3.2 mM N,N-ethylenediamine (Montgomery and Dymock, 1962). Samples were held in the dark for 15 minutes prior to absorbance measurements at 510 nm.

2.2 Voltammetry

2.2.1 Microelectrodes

Oxygen, organic-Fe(III), total sulfides, iron sulfide, Fe(II), Mn(II) voltammetric analyses of sediment pore waters and samples from microbial incubations were performed with gold-mercury amalgam (Au/Hg) microelectrodes (Brendel and Luther 1995). The Au/Hg microelectrode consists of a gold wire plated with a mercury solution to form a thin mercury film. A three-electrode cell consisting of an Au/Hg amalgam working electrode, an Ag/AgCl reference electrode, and a platinum counter electrode was used for all voltammetric analyses. Voltammetric techniques included linear sweep (Oxygen), cyclic (sulfides), and cathodic square wave (organic-Fe(III), Fe(II), Mn(II)) voltammetry (Davison et al. 1988; Brendel and Luther 1995). In voltammetry, a voltage is scanned between the working and reference electrodes as a function of time. When an appropriate potential for electron transfer between the working electrode and a redox active species in the solution is reached, a current that is proportional to the concentration of that species in solution flows between the working and counter electrodes (Taillefert et al., 2000b). The potential at which the current in measured can be used to identify the species in solution. For linear sweep voltammetry, a potential is applied between the working and reference electrode and swept typically between -0.1 and -1.8 volts. Oxygen

and peroxide current responses are observed as stair-step increases in the baseline current. The concentration of oxygen is calibrated to oxygen saturated solution of similar ionic matrix (Luther et al. 2008). Cyclic voltammetry is similar to linear sweep except that the potential is swept in one direction then swept back to the initial potential. Square wave voltammetry is a pulsed voltammetric technique with a square wave function superimposed onto a stair step potential sweep resulting in both a forward and reverse potential scans within a small potential range (Osteryoung and Osteryoung 1985). A positive current flow is measured following the forward potential jump and a negative current flow is measured following the reverse potential jump. The reverse current (negative) is subtracted from the forward current (positive) and the resulting current difference provides greater sensitivity than other voltammetric techniques (Fig 2.1). The potential is then stepped to the next potential range where forward and reverse scans are performed with current measured at the end of each scan. Square wave voltammetry provides faster scans, with greater sensitivity than traditional voltammetric methods (Osteryoung and Osteryoung 1985). Square wave voltammetry produces peaks centered at the redox potential making data analysis easier than the waves generated in linear sweep voltammetry (Ramaley and Krause 1969). The peak width provides information about the number of electron transferred during the reaction at the electrode. For reversible reactions, the theoretical half-width is 90.5 mV divided by the number of electrons transferred (Ramaley and Krause 1969). In cathodic square-wave voltammetry, potentials are scanned from positive to negative values, and the resulting current is represented graphically versus the potential applied (Fig 2.1). An example scan acquired in anoxic sediment porewaters displays the broad organic-Fe(III) peak at -0.3 V

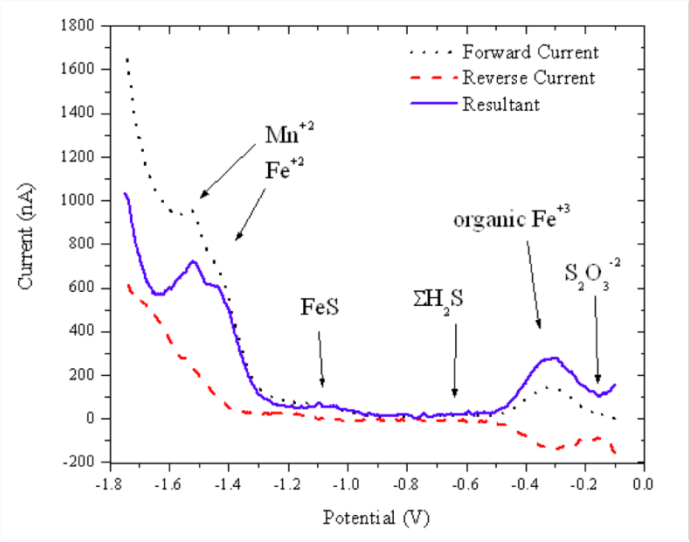

Figure 2.1 Cathodic square wave voltammagram of sediment porewaters. Label indicate the potentials for the reduction of thiosulfate (-0.15 V), organic-Fe(III) (-0.35 V), total sulfide (-0.63 V), FeS (-1.1 V), Fe(II) (-1.4 V), and Mn(II) (-1.6 V).

representative of a one electron transfer from Fe(III) to Fe(II). A set of narrow, overlapping peaks are visible for the reduction of Fe(II), -1.4 V, and Mn(II), -1.6 V. These peaks are one-half the half-width of the organic-Fe(III) peak due to the two electron transfer for the reduction of Fe(II) and Mn(II). If present, thiosulfate at -0.15 V, total sulfide at -0.63 V, and FeS -1.1 V would also have been detected in the same cathodic square-wave voltammogram. Oxygen is calibrated from the calculated oxygen saturation for a fully oxygenated sample at a given temperature and ionic strength. Manganese is calibrated with Mn(II) solution prepared from manganese chloride salts. Fe(II) and total sulfide are referenced to the manganese calibration by known calibration relationships between these species and Mn(II). Unfortunately the current sensitivity of organic-Fe(III) complexes depends on the nature of the organic ligand binding iron (Taillefert et al. 2000a). Without knowing the organic ligand binding the iron in solution

the concentration cannot be determined directly. Therefore, organic-Fe(III) measurements are typically reported in current intensity units.

2.2.2 Microelectrode Screening Array (MESA)

A Microelectrode Screening Array (MESA) for voltammetric detection of soluble organic-Fe(III) complexes was constructed to screen large numbers of mutants in the individual 300 μL wells of a 96-well tray (8 x 12 matrix). MESA consists of an electrode holder with eight removable 100 μm diameter Au/Hg amalgam working electrodes and eight permanent 0.5 mm diameter Ag/AgCl reference and 0.5 mm diameter platinum counter electrodes mounted on a manual micromanipulator (Narishige). A machined aluminum tray holder with raised stops corresponding to the distance between the rows of the 96-well trays facilitated deployment of the tray from one row to another for screening (Fig. 2.2a). The array of eight counter electrodes (Fig. 2.2b) was fabricated by soldering

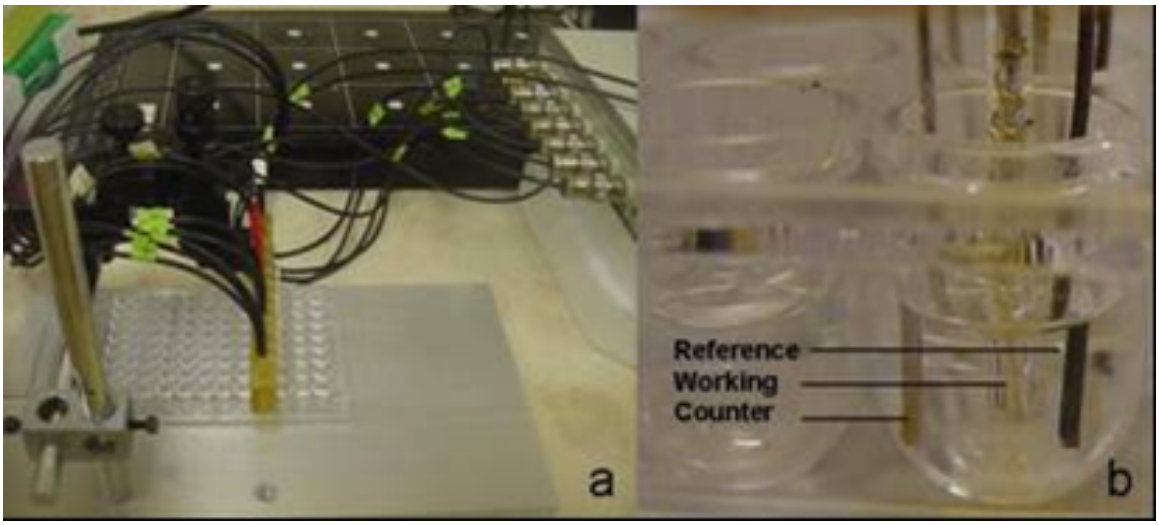

Figure 2.2 Microelectrode screening array (MESA) developed to identify Sol mutants. An array of eight Au/Hg voltammetric microelectrodes was used to analyze each row of a 96-well tray. A computer-controlled multiplexer automatically switched between working electrodes during each analysis. (a) View of MESA in a 96-well tray. (b) Interconnected platinum counter (left) and Ag/AgCl reference (right) electrodes are fixed within the resin body, while Au/Hg working electrodes (center) can be removed for polishing and storage.

eight one inch pieces of 0.5 mm platinum wire together every 0.8 cm along a 8 cm piece of striped stranded coaxial cable such that the distance between each wire was equal to the distance between the wells of a 300 μL 96-well tray. A similar array of reference electrodes was fabricated from 0.5 mm silver wire. The counter and reference arrays were placed 0.7 cm apart in a 12 cm x 1 cm x 2 cm mold such that 2 cm of the unstripped coaxial cables were incorporated within the mold and 2 cm of the wires were kept outside the mold. The mold was filled with epoxy resin and eight 5/32 inch holes were drilled between the counter and reference to receive the 3/16 inch PEEK™ tubing sheath of the working electrodes. Tapped holes were added to secure working electrodes with setscrews. The Ag/AgCl reference electrodes were conditioned by applying +9 volts for 30 seconds between the reference and counter electrodes in a 3 M KCl solution. Au/Hg working electrodes were fabricated by soldering a one-inch length of 100 μm gold wire to the end of stranded coaxial cable. The gold wire and exposed copper wire were threaded into a 1.0 mm outer diameter glass tube. The joint between the glass tube and coaxial cable was covered by a one inch piece of 3/16 inch PEEK™ tubing sheath for reinforcement and mounting in the array body. The glass end was filled with epoxy until excess epoxy was observed from all joints. After drying, the tip was sanded with 400 grit sandpaper. BNC connectors were added and electrodes were polished, plated and conditioned as previously described (Brendel and Luther 1995). Microelectrodes were first tested for quality using O_2, then calibrated with Mn^{2+}. Minor differences in electrode construction, polishing, and mercury plating generally result in electrodes that vary in mercury size, geometry, and analyte sensitivity (Osteryoung and Osteryoung,

1985; Brendel and Luther, 1995). Current intensities of each electrode were therefore normalized by multiplying the measured analyte intensity by the current intensity ratio of a Mn^{2+} standard for a given electrode to the average Mn^{2+} current intensity for the eight electrodes in the array (Eq. 2.1):

$$I_{normalized} = I_{measured} \times \frac{I_{standard}}{\text{average } (I_{standard})} \qquad \text{(Eq. 2.1)}$$

where $I_{normalized}$ is the normalized current intensity, $I_{measured}$ is the measured current intensity of the analyte of interest, $I_{standard}$ is the current intensity of a 200 uM Mn^{2+} standard, and average($I_{standard}$) is the average current intensity of the Mn^{2+} standard for the eight electrodes of the array. A Model DLK-100 potentiostat with DLK-MUX-1 eight channel electrode multiplexer (Analytical Instruments Systems, Inc.) was used for all voltammetric measurements. Working electrodes were controlled by the computer-operated DLK-MUX-1 multiplexer, while the reference and counter electrodes shared respective leads between each cell and the DLK-100A potentiostat. All voltammetric potentials are reported versus the Ag/AgCl reference electrode. All MESA analysis was performed in an oxygen-free atmosphere.

2.3 Competitive Ligand Equilibration

2.3.1 Overview

As the direct voltammetric measurement of unknown organic-Fe(III) complexes is hindered by the unknown sensitivity of the Fe(III)-ligand complex to the mercury electrode (Taillefert et al. 2000), it is necessary to find alternate techniques to quantify these complexes. Isolation of the organic-Fe(III) complexes would be ideal for studying

the speciation of soluble organic-Fe(III) in both estuarine environments and during dissimilatory iron reduction. Natural organic matter is, however, known to consist of a wide variety of organic molecules ranging from amino acids and sugars to humic and fulvic compounds (Buffle et al 1982). Isolation and identification of these organic-Fe(III) complexes has been hindered by the complex organic matrix present in both environmental samples and microbial culture experiments and the strong adsorption properties of iron oxides. Alternately, competitive ligand equilibration – adsorptive cathodic stripping voltammetry (CLE-ACSV) could be adapted to measure dissolved organic-Fe(III) complexes. In this technique, a known Fe(III) complexing ligand is added to a sample containing organic-Fe(III) to compete for free iron in the sample (Rue and Bruland 1995). The concentration of free iron, $[Fe^{3+}]$, in the sample is either increased or decreased while the change in current response of the competitive ligand-Fe(III) complex is monitored. In forward CLE-ACSV titrations, the concentration of natural and competitive ligands is held constant while the concentration of free iron, $[Fe^{3+}]$, in the samples is increased by addition of Fe(III). Conversely, in reverse CLE-ACSV titrations the natural ligand and total iron (III) concentrations are held constant while additions of the competitive ligand decrease the free Fe(III) concentration (Santos-Echeandia et al. 2008). The change in the concentration of the known organic-Fe(III) complex can be described by the iron and ligand mass balance equations and the known and unknown ligand equilibrium equations to determine ligand concentrations and conditional stability constants of the organic-Fe(III) complexes.

2.3.2 Forward Titration

A competitive ligand equilibration adsorptive cathodic stripping voltammetry (CLE-ACSV) technique modified from previous methods designed for low iron (nmol L^{-1}) in open ocean samples (Rue and Bruland 1995; Wu and Luther 1995) was used to determine the speciation of dissolved Fe(III) in filtered estuarine and porewater samples with concentrations of Fe(III) ranging between 0.5 μmol L^{-1} and 1 mmol L^{-1}. Any Fe(II) in riverine and sediment porewater samples was allowed to oxidize during dilution (10-500 times) with a 10 mmol L^{-1} Piperazine-1,4-bis(2-ethanesulfonic acid (PIPES) buffer in 0.25 mol L^{-1} NaCl containing 30 μmol L^{-1} of the competitive ligand 1-nitroso-2-napthol (NN). Each dilution was selected such that the competitive ligand was in excess of total dissolved iron. After a 2-hour equilibration, samples were divided into 10 aliquots, each receiving a ferric chloride spike ranging between 0 and 2 μmol L^{-1}. Samples were allowed to equilibrate for 8 hours prior to analysis by hanging mercury drop electrode (Metrohm VA-663) connected to a DLK-60 potentiostat (Analytical Instruments Systems). Cathodic square-wave voltammetry was used for all CLE measurements with 30 second (porewaters) or 240 second (overlying waters) deposition times at -0.1 volts with stirring followed by a 5 second equilibration time. A 150 mV s^{-1} scan rate and 35 mV pulse height was used during square-wave scans. The current height of the Fe(III)-1N2N complex was measured at -0.48 V vs. Ag-AgCl. Data from voltammetric scans were integrated using VOLTINT, a semi-automated integration software implemented in Matlab (Bristow and Taillefert 2008). A conditional binding constant of 1.42 x 10^{15} for the competitive ligand NN was determined by calibration with ethylenediaminetetraacetic

acid (EDTA) in the buffer system (10 mmol L^{-1} PIPES, 0.25 mol L^{-1} NaCl) used in all measurements (Rue and Bruland 1995).

The concentration of the natural ferric complex, [FeL], in each sample was calculated from the titration curve of the Fe(III)-NN complex measured electrochemically and the mass balance on ferric iron species in solution expressed by the following equation:

$$[Fe_T] = [FeL] + [Fe´] + [Fe_{NN}] \qquad \text{(Eq. 2.2)}$$

where $[Fe_T]$ is the concentration of total dissolved Fe(III), [FeL] is the concentration of the natural organic-Fe(III) complex exchangeable with the competitive ligand NN, [Fe'] is the concentration of inorganic and 'free' hydrated Fe(III), and $[Fe_{NN}]$ is the concentration of the Fe(III)-NN complex measured electrochemically. The point where the linear extrapolation of the titration curve intersects the x-axis yields the point of zero

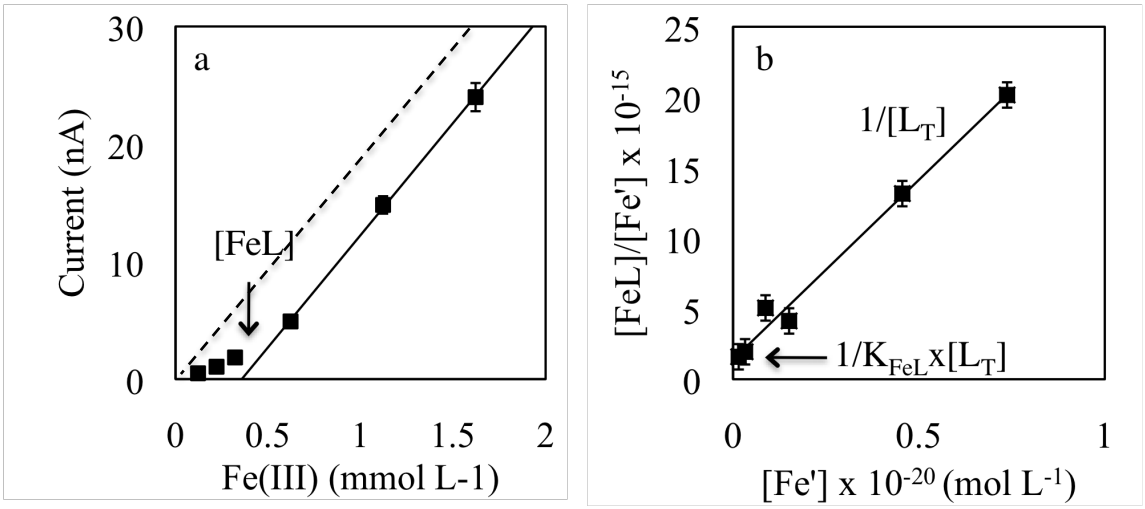

Figure 2.3 Forward CLE-ACSV titration (a) and Ruzic linearization (b) of 500 fold diluted sediment porewaters of the Satilla River Estuary. The [FeL] in the sample is determined from the x-intercept of the titration. The Ruzic linearization provides the $[L_T]$ and K_{FeL} from the slope and y-intercept respectively. Dashed line represents the theoretical FeNN calibration without a natural ligand.

current from the Fe(III)-NN complex, thus the point where [Fe_{NN}] is zero in the mass balance equation (Eq. 2.2). If iron bound to organic complexes far exceeds free or inorganically bound iron ([FeL] >> [Fe']), then the [Fe'] term is negligible in the mass balance equation (Eq. 2.2) and [Fe_T] = [FeL] at the x-intercept (Fig 2.3a). In this technique, colloidal iron that does not diffuse to the electrode or does not react with the NN and dissolved iron bound to organic ligands that are not exchanged by the NN ligand are not included in the [FeL] fraction (Wu and Luther 1995). As excess ligand is present in the sample, any Fe(II) oxidized during the equilibration is likely complexed by either the natural or the competitive organic ligand and should remain soluble. Thus, the concentration of organic-Fe(III) complexes in the initial sample can be calculated by subtracting the concentration of Fe(II) from the CLE-determined organic-Fe(III) concentration. At each point of the titration the [Fe_{NN}] can be calculated from the following equation:

$$[Fe_{NN}] = S \times i \qquad \text{(Eq. 2.3)}$$

where S is the slope of the linear portion of the titration curve, excluding any curvature approaching the x-axis, and i is the current intensity of the Fe(III)-NN complex. The free and inorganically bound Fe(III) is determined by:

$$[Fe'] = \frac{S \times i}{\alpha_{FeNN}} \qquad \text{(Eq. 2.4)}$$

where α_{FeNN} is the side reaction coefficient for the formation of the Fe(III)-NN complex. Assuming a 3:1 binding ration between NN and Fe(III), the side reaction coefficient is defined as:

$$\alpha_{FeNN} = K_{FeNN} \times [NN]^3 \qquad \text{(Eq. 2.5)}$$

where K_{FeNN} is the conditional stability constant for the Fe(III)-NN complex determined to have a Log value of 15.15 by titration with EDTA. The concentration of FeL at each titration point is determined by difference from the Fe mass balance equation:

$$[FeL] = [Fe_T] - ([Fe_{NN}] + [Fe']) \qquad \text{(Eq. 2.6)}$$

Given the concentrations of [FeL] and [Fe'] at each titration point the Ruzic linearization (Fig 2.3b) can be derived from the equations for total ligand concentration $[L_T]$ and the conditional binding constant, K_{FeL}:

$$[L_T] = [L] + [FeL] \qquad \text{(Eq. 2.7)}$$

and

$$K_{FeL} = \frac{[FeL]}{[L] \times [Fe']} \qquad \text{(Eq. 2.8)}$$

where [L] is the free ligand in solution. By substituting [L] from the K_{FeL} equation into the $[L_T]$ equation gives:

$$[L_T] = [FeL] + \frac{[FeL]}{[Fe'] \times K_{FeL}} \qquad \text{(Eq. 2.9)}$$

Multiplying both sides by [Fe']/([FeL]*$[L_T]$) yields:

$$\frac{[Fe']}{[FeL]} = \frac{[Fe']}{[L_T]} + \frac{1}{[L_T] \times K_{FeL}} \qquad \text{(Eq. 2.10)}$$

The plot of [Fe']/[FeL] against [Fe'], gives a slope of $1/[L_T]$ and a y-intercept of $1/K_{FeL}*[L_T]$.

2.3.3 Reverse Titration

Reverse CLE-ACSV titrations are similar to forward CLE-ACSV except that the concentration of competitive ligand is increased instead of the concentration of total Fe(III) (Nuester and van den Berg, 2005). In this technique, the concentration of free $[Fe^{3+}]$ decreases with the addition of the competitive ligand, making this titration the reverse of the forward titration. Reverse CLE-ACSV titrations are most sensitive when total Fe(III) is in a similar concentration to the natural ligand (Santos-Echeandia et al 2008). The competitive ligand is able to then exchange iron with the natural ligand over a range representing the entire concentration of the natural ligand. If the ratio of iron to natural ligand is low, only a small range of competition is observed during the titration. If insufficient iron is present in the sample, Fe(III) can be added to the sample to measure the complexation capacity of the ligand present in the sample. This method presents two main advantages over forward CLE-ACSV titrations. First, reverse CLE-ACSV titrations reach a much larger detection window than forward CLE-ACSV titrations. In forward CLE-ACSV titrations the detection window, the ratio of ligand concentrations and ligand strengths that allows for competition between the natural and competitive ligand, is typically within ± one decade of the $\alpha_{Fe\text{-}1N2N}$ (Eq. 2.5). In reverse CLE-ACSV the concentration of competitive ligand is typically increased by three orders of magnitude over the course of the titration. Changing the concentration of competitive ligand extends the detection window from two to five decades, greatly increasing the likelihood of

detection a ligand of interest especially in dynamic systems where the concentration or stability constant of natural ligands may change over time. Second, this technique does not require determining the sensitivity, S, of the Fe(III)-NN complex to the mercury electrode. Instead, the relative current response of the titration, or the ratio of the current intensity to the maximum current intensity observed during the titration, is evaluated by the equation:

$$X = \frac{i}{i_{max}} = \frac{[FeNN]}{[Fe_T]} \qquad \text{(Eq. 2.11)}$$

where, X, is the relative current response, i, is the current intensity for a given titration point, and, i_{max}, is the maximum observed current intensity for the titration. This ratio is equivalent to the ratio of concentration of [FeNN] to the $[Fe_T]$, assuming all the Fe(III) in the system is titratable by the competitive ligand. By substituting the Fe mass balance equation for $[Fe_T]$, the following equation is derived:

$$X = \frac{[FeNN]}{[Fe'] + [FeL] + [FeNN]} \qquad \text{(Eq. 2.12)}$$

The concentration of FeNN and Fe' can be related to the concentration of free Fe(III), $[Fe^{3+}]$, through the respective side reaction coefficients, α, in the following equations:

$$[FeNN] = \alpha_{FeNN} \times [Fe^{3+}] \qquad \text{(Eq. 2.13)}$$

and

$$[Fe'] = \alpha'_{Fe} \times [Fe^{3+}] \qquad \text{(Eq. 2.14)}$$

where α'_{FeNN} is the side reaction coefficient for the complextion of the competitive ligand NN with free iron, Fe^{3+}, and $\alpha'_{Fe'}$, the side reaction coefficient for the complexation of free iron by inorganic species and is defined in the following equation:

$$\alpha'_{Fe} = \frac{[Fe']}{[Fe^{3+}]} = 1 + \sum(\beta'_{FeX_i}[X]^i) \qquad \text{(Eq. 2.15)}$$

where β'_{FeXi} is the stability constant for iron complexes with, *i*, major anions (X) in M1 growth media at pH 7 and was determined for the growth M1 growth media used in the microbial cultures by the thermodynamic calculation program Visual MINTEQ 3.0 (Gustafson 2005). The concentration of the natural ligand during titration is determined by substituting the ligand mass balance equation (Eq. 2.7) into the FeL equilibrium equation (Eq. 2.8) to yield:

$$[FeL] = \frac{K_{FeL} \times L_T \times [Fe^{3+}]}{1 + (K_{FeL} \times [Fe^{3+}])} \qquad \text{(Eq. 2.16)}$$

By substituting the equations for [FeNN], [Fe'], and [FeL] (Eq 2.13, 2.14. and 2.16) into the relative current response equation (Eq. 2.12), the following equation is obtained to describe the titration behavior:

$$X = \frac{\alpha_{FeNN}}{\alpha'_{Fe} + \alpha_{FeNN} + \frac{K_{FeL} \times [L_T]}{(K_{FeL} \times [Fe^{3+}]) + 1}} \qquad \text{(Eq. 2.17)}$$

This equation is used to describe the S-shaped titration curve observed in the graph of the log [NN] versus the relative current response of the Fe-NN complex. The K_{FeL} and $[L_T]$

parameters can be optimized by least-squares fitting (Nuester and van den Berg 2005) which is described in Appendix A.

Alternatively, Ruzic and Scatchard linearizations can be used for the determination of the K_{FeL} and $[L_T]$ values. Both linearizations require the calculation of [FeL] and $[Fe^{3+}]$ at each point of the titration. Substituting the side reaction coefficient reaction equation for [FeNN] (Eq. 2.13) into the relative current response equation (Eq. 2.11) yields:

$$[Fe^{3+}] = \frac{X \times [Fe_T]}{\alpha_{FeNN}} \qquad \text{(Eq. 2.18)}$$

[FeNN] and $[Fe^{3+}]$ are determined by their respective side reaction equations (Eq. 2.13 and 2.14), while [FeL] is calculated by difference from the iron mass balance equation (Eq. 2.2). The Ruzic linearization can be used as described above in the section on forward CLE-ACSV titrations, however for the reverse CLE the conditional stability constants were calculated with respect to $[Fe^{3+}]$ using the following equation:

$$\frac{[Fe^{3+}]}{[FeL]} = \frac{[Fe^{3+}]}{[L_T]} + \frac{1}{[L_T] \times K_{FeL/Fe3+}} \qquad \text{(Eq. 2.19)}$$

where $K_{FeL/Fe3+}$ is the conditional stability constant for the formation of the FeL complex with respect to $[Fe^{3+}]$. Values for $K_{FeL/Fe3+}$ differ from K_{FeL} by the inorganic side reaction coefficient, α'_{Fe} (Eq. 2.14).

$$K_{FeL} = \alpha'_{Fe} \times K_{FeL/Fe3+} \qquad \text{(Eq. 2.20)}$$

If multiple ligands are within the detection window, curvature will be observed in the Ruzic linearization. In the case of multiple ligands, the Scatchard linearization can be used to determine the K_{FeL} and $[L_T]$ for up to two ligands (Rue and Bruland 1995). The Scatchard linearization is derived from combining the ligand mass balance equation (Eq. 2.7) and the FeL equilibrium equation (Eq. 2.8):

$$\frac{[FeL]}{[Fe^{3+}]} = K_{FeL/Fe3+}([L_T] - [FeL]) \qquad \text{(Eq. 2.21)}$$

If the Scatchard plot ([FeL] vs. [FeL]/[Fe^{3+}]) is linear only one ligand is present in the titrations detection window and the slope is equal to the negative of $K_{FeL/Fe3+}$ and the x-intercept is $[L_T]$. If two ligands are present, two linear relationships are observed in the Scatchard linearization, which slopes represent the negative of the conditional stability constants of the Fe(III) complex with the L1 and L2 ligands (Miller and Bruland 1997).

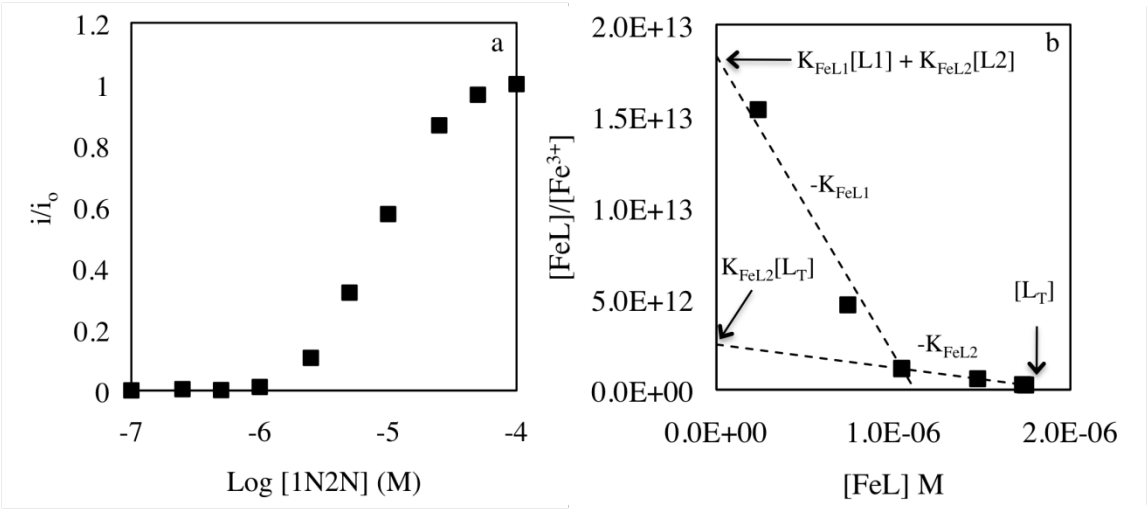

Figure 2.4 Reverse CLE-ACSV titration (a) and Scatchard linearization (b) of the supernatant of a microbial culture. The titration displays the typical S-shaped curve of the reverse CLE-ACSV titration when represented against the log of the competitive ligand concentration. The Scatchard linearization exhibits a two-ligand behavior, and two slopes can be fitted representing the L1 and L2 ligands.

The equations for the linearizations are additive such that the x-intercept of the weaker ligand, L_2 (i.e. smaller slope absolute value) is the sum of the two ligands, $[L_1]$ and $[L_2]$ or the total ligand concentration. In the single ligand case the y-intercept is $K_{FeL/Fe3+}$ x $[L_T]$. For the two ligand case, the total ligand titrated is the sum of the stronger ligand, L1, and a weaker ligand, L2:

$$[L_T] = [L_1] + [L_2] \qquad \text{(Eq. 2.22)}$$

and the y-intercept of the stronger ligand, L_1, is the sum of the y-intercepts of the two lines:

$$\text{y int}_{L1} = K_{FeL1}[L_1] + K_{FeL2}[L_2] \qquad \text{(Eq. 2.23)}$$

Combining the ligand mass balance equation Eq. 2.20 with Eq. 2.21 yields an equation for the strong ligand:

$$[L_1] = \frac{\text{y int}_{L1} - K_{FeL2}[L_T]}{K_{FeL1} - K_{FeL2}} \qquad \text{(Eq. 2.24)}$$

where K_{FeL1} and K_{FeL2} are determined from the negative slopes of the linear portions of each curve and are with respect to $[Fe^{3+}]$. The value of $[L_T]$ is the x-intercept of linear portion representing the weak ligand and $[L_2]$ is then determined by difference in the mass balance equation Eq. 2.22.

Reverse CLE-ACSV was used to determine the Fe(III) ligand concentration and the conditional stability constant in microbial cultures. Samples were taken daily and filtered through 0.2 μm, polyethersulfone syringe filters (Millipore). Total dissolved iron was determined by the ferrozine technique (Stokey 1970). Ten aliquots were diluted 100 fold with a buffer containing 10 mM piperazine-1,4-bis(2-ethanesulfonic acid (PIPES) in 0.2 M NaCl. Iron contaminations in the 0.1 M piperazine-1,4-bis(2-ethanesulfonic acid (PIPES) stock solutions were avoided by equilibrating 1 g of Chelex 100 with 500 mL of 0.1 M PIPES stock at pH 7 for 1 hour with periodic mixing. The pH of the PIPES-Chelex 100 mixture was raised with sodium hydroxide pellets until the desired pH was obtained, at which point the mixture was allowed to equilibrate for 30 minutes with periodic mixing. The pH was tested again and adjusted if necessary. Chelex 100 was removed from the PIPES stock solution through a trace metal cleaned fritted glass funnel. Buffered samples were titrated with increasing concentrations of the competitive ligand 1-nitroso-2-napthol (NN) from 0.1 μM to 100 mM from stock solutions of NN prepared in methanol then diluted by 50% with deionized water (>18.3 MΩ, Milli-Q). In samples containing only small concentrations of iron, 0.5 to 50 μM of $FeCl_3$ was added to the diluted samples prior to the competitive ligand additions. Samples were allowed to equilibrate in the dark for 4 hours prior to analysis by hanging mercury drop electrode (Metrohm VA-663) connected to a computer-controlled potentiostat (Autolab PG STAT 12). Voltammetric scan were performed using differential pulse after 3 min purge with nitrogen gas to remove oxygen. A 10 s deposition at -0.1 V was followed by a 3 s equilibration time. Scans were run from -0.2 V to -0.7 V with a step voltage was 7.5 mV and a modulation amplitude of 100 mV. The current height of the Fe(III)-NN complex

was measured at -0.48 V vs. Ag/AgCl. Data from voltammetric scans were integrated using VOLTINT, a semi-automated integration software implemented in Matlab (Bristow and Taillefert 2008).

2.4 Inductively Coupled Plasma Mass Spectrometry (ICP-MS)

2.4.1 ICP-MS standard addition analysis

Trace metal concentrations in total, filtered (0.2 μm), and ultrafiltered (10 kDa) samples from hydrothermal vent fluids were determined by ICP-MS (Agilent 7500) using a standard addition method. Samples were diluted 50 or 500 fold with 2% trace metal nitric acid (HNO_3) containing a 10 ppb multi-element internal standard (Sc, Y, In, Ho, Bi). Standard additions were prepared in two ranges, between 0.05 and 5 ppb for low concentration elements (Cr, Co, Ni, Cu, Zn, As, Cd, Ba, Pb, U) and between 10 and 5000 ppb for high concentration elements (Mn, Fe, Cu, Zn, As). Raw counts were corrected for instrument fluctuations with internal standards. Sample concentrations were determined from the negative of the x-intercept of the standard addition curve for each element. Blanks, calibration check standards, and Seawater Certified Reference Material for Trace Metals (NASS-5, National Research Council Canada, Ottawa, Canada) were analyzed for quality controls. The concentrations reported correspond to the average of three replicate sample analyses.

2.4.2 Magnesium end-member analysis

When sampling hydrothermal vents some seawater is inevitably entrained with the hydrothermal fluid either by mixing near the vent opening, entrainment of seawater

prior to exiting the vent, or as a result of seawater present in the dead space of the sample apparatus. As magnesium is removed from solution through seawater basalt interaction at temperatures greater than 150° C (Bischoff and Dickson 1975; Seyfried and Bischoff 1979), a magnesium end-member correction is applied to account for the percent of seawater mixed with the hydrothermal fluid. In this calculation, it is assumed that all magnesium is removed from the vent solution and any Mg measured in the sample is from seawater entrainment after the formation of the vent fluid (Von Damm 1990). The percentage of seawater entrainment is calculated from the mixing line of between the end-members Mg = 0 mmol kg-1 at 0% seawater and Mg = 53 mmol kg-1 at 100% seawater. From this mixing line, the percent of seawater entrained can be determined. For all other species measured, the pure vent fluid end-member concentrations can be calculated from the known seawater concentrations, the measured sample concentration, and the percent of seawater entrainment. These end-member concentrations are most accurate for high temperature vents with low seawater mixing (Von Damm 1990).

2.5 Ion Chromatography

2.5.1 Anions in Hydrothermal Vent Fluids

Chloride (Cl^-) and Sulfate (SO_4^{2-}) were determined by ion chromatography on a Dionex DX-300 Series IC with a Dionex IonPac AS14A column (4 x250 mm), AG14A guard column (4 x 50 mm), and AMMS 300 suppressor. Anions were eluted with a carbonate/bicarbonate buffer (8 mM Na_2CO_3 and 1 mM $NaHCO_3$) at 1 ml min^{-1}. Anions were detected by suppressed conductivity. Hydrothermal vent samples were diluted 50 fold prior to analysis.

2.5.2 Polysulfide species in Hydrothermal Vent Fluids

Sulfur oxy-anion concentrations in vent fluids were determined by ion chromatography (IC) with ultra violet (UV) detection based on the method of Weir et al. 1994. Separation was performed on a PRP-1 reverse phase column (150 x 4.6 mm) with 10 μm bead size (Hamilton). The eluent was made of 10 mM tetrabutylammonium bisulfate (TBA-HSO_4), 3 mM $NaClO_4$, 2 mM Na_2CO_3, 2 mM $NaHCO_3$, and 30 mM NaCl

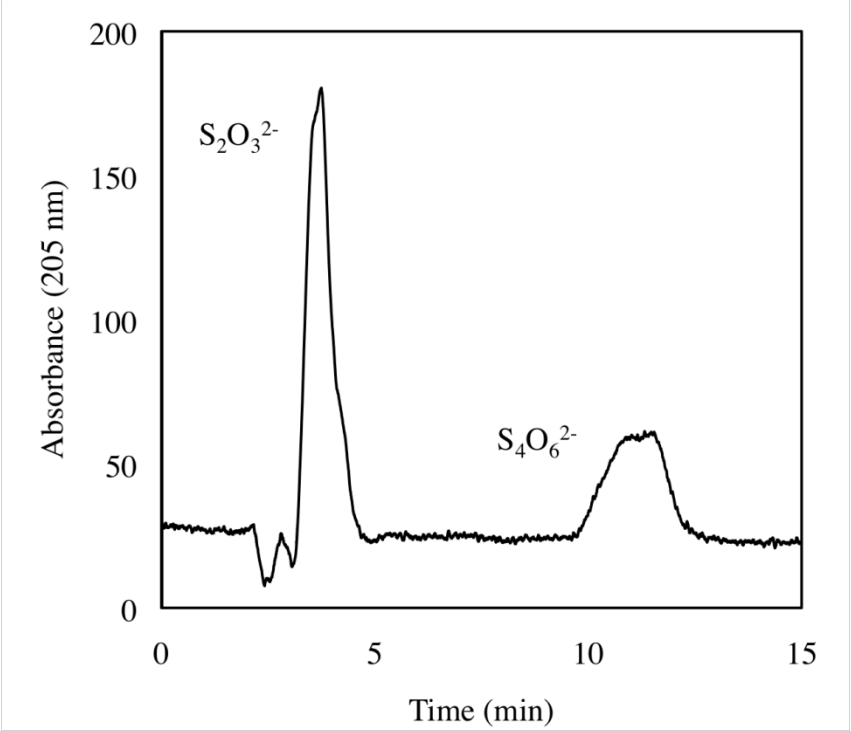

Figure 2.5 Chromatogram of polythionates in hydrothermal vent fluids. Vent sample was diluted 10 fold with eluent to minimize the system peak at 2.8 minutes. Thiosulfate, $S_2O_3^{2-}$ (0.56 mM), and tetrathionate, $S_4O_6^{2-}$ (0.027 mM), elute at 3.7 and 11.5 minutes respectively.

prepared in 25:75 acetonitrile-water. A flow rate of 0.5 ml min^{-1} was produced by a GP-50 IC pump (Dionex). Sulfur oxy-anions, thiosulfate and tetrathionate were detected by UV absorbance at 205 nm (Dionex) at 3.7 min and 11.5 min retention times respectively. Samples were degassed for 10 min with UHP nitrogen and diluted 10 times in the eluent

prior to injection to reduce background interference. A 20 µl injection loop was used with a Rheodyne 7125 injector. Unlike the work by Weir et al. 1994 no preconcentration was used for this method because of the higher thiosulfate and tetrathionate concentrations expected in hydrothermal vent fluids. Linear calibrations were established from 2 to 100 µM with standards prepared from sodium thiosulfate and sodium tetrathionate salts.

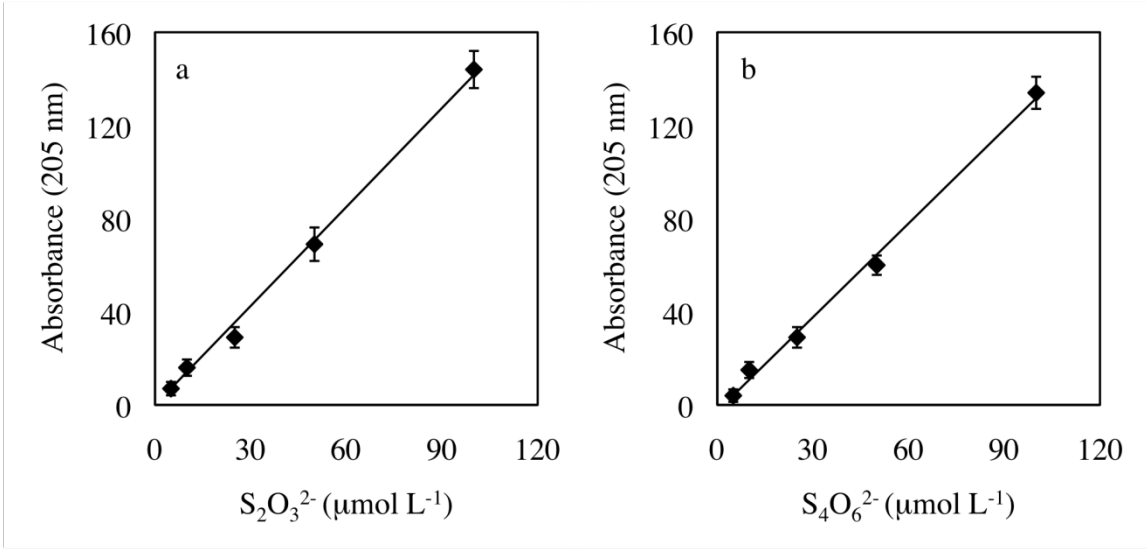

Figure 2.6 Calibration curves of sodium thiosulfate (a) and sodium tetrathionate (b).

CHAPTER 3

THE ROLE OF SULFUR IN THE FLUX OF IRON AT HYDROTHERMAL VENT FLUIDS FROM 9° NORTH, EAST PACIFIC RISE

3.1 Abstract

Hydrothermal vents produce high temperature reduced fluids rich in iron and sulfides and support a unique community of organisms including tubeworms, crabs, and mussels. These highly dynamic systems may provide a significant source of iron to high nutrient low chlorophyll zones of the surface ocean. The transport of metals from vents may be increased by the presence of organic ligands or the formation of colloidal iron-sulfide minerals. Here, we describe the chemistry of hydrothermal vent fluids from 9° North at the East Pacific Rise (EPR). Analysis of the size distribution of iron in most of the vents reveals that it is mainly found in the truly dissolved fraction (<10 kDa). At the highest temperature vent, however, 82% of the iron is under the form of colloids (10 kDa to 0.2 microns). In contrast to the large volume, high temperature, black smokers that produce 1.5 to 3 mM total Fe, the smaller, younger vent produces about 0.24 mM of total iron in its hydrothermal fluids. This vent also displays a large removal of chloride during fluid formation, which suggests subsurface phase separation with possible halite formation in the subsurface. The vents of 9^0 North produce large amounts of sulfur from the chemical reduction of sulfate through water-rock interactions. The sulfide emitted from these vents is oxidized through either biological or chemical pathways, and all vent fluids sampled contained thiosulfate as intermediate product of sulfide oxidation that

could be further used as electron acceptor for the oxidation of organic carbon. Half of the vent fluids also contained tetrathionate, a possible intermediate in the oxidation of sulfides to sulfate. Results of this study reveal that the hydrothermal vents of 9° North are part of a dynamic, evolving hydrothermal vent system that is a source of iron to the pelagic ocean and possibly beyond.

3.2 Introduction

Iron is a limiting nutrient in the surface ocean (Martin et al. 1990) due to its low solubility in oxic conditions (Millero 1998). The stimulation of primary production by relieving iron limitation in high nutrient low chlorophyll (HNLC) zones has been proposed to reduce atmospheric carbon dioxide (Breitbarth et al. 2010). The sources of iron to support primary production in the oceans have not been fully resolved (Tagliabue et al. 2009; Boyd et al. 2010) and have to be quantified to understand the biogeochemical cycling of iron in the surface oceans. Sources of iron to the surface ocean include eolian depositions (Fung et al. 2000), riverine inputs (Martin and Maybeck 1979), continental shelf and estuarine sediments (Elrod et al. 2004), icebergs (Raiswell et al. 2006; Raiswell et al. 2008), and hydrothermal vents (Tagliabue et al. 2010). Eolian iron inputs, by providing a flux of 1-10 x 10^9 mol Fe yr^{-1} (Fung et al. 2000), are considered one of the dominant sources of iron to the open ocean despite its low solubility in seawater (1-10%). Riverine inputs to the upper ocean are geographically limited and largely consist of particulate iron (Martin and Maybeck 1979; Poulton and Raiswell 2002), which is mostly lost to sedimentation prior to reaching the continental shelf. Conversely, rivers draining organic-rich peatlands provide an estimated 12 x 10^9 mol Fe yr^{-1} as dissolved organic-Fe(III) complexes to ocean margins (Krachler et al. 2010, Chapter 4 of this thesis).

Continental shelf sediments may also provide a source of dissolved iron to the surface waters in upwelling zones, and approximately 2.2 x 10^9 mol Fe yr^{-1}, extrapolated from benthic flux measurements of dissolved iron, is estimated to reach the photic zone (Elrod et al. 2004). Similarly, primary productivity in the Southern Ocean may be stimulated by iron from glacial sediments, and a flux of 1 x 10^8 mol Fe yr^{-1} is estimated to be delivered by the melting of icebergs (Raiswell et al. 2008). Finally, hydrothermal vents were initially disregarded as an important source of iron to the photic zone due to the rapid formation of particles upon oxidation in seawater; however, recent global models suggest that a net flux of 9 x 10^8 mol Fe yr^{-1} may enter the ocean from hydrothermal sources (Tagliabue et al. 2010). While the magnitude of the hydrothermal vent flux of iron is considerably lower than other sources, it is proposed that hydrothermal vents provide a more consistent source of iron on millennial time scales (Tagliabue et al. 2010). Organic ligands have been shown to stabilize iron fluxing from hydrothermal sources (Bennett et al. 2008; Toner et al. 2009) and recently proposed to account for 10% of the flux of iron in deep waters (Sander and Kochinsky, 2011). Additionally, pyrite nanoparticles have been shown to oxidize more slowly than aqueous Fe(II) and FeS and are thus expected to sink more slowly than larger particles facilitating the delivery of iron to greater distances (Yucel et al. 2011). Nanoparticulate pyrite is suspected to form within the vent prior to interaction with seawater by the reaction of FeS with sulfide (Yucel et al. 2011).

Hydrothermal vents support a unique biological community that is not driven by photosynthesis, making it of interest as an analog for the evolution of life of earth or other planets (Corliss et al. 1981; Russell and Hall 1997). Chemosynthetic microorganisms oxidize sulfide, methane, or hydrogen producing organic compounds

that are used by the host megafauna (Takai et al. 2005; Petersen et al. 2011). These symbionts are associated with both tubeworms (*Rifta* and *Tevnia*) and mussels (*Bathymodiolus*) of hydrothermal vent systems and are the primary source of organic carbon to these systems (Childress and Fisher 1992; Dubilier et al. 2008).

The oxidation of sulfide at hydrothermal vents can be chemical (Pyzik and Sommer 1981; Yao and Millero 1995) or biological (OBrien and Vetter 1990). The oxidation of sulfide by oxygen, while thermodynamically favorable, is kinetically slow below a pH of 9 (Yao and Millero 1995; Luther et al. 2011). As the kinetics of iron oxidation is much faster at circumneutral pH than that of reduced manganese (Millero et al. 1995; Sung and Morgan 1981), it is possible that reduced iron, through the formation of an oxidized metal intermediate, catalyzes the chemical oxidation of sulfide (Boudreau 1991). The most common product from the oxidation of sulfide by iron oxides is elemental sulfur (Afonso and Stumm 1992), though thiosulfate formation may occur by surface reaction between the unstable HS radical produced during the reduction of ferric ion by bisulfide (Pyzik and Sommer, 1981). The oxidation of pyrite may also produce oxidized sulfur species in hydrothermal vent fluids, including thiosulfate formed in the presence of molecular oxygen and dissolved Fe(III) (Luther 1987), though most laboratory investigations on the oxidation of pyrite dissolved Fe(III) report sulfate as the main product of oxidation at low pH (e.g., Mekibben and Barnes, 1986; Willamson and Rimstidt 1994) and a mixture of sulfate, thiosulfate, and sulfite at high pH (Bonnissel et al., 1998).

The 9° North vent system was first discovered in 1989 (Fornari and Embley 1995) and is a highly dynamic system on the fastest spreading ridge at 10 cm yr^{-1}. Lava flows

in 1991 (Von Damm 2000) and seismic activity in 2006 disrupted the vent communities and allowed for the observations on the reestablishment of these unique communities (Adams and Mullineaux 2008; Nees et al. 2008). The objectives of this study were to evaluate the composition of hydrothermal vent fluids at 9° North on the EPR two years after the 2006 eruption to determine the role of this hydrothermal system as a source of iron to the ocean. The distribution of metals among the particulate, colloidal, and truly dissolved fractions was quantified as they exit the vents, and their role in the oxidation of sulfide to thiosulfate in this highly unique ecosystem was evaluated.

3.3 Materials and Methods

The study site consists of five hydrothermal vents at 9° North along the East Pacific Rise (Fig. 3.1). Samples were collected during DSV *Alvin* dives (dive #4403, 4405, 4407) from the R/V *Atlantis* between June 8th and June 12th of 2008 (Table 3.1). Each vent supported a community of tubeworms, mussels, and crabs. One vent, Bio-9, was sampled more than twice. Water samples were collected in titanium "majors" bottles operated by the pilot of the DSV *Alvin*. Temperatures were measured with the *Alvin* high temperature probe, which were calibrated shipboard. Additionally, ΣH_2S was measured by voltammetry at or near the site of water sampling using gold amalgam microelectrodes and an ISEA III (Analytical Instrument Systems, Inc.) on board the *Alvin*. Shipboard measurements of pH, major anions, polythionates, and dissolved iron were performed within four hours of sample retrieval. All samples were prepared in acid washed Nalgene™ low-density polyethylene bottles. Fifty milliliters of unfiltered vent fluid was collected directly from the "majors" bottles and stored in 0.3 M trace metal grade nitric

acid (Fisher) for total metals analysis by inductive coupled plasma mass spectrometry (ICP-MS). Acid washed vacuum filter bottles (500 mL, Nalgene™) were directly filled with vent waters using an acid washed Tygon™ tubing connected to the "majors" bottles to minimize atmospheric contact. Sample waters were filtered through 0.22 μm mixed cellulose filters (Millipore), stored in duplicate acid washed Nalgene™ low-density polyethylene bottles, until analysis. A 50 ml aliquot was acidified to a final concentration of 0.3 M with trace metal grade nitric acid for ICP-MS analyses. Another filtered aliquot was ultrafiltered to 10 kDa using centrifugal ultrafilters (Vivaspin 20, Sartorius Biolab Products) for 5 mins at 3000 revolutions per minute, then acidified to a final concentration of 0.3 M with trace metal grade nitric acid for ICP-MS analysis. Chloride (Cl^-) and Sulfate (SO_4^{2-}) concentrations were quantified in the 0.2 μm filtered samples diluted 50 folds by ion chromatography on a Dionex DX-300 Series IC with a Dionex IonPac AS14A column (4 x250 mm), AG14A guard column (4 x 50 mm), and AMMS 300 suppressor. Anions were eluted with a carbonate/bicarbonate buffer (8 mM Na_2CO_3 and 1 mM $NaHCO_3$) at 1 ml min^{-1} and detected by suppressed conductivity (Michalski 2006).

Table 3.1 - Location of Vents and Characteristics of the Hydrothermal Fluids Collected

Vent	Latitude	Longitude	Depth	Date	Dive	Temp	Description
	°N	°W	m			°C	
Bio-9 A	9°50.30'	104°17.47'	2504	June 8, 2008	4403	340	Black smoker, high flow
P Vent	9°50.27'	104°17.47'	2506	June 8, 2008	4403	373	Black smoker, high flow
Tica	9°50.40'	104°17.49'	2507	June 8, 2008	4403	276	New small vent
Bio-9 B	9°50.26'	104°17.48'	2504	June 10, 2008	4405	360	Black smoker, high flow
Bio Vent	9°50.96'	104°17.61'	2502	June 12, 2008	4407	350	Black smoker, high flow
MKR 35	9°49.72'	104°17.37'	2504	June 12, 2008	4407	10	Diffuse flow, *Rifta* colony

Shipboard measurements of pH, major anions, polythionates, and dissolved iron were performed within four hours of sample retrieval. All samples were prepared in acid washed Nalgene™ low-density polyethylene bottles. Fifty milliliter of unfiltered vent fluid was collected directly from the "majors" bottles and stored in 0.3 M trace metal grade nitric acid (Fisher) for total metals analysis by inductive coupled plasma mass spectrometry (ICP-MS). Acid washed vacuum filter bottles (500 mL, Nalgene™) were directly filled with vent waters using an acid washed Tygon™ tubing connected to the "majors" bottles to minimize atmospheric contact. Sample waters were filtered through 0.22 μm mixed cellulose filters (Millipore), stored in duplicate acid washed Nalgene™ low-density polyethylene bottles, until analysis. A 50 ml aliquot was acidified to a final concentration of 0.3 M with trace metal grade nitric acid for ICP-MS analyses. Another filtered aliquot was ultrafiltered to 10 kDa using centrifugal ultrafilters (Vivaspin 20, Sartorius Biolab Products) for 5 mins at 3000 revolutions per minute, then acidified to a final concentration of 0.3 M with trace metal grade nitric acid for ICP-MS analysis. Chloride (Cl^-) and Sulfate (SO_4^{2-}) concentrations were quantified in the 0.2 mm filtered

samples diluted 50 folds by ion chromatography on a Dionex DX-300 Series IC with a Dionex IonPac AS14A column (4 x250 mm), AG14A guard column (4 x 50 mm), and AMMS 300 suppressor. Anions were eluted with a carbonate/bicarbonate buffer (8 mM Na_2CO_3 and 1 mM $NaHCO_3$) at 1 ml min^{-1} and detected by suppressed conductivity (Michalski 2006).

Total dissolved sulfides ($\Sigma H_2S = H_2S + HS^- + S^{(0)} + S_x^{2-}$) and aqueous iron sulfide complexes ($FeS_{(aq)}$) in vent samples were determined by voltammetric analyses with gold-mercury amalgam (Au/Hg) microelectrodes (Brendel and Luther 1995). Au/Hg microelectrodes were made of a gold wire plated at -0.1 V in a mercury solution to form a thin mercury film. A three-electrode cell system consisting of a Au/Hg amalgam working electrode, a Ag/AgCl reference electrode, and a platinum counter electrode was used for all voltammetric analyses. Voltammetric techniques used included cyclic voltammetry and cathodic and anodic square wave voltammetry with a scan rate of 200 mV/s, a preconcentration step of 10 sec at -0.1 V, and a pulse amplitude of 50 mV for the square wave technique. A conditioning step at -0.9V for 10 s was included when the cyclic and cathodic square wave voltammetric techniques were used to clean the electrodes between measurements. Electrodes were calibrated with a solution of known sulfide concentration.

Sulfur oxy-anion concentrations in vent fluids were determined in 10 or 100 fold diluted samples by ion chromatography (IC) with ultra violet (UV) detection based on the method of Weir et al. 1994. Separation was performed on a PRP-1 reverse phase column (150 x 4.6 mm) with 10 mm bead size (Hamilton). The eluent was made of 10 mM tetrabutylammonium bisulfate (TBA-HSO_4), 3 mM $NaClO_4$, 2 mM Na_2CO_3, 2 mM

$NaHCO_3$, and 30 mM NaCl prepared in 25:75 acetonitrile-water. A flow rate of 0.5 ml min^{-1} was produced by a GP-50 IC pump (Dionex). Sulfur oxy-anions, thiosulfate and tetrathionate were detected by UV absorbance at 205 nm (Dionex) at 3.7 min and 11.5 min retention times respectively. Samples were degassed for 10 min with UHP nitrogen and diluted 10 times in the eluent prior to injection to reduce background interference. A 20 ml injection loop was used with a Rheodyne 7125 injector. Unlike the work by Weir et al. 1994, no preconcentration was used for this method as the expected concentrations from these samples is much higher than normal seawater. Linear calibrations were established from 2 to 100 μM with standards prepared from sodium thiosulfate and sodium tetrathionate salts. Detection limits in vent samples for thiosulfate (0.67 mM) and tetrathionate (0.02 mM) were calculated as three times the standard deviation of the lowest standard.

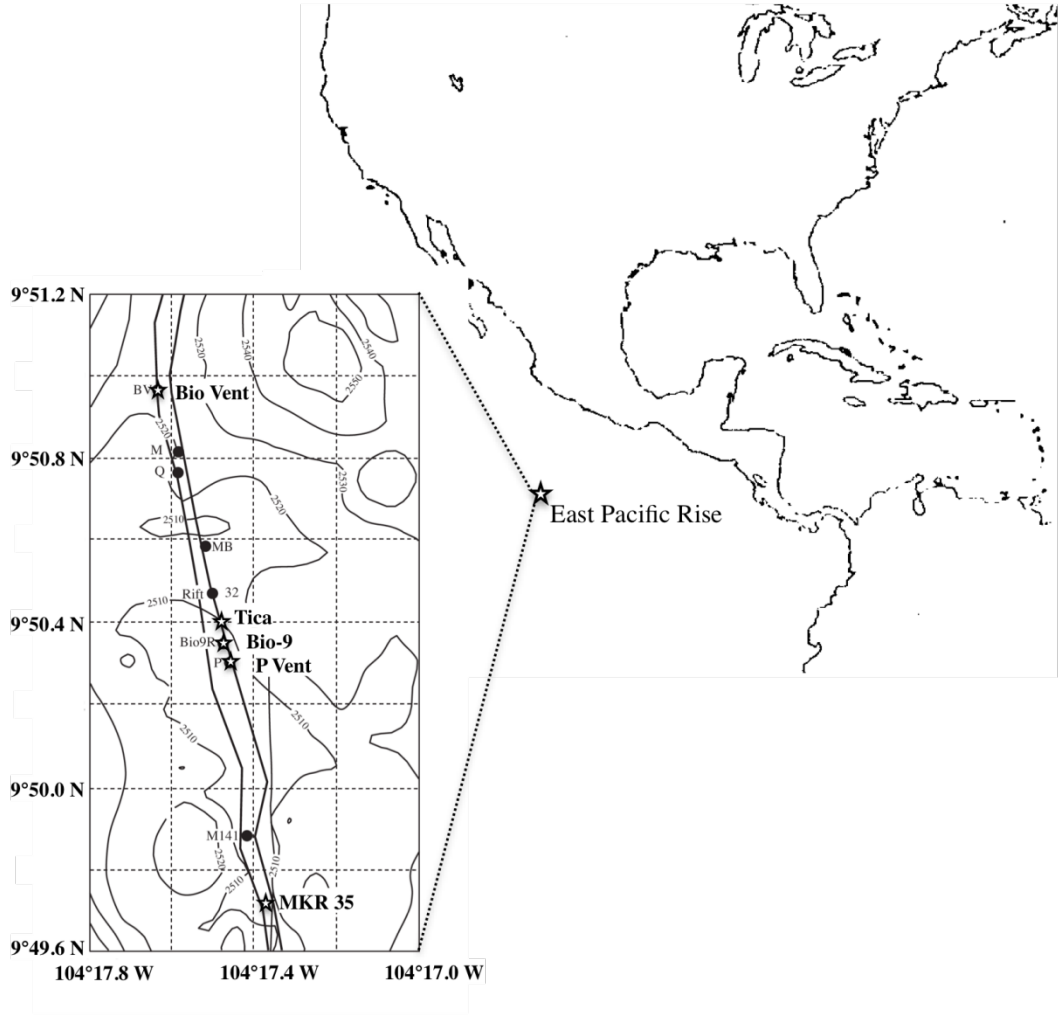

Figure 3.1 – Map of the 9° North study site at the East Pacific Rise. The five locations sampled include (from north to south) Bio Vent, Tica, Bio-9, Pvent, and MKR 35. Each of the vents is positioned along the spreading axis of the EPR (map reproduced and modified from Lein et al. 2006).

Total dissolved iron, including soluble species and colloids smaller than 0.2 μm, was determined by the ferrozine method after reduction by hydroxylamine (Stookey 1970). Detection limits for total iron by this method were 0.24 ± 0.03 μmol L^{-1}.

Trace metal concentrations in unfiltered, filtered (0.2 μm), and ultrafiltered (10 kDa) samples from hydrothermal vent fluids were determined at the Georgia Institute of Technology by ICP-MS (Agilent 7500) using a standard addition method. Samples were

diluted 50 or 500 fold with 2% trace metal nitric acid (HNO_3) containing 10 ppb multi-element internal standard (Sc, Y, In, Ho, Bi). Elemental standard additions were prepared in two ranges for low concentration elements (Cr, Co, Ni, Cu, Zn, As, Cd, Ba, Pb, U) and high concentration elements (Mg, Mn, Fe, Cu, Zn, As). Low concentration elements were calibrated with five standard additions from 0.05 to 5 ppb. High concentration elements were calibrated with five standard additions from 10 to 5000 ppb. Raw counts were corrected for instrument fluctuations with internal standards (Mg, Cr, Mn, and Fe were corrected with Sc), (Co, Ni, Cu, Zn, and As were corrected with Y), (Cd was corrected with In), and (Ba, Pb, and U were correct with Ho). Sample concentrations were determined from the negative of the x-intercept of the standard addition curve for each element. The fraction of metals < 10 kDa was assumed to consist of truly dissolved metals only, while the fraction filtered through 0.2 μm filters was assumed to include both the colloidal and truly dissolved metal fractions. Finally, the particulate metal fraction was determined from difference between the metal concentration measured in unfiltered and 0.2 μm-filtered samples. The concentration of all trace elements shown represents the average of three replicate analyses.

3.4 Results

The hydrothermal vents sampled ranged from high temperature (373 $^{\circ}$C) black smokers to low temperature (10 $^{\circ}$C) diffuse flow vents (Table 3.2) and were located at a depth of approximately 2500 m along the axis of the EPR spreading ridge (Fig. 3.1, Table 3.1).

Table 3.2 - Chemical Analysis of Vent Samples from Bio-9, P-vent, Tica, Bio-vent, and MKR 35. All measurements were made shipboard within 4 hours after collecting the samples.

	% Sea water	Temp °C	pH	Cl^- mmol L^{-1}	SO_4^{2-} mmol L^{-1}	Fe^{2+} mmol L^{-1}	ΣH_2S mmol L^{-1}	$S_2O_3^{2-}$ mmol L^{-1}	$S_4O_6^{2-}$ mmol L^{-1}	Cl/SO4
Bio-9 A	97.1	340	5.50	519	20.80	135	n.d.	6.6	0.48	25
P-vent	6.6	373	3.25	396	< 2.5	2523	n.d.	7.3	<0.02	309
Tica	5.3	276	3.80	180	< 2.5	195	n.d.	5.6	0.27	201
Bio-9 B	36.1	360	2.30	407	6.80	1200	6	2.2	0.02	60
Bio-Vent	5.1	350	2.97	372	<2.5	2112	3	5.7	0.09	149
MKR 35	97.0	10	6.46	531	21.28	<0.5	0.10	5.9	0.02	25

n.d. = not determined

The percentage of seawater in the vent samples was calculated from the magnesium concentration measured in the samples and the mixing line between pure vent fluids, assuming vent fluids are free of magnesium, and seawater which contains 53 mmol L^{-1} of magnesium (Fig. 3.2A). The contribution of seawater entrained in the vent samples varied from a low percentage at Bio-vent, P-vent, and Tica to predominantly seawater at Bio-9 A and MKR 35. The vent samples with minimal (< 40%) seawater content also displayed low pH (< 3.8) typical of hydrothermal vents in this area (Von Damm 2000) while vent samples with larger seawater content (Bio-9 A and MKR 35) displayed higher pH values (Table 3.2).

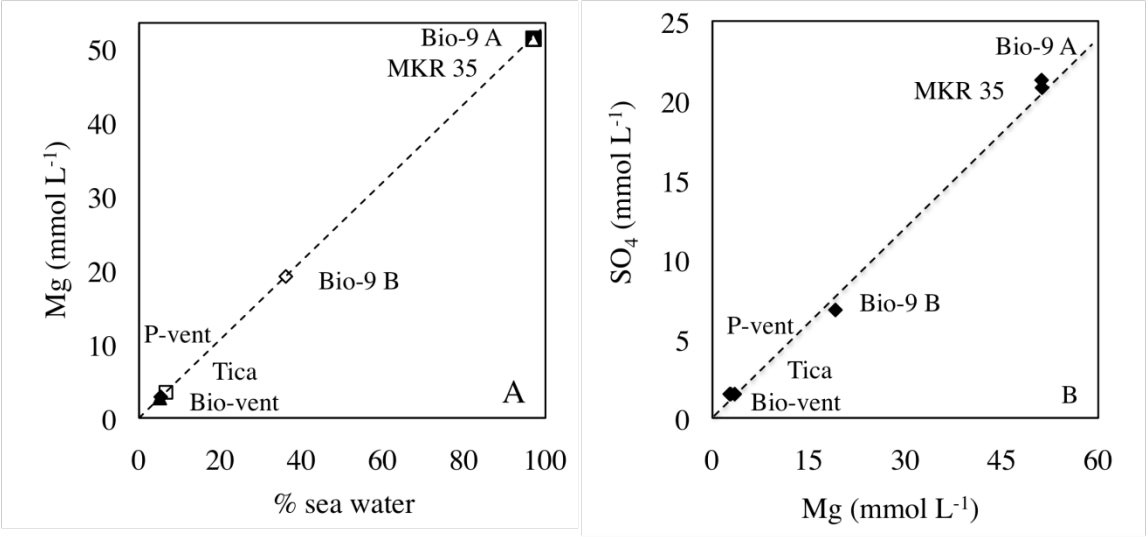

Figure 3.2 – (A) The percent seawater content in the vent samples calculated from the magnesium concentration in the samples. (B) The sulfate concentrations of the vent fluids

correlate strongly ($R^2 = 0.997$) to the magnesium concentrations, consistent with complete reduction of sulfate during the creation of the vent fluid.

Sulfate concentrations in the high purity vent samples (P-vent, Tica, Bio-vent) were predictably low for highly reduced hydrothermal vent fluids, whereas sulfate concentrations at the other vents correlated with the magnesium concentrations and were thus consistent with the percentage of seawater entrained with these samples (Fig. 3.2B). Indeed, shipboard measurements of ΣH_2S species by gold amalgam microelectrodes voltammetry revealed that the highest sulfide concentrations were found at Bio-9 B, with 6 mmol L^{-1}, compared to 3 and 0.1 mM at Bio-vent and MKR 35 (Table 3.2). Interestingly, Bio-9 B produced the lowest polythionate concentrations with only 2.2 +/- 0.4 mmol L^{-1} and tetrathionate concentration of 0.02 +/- 0.01 mmol L^{-1}. Thiosulfate concentrations in all vent samples were 10 to 100 times higher than tetrathionate concentrations. The highest thiosulfate concentration was measured in the P-vent samples (7.3 +/- 0.3 mmol L^{-1}) while tetrathionate was below the detection limit (0.02 mM) of the IC technique. The highest tetrathionate concentrations (0.48 mM) and second highest thiosulfate concentrations were observed at Bio-9 A. Bio-9 B, a relatively pure sample, produced 2.2 mM of thiosulfate and 0.02 mM tetrathionate. The vent samples from Tica, Bio-vent, and MKR 35 produced similar thiosulfate concentrations, between 5.6 to 5.9 mM, while the concentration of tetrathionate in the Tica vent sample (0.2 mM) was three times greater than that at Bio-vent (0.09 mM) and nearly 14 times greater than that at Bio-9 B (0.02 mM).

The distribution of metals between the particulate (>0.2 μm), the colloidal (0.2 μm to 10kDa), and the truly dissolved (<10kDa) fractions was determined in each vent

fluid (Fig. 3.3, Fig. 3.4, and Fig. 3.5). Iron was the most abundant metal in each of the samples and found primarily in the truly dissolved fraction with the notable exceptions of P-vent, MKR 35, and Bio-9 A. Iron in the MKR 35 and Bio-9 A samples was predominantly detected in the particulate fraction while it was mainly found in the colloidal fraction at P-vent. Manganese was the second most abundant metal in most of the vents samples and primarily under the form of truly dissolved manganese. Zinc and copper were found almost completely in the particulate fraction. Barium and chromium were typically the next most abundant metals and were predominantly found in the dissolved fraction. Cobalt, lead, and cadmium displayed low concentrations and were found in the particulate fraction in the majority of samples. Finally, nickel, arsenic, and uranium were all found in low concentrations and primarily in the truly dissolved fractions of the vent fluids of 9^0 North.

3.5 Discussion

Hydrothermal vents, such as those of 9° North at the EPR promote and support the formation of unique biological communities by creating extreme chemical and thermal gradients. In addition hydrothermal vents may provide a source of iron to the photic zone to support photosynthesis in areas of iron limitation (Tagliabue et al. 2009). For hydrothermal vents to be a viable source of iron to the surface ocean, iron must be maintained in a stable form that minimizes losses to precipitation. In this study the chemistry of the vent fluids and the speciation of trace metals between the particulate, colloidal, and truly dissolved fractions were investigated to determine the potential mechanisms involved in the preservation of metals in the dissolved phase.

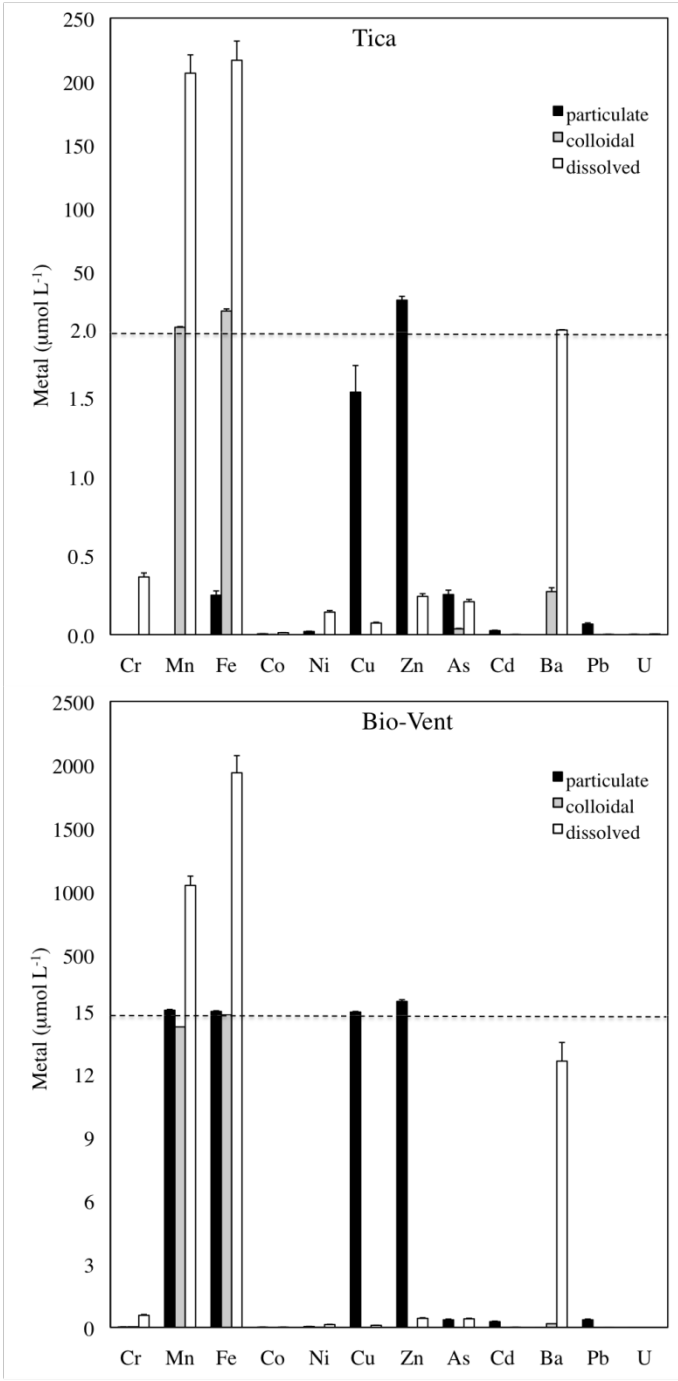

Figure 3.3 – Metal distribution between the particulate (> 0.2 μm), colloidal (10 kDa-0.2 μm), and truly dissolved (<10 kDa) fractions determined in hydrothermal vent fluids from Tica and Bio-vent vents at 9^0 North. Note the break in the scale of the y-axis as highlighted by the dashed line.

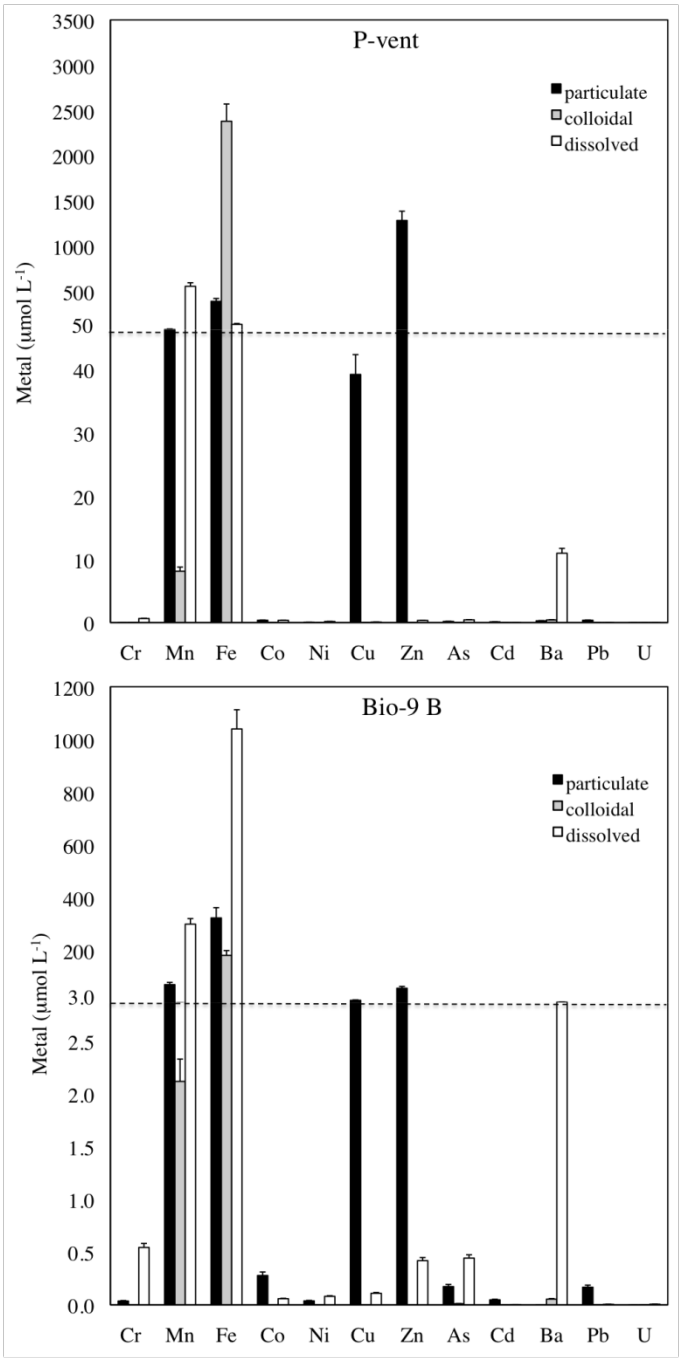

Figure 3.4 – Metal distribution between the particulate (> 0.2 μm), colloidal (10 kDa-0.2 μm), and truly dissolved (<10 kDa) fractions determined in hydrothermal vent fluids from P-vent and Bio-9 B vents at 9^0 North. Note the break in the scale of the y-axis as highlighted by the dashed line.

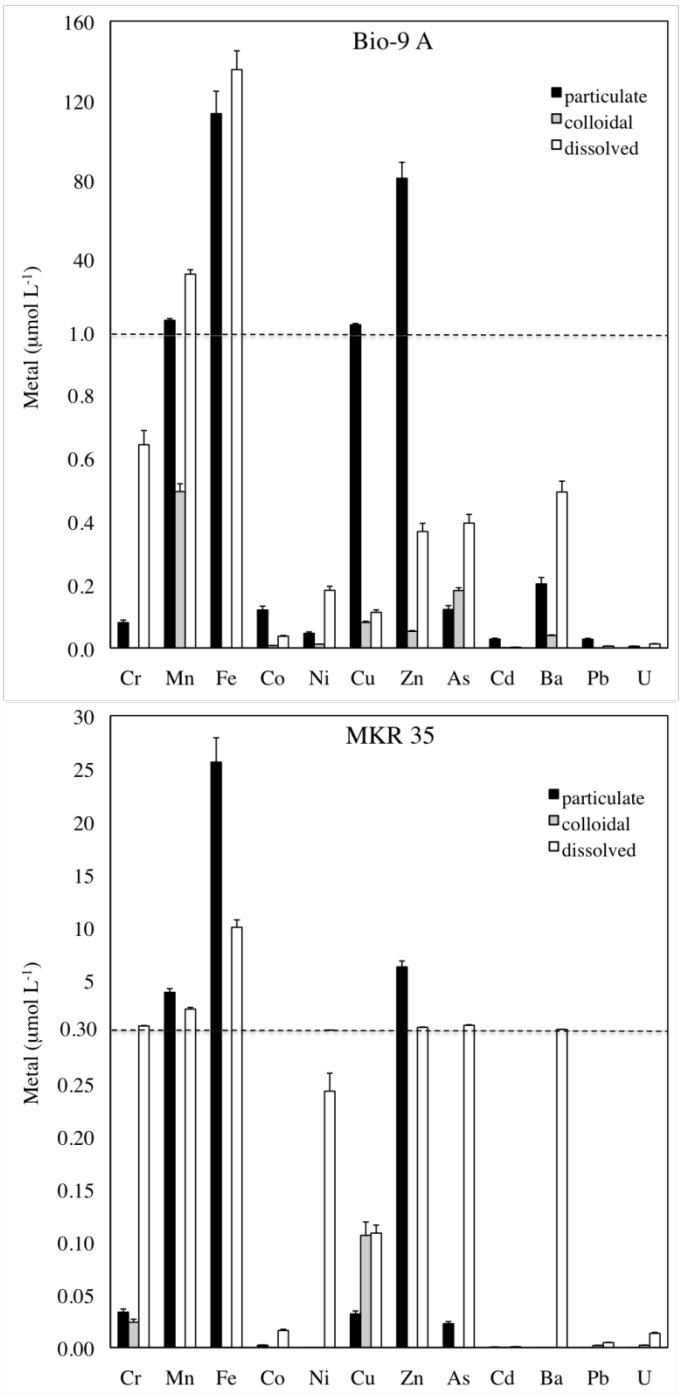

Figure 3.5 – Metal distribution between the particulate (> 0.2 μm), colloidal (10 kDa-0.2 μm), and truly dissolved (<10 kDa) fractions determined in hydrothermal vent fluids from Bio-9 A and MKR 35 vents at 9^0 North. Note the break in the scale of the y-axis as highlighted by the dashed line.

The chloride concentrations of Bio-9 A and MKR 35 reflected the high seawater content entrained in these samples (as determined from the Mg content) with concentrations above 519 mmol L^{-1} (Table 3.2). Conversely, samples containing less than 40% seawater entrainment displayed evidence of removal of chloride from seawater during the formation of the vent fluids (Fig. 3.6A). The Tica vent shows the lowest end member chloride concentrations, 180 mM, or just 33% of the ambient seawater chloride concentration. Previous studies of the 9° North hydrothermal vent field found depleted Cl^- end member concentrations in vent north of 9°45' N and enriched Cl^- concentrations south of 9°45' N (Van Damm 2000). All of the vents sampled in this study were located north of 9°45' N and are consistent with the removal of Cl^- through phase separation and formation of halite below the surface. During phase separation, vent fluids are mainly composed of vapors containing low Cl^- concentrations while brines or halite form in the subsurface. As vents age, however, the brine reincorporates the vent fluids, thus creating Cl^- concentrations in excess of seawater values (Van Dover 2000). The chloride data thus suggest vents of different age that should be reflected in the trace metal composition of their fluids.

Table 3.3 - Pure Vent Fluid Concentraion of Trace Metals at P-vent, Tica, Bio-9, and Bio-vent Estimated from the Mixing of Seawater with vent fluid. The Percent of Seawater Entrained in each Sample and the Average Trace Metal Composition of Seawater are Provided for Comparison.

	% Sea water	Cr	Mn	Fe	Co	Ni	Cu	Zn	As	Cd	Ba	Pb	U
		µmol L^{-1}	µmol L^{-1}	µmol L^{-1}	µmol L^{-1}	µmol L^{-1}	µmol L^{-1}	µmol L^{-1}	µmol L^{-1}	µmol L^{-1}	µmol L^{-1}	µmol L^{-1}	µmol L^{-1}
P-vent	6.6	0.70	688	3111	0.79	0.24	42.0	1374.4	0.68	0.121	12.45	0.40	0.001
Tica	5.3	0.37	224	249	0.02	0.16	1.7	29.2	0.52	0.027	4.12	0.07	0.005
Bio-9 B	36.1	0.86	585	2420	0.49	0.12	18.9	90.8	0.96	0.078	7.39	0.27	0.002
Bio-Vent	5.1	0.65	1186	2125	0.03	0.19	51.9	140.4	0.80	0.301	13.30	0.38	0.002
Sea water	100.0	0.004	0.007	0.061	0.007	0.112	0.014	0.076	0.035	0.001	0.153	0.000	0.014

The pure vent fluid concentrations of each trace metal was determined from the end member of the mixing line between the concentration of trace metal measured as a

function of the percent seawater in the sample and the average seawater concentration of each metal (Fig. 3.5B). Only vent samples with < 40% seawater mixing (Bio-9 B, P-vent, Tica, and Bio-vent) were considered in this calculation (Table 3.3). Vent samples with > 90% seawater were not considered for end-member analysis due to the large error associated with the calculation of the vent fluid composition. The three mature black smokers displayed the highest iron content, including concentrations greater than 3 mmol L^{-1} at P-vent, and were approximately 10 times more concentrated than the younger Tica vent (Table 3.3). These Fe concentrations are similar to Fe concentrations observed in high temperature vents during previous studies (Von Damm 2000; Demina et al. 2007) and suggest the vents of 9° North represent a significant source of iron to the pelagic ocean. Shipboard measurements of ferrous iron provided similar results to the end member values (Table 3.2) indicating the majority of dissolved iron emanating from the vent is in the reduced form. The concentration of other trace metals was generally lower in the Tica vent than the mature black smokers with the exception of nickel and uranium, both of which displayed relatively high concentrations in seawater compared to hydrothermal vent fluids. Overall, iron was the most abundant metal in each of the end member vent fluids followed by manganese, zinc, copper, and barium. Together these metals composed greater than 99.7 % of the metals analyzed in pure vent fluids.

The distribution of iron between particulate, colloidal, and truly dissolved fractions may provide insights into the formation of particles and the potential of the iron species to travel greater distance and supply this limiting nutrient for primary production. Not surprisingly, 45% and 86% of iron in the Bio-9 A and MKR 35 samples, which

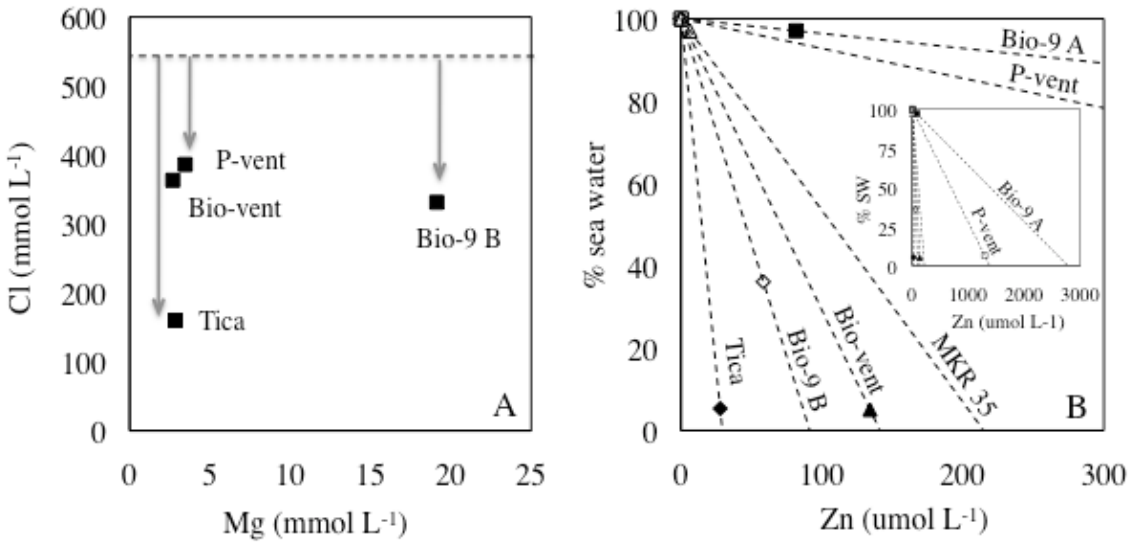

Figure 3.6 – (A) End member concentrations of Cl^-, corrected for the presence of seawater Cl^- suggest subsurface removal of Cl^- through phase separation. The phase separation is most pronounced at the younger Tica vent. (B) End member calculations for Zn based on the percent seawater entrained in the vent sample and the average concentration of Zn in seawater. Endmember vent fluid concentrations are obtained from the x-intercept for each vent. Vents with lower seawater content (Bio-9 B, P-vent, Tica, and Bio-vent) provide end member values of higher precision.

contained a high percentage of oxygenated seawater, was under the form of particles, suggesting that oxidation by dissolved oxygen and formation of large particles prevented iron to be transported away from the vents (Yucel et al. 2011). In contrast, iron in the Tica, Bio-9 B, and Bio-vent samples was mainly found in the truly dissolved fraction (< 10kDa). These samples contained little seawater such that oxidation did likely not affect the speciation of iron. These findings suggest that iron fluxing out of these vents should precipitate relatively rapidly when exposed to seawater. In contrast, the P-vent sample contained 86% colloidal iron (0.2 micron-10 kDa) and less than 1.5% iron in the truly dissolved fraction. These findings are consistent with the observed production of pyrite nanoparticles at high temperature and pressure by Yucel et al. 2011 and suggest iron from P-vent is able to travel at greater distances from the vent field than the other black smoker

vents (Bio-vent and Bio-9) (Yucel et al. 2011). The temperature, pH, and Cl^-, content of P-vent were similar to Bio-vent, while P-vent in general displayed higher concentrations of metals than the other vents sampled and produced the highest concentrations of thiosulfate.

Thiosulfate may form through the biological or chemical oxidation of reduced sulfur (Luther et al. 2001; Takai et al. 2005). The oxidation of sulfide by microorganisms is unlikely in samples that consist predominantly of pure vent fluid from high temperature vents, suggesting the oxidation of these fluids is chemical. Thiosulfate can form from the oxidation of sulfide (Millero 1998) or pyrite (Luther 1987), and oxidants for these reactions may include dissolved oxygen or Fe(III) . The oxidation of dissolved sulfides by Fe(III) is likely not significant in the vent fluids of 9^0 North due to the fact that little dissolved Fe(III) was observed in any of the hydrothermal vent fluids and the low pH (< 3.8 in Table 3.2) should limit iron oxidation (Yao and Millero, 1996) . Thiosulfate may also be produced by the oxidation of polysulfide formed during sulfide oxidation, but thiosulfate is the preferred product at high pH (pH.8.5) only (Gartman et al. 2011). As alternative to the oxidation of dissolved sulfides, the oxidation of pyrite may represent a source of oxidized sulfur species. Pyrite nanoparticles form in the vent fluid prior to exposure to seawater and may represent 10% of total dissolved iron in the vents at 9^0 North (Yucel et al. 2011). The oxidation of pyrite by oxygen is likely not the main mechanism of production of intermediate oxidized sulfur species (i.e. thiosulfate and tetrathionate) in these fluids, as the production of thiosulfate from pyrite oxidation by dissolved oxygen is more favorable at high pH (Howarth and Teal 1979; Pyzik and Sommer 1981; Bonnissel-Gissiner et al. 1998) while tetrathionate production, which

proceeds through adjacent surface complexes of thiosulfate and oxygen on the surface sites of pyrite to facilitate electron transfer, is favored at pH < 7.5 (Xu and Schoonen 1995). Indeed, tetrathionate was only detected in two samples (Bio-9 A and Tica), both of which displayed low Fe concentrations, but not in the sample displaying the highest thiosulfate concentration (P-Vent). In turn, several lines of evidence suggest that thiosulfate is likely produced as a result of the oxidation of pyrite by low concentrations of dissolved Fe(III) in the absence of significant concentrations of dissolved oxygen. First, the oxidation of pyrite by dissolved Fe(III) is faster than the oxidation by dissolved oxygen because the positive σ-orbital overlap between pyrite and Fe(III) helps adsorption of Fe(III) to the reduced mineral, while oxygen does not have σ orbitals available for binding (Luther 1987). Additionally, the product of the oxidation of pyrite with Fe(III) gains bond energy as the electron is transferred from the π* antibonding orbital of pyrite disulfur to a bonding orbital of the Fe(III), and the t2g of the iron is simultaneously stabilized. If dissolved Fe(III) is assumed to be the primary oxidant of pyrite (i.e. in the absence of dissolved oxygen) and the oxidation stops with the production of thiosulfate, due to the limited concentrations of Fe(III) available without dissolved oxygen, the time required to produce the millimolar thiosulfate concentration detected in the vent samples can be estimated. Under vent like conditions of high Fe(II), 2 mM, low Fe(III), 0.01 mM, and a pH of 3 (Table 3.2), the rate of pyrite oxidation is calculated to fall between 23 μmol L^{-1} min^{-1} and 215 μmol L^{-1} min^{-1} depending on the rate law used (McKibben and Barnes 1986, Williamson and Rimstidt 1994). Based on these rates, it would take 9.3 to 87.7 minutes to produce 2 mM of thiosulfate from the oxidation of pyrite by even small concentrations of dissolved Fe(III). Nanoparticulate pyrite resists oxidation at low

temperature and has been proposed to represent a source of dissolved iron at distance from the hydrothermal vents (Yucel et al. 2011). Simultaneously, rate laws for pyrite oxidation in the presence of small concentrations of dissolved Fe(III) suggest pyrite may be partially oxidized rapidly in the anoxic vent fluids. Indeed, vent fluids of P-vent contained the highest concentrations of colloidal Fe and thiosulfate. These findings suggest the formation of thiosulfate in the high temperature, low pH vent fluids is most likely due to the oxidation of nanoparticlate pyrite by small concentrations of dissolved Fe(III).

The Tica vent sample produced relatively low total metal concentrations than the other vents with similar seawater entrainment (Table. 3.3). The Tica vent was much smaller and younger than the black smokers (Bio-9, P-vent, Bio-vent), and its temperature was nearly 100 $^{\circ}$C less than the hottest vent (P-Vent). Simultaneously, chloride concentrations were the lowest measured (i.e., one third of seawater concentration), suggesting subsurface boiling produced vent fluids depleted in Cl^- and brines trapped in the oceanic crust (Von Damm, 1990). This behavior is consistent with recent magmatic eruptions or shallow intrusions (Von Damm 2000) and suggests that Tica is a younger vent than the nearby Bio-9 and P-vents. Tica fluids also displayed unusually elevated U concentrations compared to the other vents, as U, in the same manner as magnesium, is typically removed from vent fluids (Van Damm 2000). In general the chalcophilic trace metals Cu, Zn, Cd, and Pb are found primarily in the solid phase associated with Fe and Mn (Faure 1998). The lithophilic trace metals Ba, Cr, and U are more often found in the truly dissolved phase. Cobalt and nickel often form sulfide minerals but are considered siderophiles. In the vents of 9° North, Co is primarily found

with the particulate Fe phase and Ni in the dissolved fraction along with the chalcophile As. Interestingly, the Tica vent plume has previously been shown to contain particulate organic carbon capable of stabilizing Fe(II) within hydrothermal vent plume particles (Toner et al. 2009), however, very little colloidal and no particulate iron was observed in these vent fluids. If organic carbon is present, it may be able to maintain Fe in the truly dissolved and colloidal fractions minimizing the production of larger particles as Tica contained the lowest particulate fraction as a percent of the total.

The correlation between chloride and metal end-members can be used to further understand the chemical processes that affect the composition of hydrothermal vent fluids (Von Damm 2000). Unfortunately, only four samples were of high enough purity to perform the end-member analysis (Tica, P-vent, Bio-vent, Bio-9 B). Fe, Pb, Mn, and Cu concentrations correlate the best with Cl^- concentrations, whereas Ni, As, and Zn correlate poorly with Cl^- (Fig. 3.7). Mn^{2+}, Cu^{2+}, Zn^{2+}, and Pb^{2+} display high rates of water loss than Fe^{2+} and should be stabilized in vent fluids under the form of chloro complexes which compete with sulfide for the binding of these metals (Morse and Luther, 1999). Zinc, however, forms strong sulfide precipitates that may prevent formation of chloro complexes in the vent fluids. Similarly, Ni^{2+} displays much lower rates of water loss and is likely not significantly complexed by chloride, while As is an oxyanion that does not form stable chloro complexes. Most of the other metals, including Ba, Cd, Co, and Cr display a general increase with Cl^- concentration but do not correlate strongly. These metals either are characterized by intermediate (Co^{2+}, Ba^{2+}) or high (Cd^{2+}) rates of water loss or have to be reduced to form stable chloro complexes (Cr^{3+}). Finally, a notable exception was found in the negative correlation between Cl^- and U.

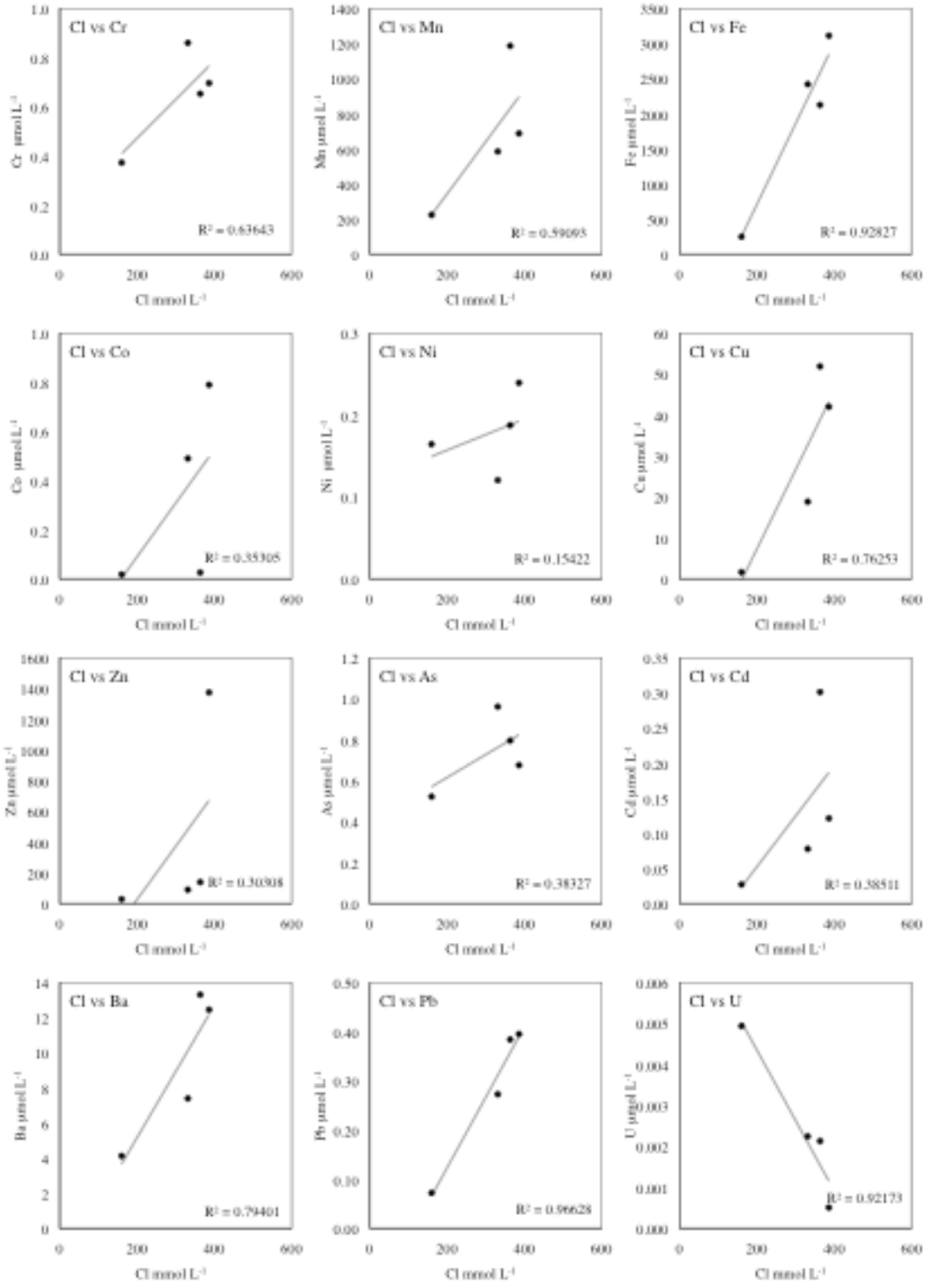

Figure 3.7 – Endmember ratios of Cl^- and trace metals from P-vent, Bio-9B, Bio-vent, and the Tica hydrothermal vent from 9^0 North.

Uranium is the only metal, other than Mg, that is present in higher concentration in seawater than in vent fluids (Table 3.3). Uranium is not soluble in the reduced form, such that highly reduced hydrothermal fluids with low chloride should contain low concentrations of dissolved uranium. It is possible, however, that uranium is remobilized by oxidation as the hot fluids carrying reduced uranium particles exits the vent. This hypothesis has to be verified in future studies.

The sources of iron to the oceans are not fully resolved and hydrothermal vents have been suggested to respresent a stable long-term iron source (Tagliabue et al. 2010). The vents of 9° North are actively producing iron rich fluids and provide a source of iron to the pelagic zone. The high colloidal nature of iron at P-vent suggests small buoyant iron sulfide particles may provide a source of iron beyond the pelagic zone. Based on their depleted end member Cl^- content, all vents sampled in this study are in the young, hot develping stage and the creation of brines or halite is expected though subsurface phase separation. Thiosulfate, an intermediate product of sulfur oxidation, is measured in all of the vent samples collected and suggests the oxidation of pyrite by small concentrations of dissolved Fe(III) may regulate the formation of pyrite in these vents. Together these results provide a snapshot of the vent chemistry at 9° North and show the importance of hydrothermal vents in deep ocean environments.

3.6 Acknowledgements

We would like to thank the Captain and crew of the R/V *Atlantis* and the crew of the DSV *Alvin*. We would like to thank Dr. George W. Luther for providing the opportunity to study the hydrothermal vents of 9^0 North. Funding for this research came from the IDEA of Biocomplexity Program of the NSF.

CHAPTER 4

THE FLUX OF SOLUBLE ORGANIC-IRON(III) COMPLEXES FROM SEDIMENTS REPRESENTS A SOURCE OF STABLE IRON(III) TO ESTUARINE WATERS AND TO THE CONTINENTAL SHELF

This is a reprint of an article whose final and definitive form has been published in Limnology and Oceanography, authored by Jones, M. E.; Beckler, J. S.; and Taillefert, M. entitled The flux of soluble organic-iron(III) complexes from sediments represent a source of stable iron(III) to estuarine waters and to the continental shelf.

4.1 Abstract

Iron speciation in the Satilla River Estuary was investigated using competitive ligand equilibration – adsorptive cathodic stripping voltammetry (CLE-ACSV) with the ligand 1-nitroso-2-naphthol (1N2N). The black water Satilla River contains high concentrations of dissolved organic matter and iron, suggesting it could provide a source of dissolved iron to the continental shelf. Total dissolved iron in the water column decreases along the estuary, likely due to flocculation and precipitation processes associated with the increase in salinity. Simultaneously, the percentage of dissolved organic-Fe(III) complexes measured by CLE-ACSV in overlying waters of sediment

cores increases with salinity. The speciation of dissolved iron in the porewaters indicates that these complexes originate in the underlying sediments. Diffusive fluxes calculated from depth profiles in the sediments indicate that only 8% of the sedimentary flux of Fe(III) is delivered to the continental shelf during low riverine discharge. During normal flow conditions, however, the sediment flux of Fe(III) represents 63% of the total riverine flux of Fe(III). These findings suggest the flux of dissolved iron to the continental shelf is controlled by the sedimentation of iron in the estuary and the remobilization of soluble organic-Fe(III) complexes produced either during iron reduction deep in the sediment or oxidation of Fe(II) close to the sediment-water interface. The Satilla River Estuary provides 5 to 8 times higher concentrations of dissolved Fe(III) than the average major world rivers, suggesting that it is, along with other small blackwater rivers, currently underrepresented in world average river flux calculations.

4.2 Introduction

The importance of iron for primary productivity in the open ocean is well documented and iron fertilization experiments have shown that iron additions can enhance primary productivity in High Nutrient Low Chlorophyll (HNLC) zones (Breitbarth et al. 2010). Iron is considered a limiting nutrient in marine waters as the low solubility of Fe(III) limits the concentration of dissolved iron (< 0.4 μm) available for biological uptake in oxic waters (Millero 1998). Organic ligands, including fulvic and humic acids, siderophores, and extracellular polymeric substances (EPS), and cell lysis products increase its solubility in seawater by 3 to 17 fold (Hunter and Boyd 2007) and play an important role in the bioavailability of iron in the oceans. Initially, the biological

uptake of iron was presumed to be proportional to the inorganic free iron concentration, however, over the last decade it appeared obvious that the solubility of iron alone does not fully explain iron bioavailability (Breitbarth et al. 2010). Two current models of biological iron uptake include either the direct uptake of organically bound Fe(III) (Salmon et al. 2006) or uptake of Fe(II) after reduction of organically bound Fe(III) either biotically or abiotically to release the organic ligand or weaken the organic Fe(III) complex (Shaked et al. 2005).

Primary sources of iron to the upper ocean have been debated since the recognition of iron as a limiting nutrient (Martin et al. 1990). By providing a flux of 1-10 x 10^9 mol Fe yr^{-1}, wind driven, atmospheric inputs of land-derived particulate iron is still considered the dominant source of iron to the open ocean despite its limited solubility in seawater (1-10%) (Fung et al. 2000). The heterogeneous distribution of eolian iron inputs, however, leaves large areas of the Arctic, Antarctic, and Southern Pacific Oceans without atmospheric iron source such that alternative sources of iron are required to explain the biological activity observed in these areas (Moore et al. 2002). Primary productivity in the Southern Ocean may be stimulated by iron delivered from icebergs and through the upwelling of deep waters enriched with iron from hydrothermal vents (Raiswell et al. 2008; Tagliabue et al. 2010). Continental shelf sediments may provide a source of particulate iron (Bruland et al. 1991) to the ocean, and the lateral advection of particulate iron mobilized from continental shelf sediments has been proposed to provide iron to the HNLC zones of the North Pacific Ocean (Lam et al. 2008). In addition, dissolved iron diffusing out of margin sediments can be transported to the surface waters in upwelling zones (Elrod et al. 2004). Although the exact composition of dissolved iron

is often not measured, a small fraction (< 20 nmol L^{-1}) may be stabilized by organic ligands (Bruland et al. 2001; Buck et al. 2007) while a significant fraction may be found under the form of colloids (Bruland et al. 1991) or nanoparticles (Raiswell et al. 2006). Overall, benthic fluxes of 2.2 x 10^9 mol Fe yr^{-1} to the photic zone (Elrod et al. 2004) have been extrapolated from these measurements of dissolved iron, corresponding to a sediment flux of 36 - 89 x 10^9 mol Fe yr^{-1} globally (Raiswell et al. 2006). Finally, riverine inputs to the upper ocean are geographically limited and highly variable between river systems depending on discharge, the type of soil eroded, and the organic matter content. Particulate iron, which makes up the majority of the total iron flux from rivers (Martin and Maybeck 1979; Poulton and Raiswell 2002) is mostly lost to sedimentation prior to reaching the continental shelf, though large particulate loads to continental shelves are observed during times of high river discharge (Buck et al. 2007). Similarly, the majority of dissolved riverine iron is lost to sediments through flocculation and precipitation reactions during estuarine mixing (Boyle et al. 1977). Dissolved iron, however, may be stabilized by organic ligands, including riverine dissolved organic matter (DOM) (Perdue et al. 1976; Gerringa et al. 2007) or DOM from sediments (Burdige et al. 1992), and it has been shown that 2% to 20% of dissolved riverine iron may be exported to the continental shelf depending on the riverine DOM content (Perdue et al. 1976; Boyle et al. 1977). Overall, the flux of dissolved iron (< 0.45 μm) from riverine sources has been estimated at 1.5 – 26 x 10^9 mol Fe yr^{-1} based on the average concentration of dissolved iron (40 nmol Fe L^{-1}) in the major world rivers (Martin and Meybeck 1979; Poulton and Raiswell 2002). Conversely, rivers draining organic-rich peatlands provide an estimated 12 x 10^9 mol Fe yr^{-1} as dissolved organic-Fe(III)

complexes to ocean margins (Krachler et al. 2010). These findings suggest that small rivers containing high DOM are capable of delivering considerable organic-Fe(III) complexes to the surface ocean and may be underrepresented in world riverine flux calculations. In addition, estuarine sediments may not only represent a sink of riverine iron, they may also provide a source of iron complexes to the surface waters, though direct evidence of this flux and its magnitude is still lacking.

The Satilla River Estuary in South Georgia, is fed by a high DOM, high dissolved iron, and low pH blackwater river. Precipitation and flocculation of dissolved iron from the estuarine mixing of riverine and seawater result in the generation of organic and iron rich estuarine sediments (Beck et al. 1974), and it has been suggested that estuarine mixing effectively removes all the iron from the Satilla River Estuary (Windom et al. 1971). Recently, however, organic-Fe(III) complexes have been detected ubiquitously in sediments along this estuary using voltammetric microelectrodes (Meiggs and Taillefert, in press), suggesting that these complexes could diffuse across the sediment-water interface. Unfortunately, direct quantification of these complexes by voltammetric microelectrodes is impossible without knowing the composition of the organic ligands (Taillefert et al. 2000). Alternately, competitive ligand equilibration – adsorptive cathodic stripping voltammetry (CLE-ACSV) could be adapted to measure the flux of dissolved organic-Fe(III) complexes across the sediment-water interface. In this technique, natural samples are first equilibrated with a known organic ligand that competes with the natural organic complexes and then titrated with increasing concentrations of Fe(III) to determine the concentration and conditional stability constant of the natural organic-Fe(III) complexes from speciation calculations (Rue and Bruland

1995; Wu and Luther 1995). CLE-ACSV is able to differentiate soluble iron species and small colloids that are able to diffuse to the electrode surface from non-labile dissolved and colloidal species that do not interact with the known complexing ligand or from colloids that are too large to diffuse to the electrode (Wu and Luther 1995; Gerringa et al. 2008). This technique is typically used to determine the speciation of Fe(III) in seawater at extremely low iron concentrations (< 1 nmol L^{-1}). Recently, however, CLE techniques have been applied to estuarine waters containing higher iron concentrations (20 – 500 nmol L^{-1}), thus providing new information about the speciation of Fe(III) in the transition from fresh to seawater (Buck et al. 2007; Gerringa et al. 2007).

The objectives of this study were to quantify the fraction of soluble iron preserved in the water column during estuarine mixing, characterize the speciation of dissolved Fe(III) in the overlying waters and sediment porewaters, quantify the diffusive flux of oxidized iron species from the sediments of the Satilla River Estuary, and determine the importance of these estuarine sediments as a supply of dissolved iron to the continental shelf.

4.3 Methods

4.3.1 Site description

The Satilla River Estuary, located in the coastal plain of Georgia in the southeastern United States (Fig. 4.1), typically displays an average discharge of less than 75 m^3 s^{-1} and drains an area of 9140 km^2 (Blanton et al. 2003). The Satilla River drainage basin is characterized by poorly drained soils and swamps with abundant vegetative matter (Beck et al. 1974). Fine grain sediment sources include retention of riverine material and the recycling of salt-marsh and tidal flat sediments within three zones

separated by large sand shoals (Blanton et al. 2003). Sediment loads range between 10 and 5000 mg L^{-1}, and sedimentation rates up to 0.43 cm yr^{-1} were estimated from the ^{137}Cs sediment record in the upper Satilla River sediments (Alber et al. 2003). The high porosity (0.9) and unconsolidation of these sediments suggest rapid deposition at the interface between fresh and salt waters. The Satilla River Estuary sediments have been shown to provide large but variable fluxes of ammonium, phosphate, and silicate to the overlying water attributed to a combination of diffusive and advective forcing (Jahnke et al. 2003). High dissolved organic carbon (DOC) (19.1 ± 8.1 mg C L^{-1}), low pH (5.7), and high dissolved iron (6.6 μmol L^{-1}) and Mn (0.76 μmol L^{-1}) typify the freshwater inputs (Windom et al. 1971; Beck et al. 1974). Iron concentrations decrease by 2 to 3 times

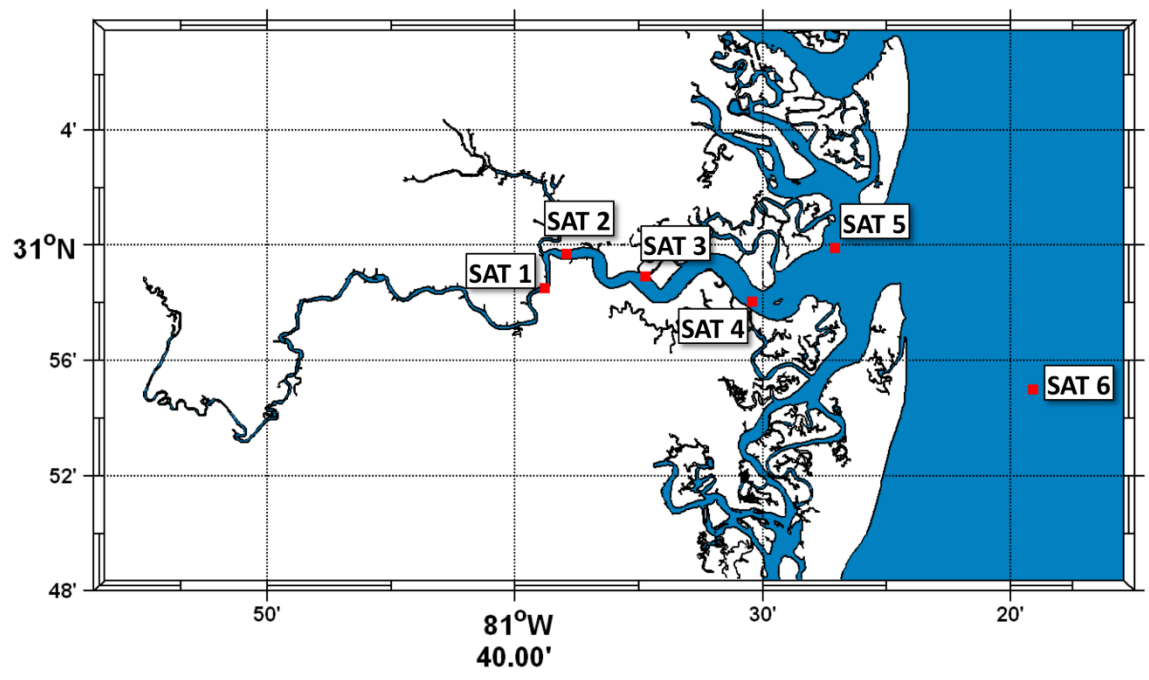

Figure 4.1 – Map of the Satilla River Estuary study site in Georgia (U.S.A). Samples were collected between July 2007 and January 2008 during cruises aboard the R/V *Savannah*. Sample locations are marked (SAT 1-5) and cover a broad salinity range (0-33 g kg^{-1}).

along the river, consistent with loss due to flocculation and precipitation during estuarine mixing (Windom et al. 1971). In this study, five locations were selected for sediment sampling along the length of the estuary from near the mouth to 28 km upstream (Table 4.1). Salinities in this area historically span between 0 and 33 with deposits ranging from fine-grained muddy sediments to mixtures of sand and mud in morphology. River discharge for the sampling periods were obtained from the United State Geological Survey Atkins station gauge No. 02228000 (http://lpdaac.usgs.gov).

Table 4.1 - Characterization of the Satilla River Estuary sediments (Alber et al., 2003)

Station	Distance up river (km)	Salinity range (1994-1999) (g kg^{-1})	Dominant sediment type	Accumulation rate (cm yr^{-1})
SAT 1	28	0-13	fine grained	na
SAT 2	25	0-15	fine grained	0.46
SAT 3	19	0-20	sandy mud	na
SAT 4	10	10-30	sandy mud	na
SAT 5	5	22-33	fine grained	0.3

na = not availible

4.3.2 Sample collection

All samples were collected aboard the R/V *Savannah* during four cruises along the Satilla River Estuary (Fig. 4.1) between July 2007 and January 2008, at the end of a prolonged period of drought (Meiggs and Taillefert, in press). Surface (1 m below surface) and bottom (1 m above sediment) water samples were collected twice (November 2007 and January 2008) along the salinity gradient of the lower 30 km of the Satilla River Estuary. Acid washed vacuum filter bottles (500 mL, Nalgene™) were directly filled with river water using an acid washed Tygon™ tubing and a peristaltic pump (flow rate: 50 mL min^{-1}). Sample waters were filtered through 0.22 μm mixed

cellulose filters (Millipore), stored in duplicate acid washed Nalgene™ low-density polyethylene bottles, and frozen until analysis. Total dissolved iron, including soluble species and colloids smaller than 0.2 μm, was determined by the ferrozine method after reduction by hydroxylamine (Stookey 1970). Detection limits for total iron by this method were 0.24 ± 0.03 μmol L^{-1}. Simultaneously, temperature and salinity were recorded from shipboard measurements at the time of collection.

Sediment cores were collected in 70 mm inner diameter polycarbonate core barrels with overlying water using a single corer. Temperature of the overlying water was measured with a digital thermocouple thermometer (Thermolyne) while salinity was measured with a refractometer (Fisher Scientific). Depth profiles of dissolved oxygen, manganese, iron, and sulfide were obtained with a millimeter resolution to a depth of 12 cm using Au-Hg voltammetric microelectrodes (Brendel and Luther 1995; Tercier-Waeber and Taillefert 2008) coupled to a DLK-60 potentiostat and automated micromanipulator (Analytical Instrument Systems, Inc.). Sediment cores were sectioned under nitrogen atmosphere in a glove bag (Sigma-Aldrich) to minimize oxidation. Sections of approximately 1 cm were centrifuged in 50 mL tubes for 5 mins at 3000 revolutions per minute under nitrogen atmosphere. Porewaters were then decanted and filtered through 0.2 μm, polyethersulfone syringe filters (Millipore), and total dissolved iron and Fe(II) were measured by the ferrozine method with and without hydroxylamine (0.2 mol L^{-1}) at pH 1 (Stookey 1970) to determine dissolved Fe(III) by difference. Simultaneously, soluble organic-Fe(III) complexes were qualitatively detected in filtered porewaters by cathodic square wave voltammetry using gold amalgam (Au-Hg) voltammetric microelectrodes (Brendel and Luther 1995; Tercier-Waeber and Taillefert

2008). Overlying water samples for competitive ligand equilibration were analyzed on board the R/V *Savannah* within one hour after collection. Porewater samples for competitive ligand equilibration were frozen until analysis within one month at the Georgia Institute of Technology.

A competitive ligand equilibration adsorptive cathodic stripping voltammetry (CLE-ACSV) technique modified from previous methods designed for low iron (nmol L^{-1}) open ocean samples (Rue and Bruland 1995; Wu and Luther 1995) was used to determine the speciation of dissolved Fe(III) in filtered estuarine and porewater samples with concentrations of Fe(III) ranging between 0.5 μmol L^{-1} and 1 mmol L^{-1}. Any Fe(II) in riverine and sediment porewater samples was allowed to oxidize during dilution (10-500 times) with a 10 mmol L^{-1} Piperazine-1,4-bis(2-ethanesulfonic acid (PIPES) buffer in 0.25 mol L^{-1} NaCl containing the competitive ligand 1-nitroso-2-napthol (1N2N) in 50% methanol at a final concentration of 30 μmol L^{-1}. Each dilution was selected such that the competitive ligand was in excess of total dissolved iron. After a 2-hour equilibration, samples were divided into 10 aliquots, each receiving a ferric chloride spike ranging between 0 and 2 μmol L^{-1}. Samples were allowed to equilibrate for 8 hours prior to analysis by hanging mercury drop electrode (Metrohm VA-663) connected to a DLK-60 potentiostat (Analytical Instruments Systems). Cathodic square-wave voltammetry was used for all CLE measurements with 30 second (porewaters) or 240 second (overlying waters) deposition times at -0.1 volts with stirring followed by a 5 second equilibration time. A 150 mV s^{-1} scan rate and 35 mV pulse height was used during square-wave scans. The current height of the Fe(III)-1N2N complex was measured at -0.48 V vs. Ag-AgCl. Data from voltammetric scans were integrated using VOLTINT, a semi-

automated integration software implemented in Matlab (Bristow and Taillefert 2008). A conditional binding constant of 1.42×10^{15} for the competitive ligand 1N2N was determined by calibration with ethylenediaminetetraacetic acid (EDTA) in the buffer system (10 mmol L^{-1} PIPES, 0.25 mol L^{-1} NaCl) used in all measurements (Rue and Bruland 1995).

The concentration of the natural ferric complex, [FeL], in each sample was calculated from the titration curve of the Fe-1N2N complex measured electrochemically and the mass balance on ferric iron species in solution expressed by the following equation:

$$[Fe_T] = [FeL] + [Fe'] + [Fe_{1N2N}] \qquad \text{(Eq 4.1)}$$

where $[Fe_T]$ is the concentration of total dissolved Fe(III), [FeL] is the concentration of the natural organic-Fe(III) complex exchangeable with the competitive ligand 1N2N, [Fe´] is the concentration of inorganic and 'free' hydrated Fe(III), and $[Fe_{1N2N}]$ is the concentration of the Fe(III)-1N2N complex measured electrochemically. The point where the linear extrapolation of the titration curve intersects the x axis yields the point of zero current from the Fe(III)-1N2N complex, thus the point where $[Fe_{1N2N}]$ is zero in the mass balance equation (Eq. 4.1). If iron bound to organic complexes far exceeds free or inorganically bound iron ([FeL] >> [Fe´]), then the [Fe´] term is negligible in the mass balance equation (Eq. 4.1) and $[Fe_T]$ = [FeL] at the x-intercept. In this technique, colloidal iron that does not diffuse to the electrode or does not react with the 1N2N and dissolved iron bound to organic ligands that are not exchanged by the 1N2N ligand are not included in the [FeL] fraction. As excess ligand is present in the sample, any Fe(II)

oxidized during the equilibration is likely complexed by either the natural or the competitive organic ligand and should remain soluble. Thus, the concentration of organic-Fe(III) complexes in the initial sample can be calculated by subtracting the concentration of Fe(II) from the CLE-determined organic-Fe(III) concentration. Raw titration data were also transformed using Ruzic linearization methods (Ruzic 1982) to calculate the conditional stability constant of the natural organic-Fe(III) complex and total natural ligand concentration whenever possible using the equation:

$$\frac{[Fe']}{[FeL]} = \frac{[Fe']}{[L_T]} + \frac{1}{[L_T] \times K_{FeL}} \qquad \text{(Eq. 4.2)}$$

where $[L_T]$ is the total natural ligand concentration and K_{FeL} is the conditional stability constant of the FeL complex. The total ligand concentration is determined from the slope of the linearized titration data, and the conditional stability constant is determined from the y-intercept. Additional Fe(III) from the oxidation of Fe(II) should not affect the calculation of total ligand concentration or conditional stability constant as they are both independent of the concentration of iron in the samples.

Diffusive flux of dissolved Fe(III) from sediment cores was calculated using Fick's first law according to:

$$\text{FLUX} = -\phi_{sed} D_{orgFe} \left(\frac{\partial C_{Fe(III)}}{\partial z} \right)_{0\text{-}4\,cm} \qquad \text{(Eq. 4.3)}$$

where FLUX is the diffusive flux (μmol m^{-2} d^{-1}) across the first 4 cm of sediment, ϕ_{sed} is the sediment porosity, D_{orgFe} is the molecular diffusion coefficient (cm m^{-2} d^{-1}), $C_{Fe(III)}$ is

the concentration of dissolved Fe(III), and z is depth in the sediment. A sediment porosity of 0.7 obtained from previous studies (Jahnke et al. 2003) was used to reflect the sediment consolidation throughout the estuary. The temperature dependent molecular diffusion coefficients for organic-Fe(III) complexes were calculated from the equation:

$$D_{orgFe} = (3.125 \times 10^{-12} \times T) - 8.45 \times 10^{-11} \qquad \text{(Eq. 4.4)}$$

where T is the temperature of the core overlying water (°C). The diffusion equation was derived from experimental results of the temperature dependent diffusion of 1 kDa humic acids (Cornel et al., 1986).

4.4 Results

4.4.1 Total iron vs. salinity

Total dissolved iron was measured during a transect along the Satilla River Estuary in low discharge (4.25 $m^3 s^{-1}$) and normal flow (60 $m^3 s^{-1}$) conditions. Similar total dissolved iron concentrations were observed in surface and bottom water at salinities greater than 15 g kg^{-1} in both low and normal flow conditions (Fig. 4.2). At stations with

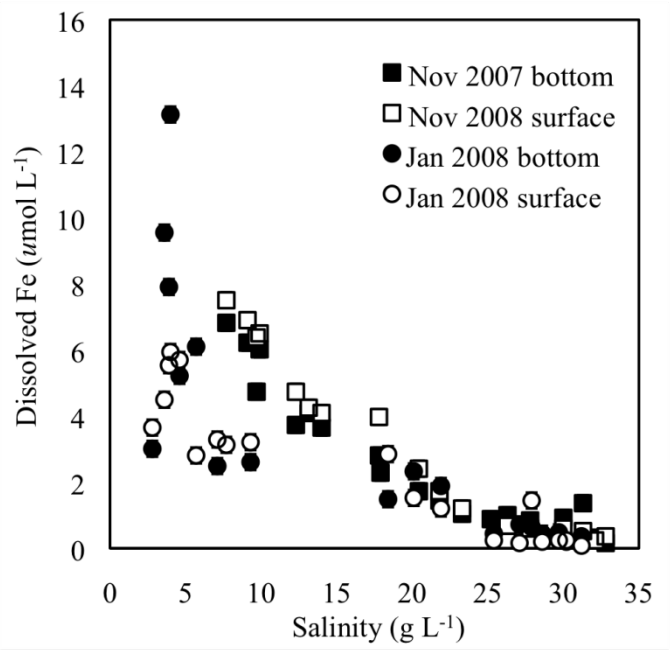

Figure 4.2 – Total dissolved iron as a function of salinity in surface waters, 1 m below surface (closed symbols), and in bottom waters, 1 m above sediment (open symbols). Data were collected during drought, November 2007, (squares) and normal, January 2008, (circles) river conditions. Loss of dissolved iron is consistent with estuarine mixing. Both conservative (dilution) and non-conservative (flocculation and precipitation) are observed. Error bars represent the standard deviation of triplicate measurements.

salinities less than 15 g kg^{-1}, however, little agreement was found between sampling dates: dissolved iron concentrations reached 13 μmol L^{-1} in the freshwater end of the estuary (S=3 g kg^{-1}) during the normal flow conditions, while they reached only 7 μmol L^{-1} at the freshwater end (S=8 g kg^{-1}) in low flow conditions. Dissolved iron was rapidly lost with increasing salinity and reached a minimum of 0.34 ± 0.11 μmol L^{-1} during low discharge and 0.19 ± 0.08 μmol L^{-1} during normal flow conditions at the mouth of the estuary. Overall, 98% of dissolved iron was lost between the lowest (S = 3 g kg^{-1}) and highest (S = 33 g kg^{-1}) salinity stations. No visible differences in concentration were observed between the surface and bottom samples at most stations with the notable

exception of four low salinity stations during normal flow conditions. At these stations the concentration of iron in the bottom waters exceeded the surface waters by 2 μmol L^{-1} to 7 μmol L^{-1}.

4.4.2 Iron speciation in overlying waters

The speciation of iron in the overlying waters obtained from sediment cores was investigated during normal river flow conditions in January 2008. Total dissolved Fe(III) in the overlying waters did not follow the same trend observed in the bulk river water (Table 4.2). Total dissolved Fe(III) was highest at Satilla 4 (SAT 4), the most saline

Table 4.2 - Iron speciation by CLE-ACSV titration of sediment overlying waters (January 2008)

Site	Salinity (g kg^{-1})	Total dissolved Fe ($u$mol L^{-1})	[FeL] ($u$mol L^{-1})	% Fe as [FeL]
SAT 1	7	7.0 ± 0.4	3.6 ± 0.8	52 ± 22
SAT 2	10	3.9 ± 0.2	2.6 ± 0.7	66 ± 27
SAT 3	15	5.5 ± 0.3	5.1 ± 1.0	94 ± 20
SAT 4	20	8.4 ± 0.4	8.7 ± 2.8	104 ± 32

station (8.4 ± 0.4 μmol L^{-1}, S=20 g kg^{-1}) while it was lowest at Satilla 2 (SAT 2), a moderately saline station (3.9 ± 0.2 μmol L^{-1}, S=10 g kg^{-1}). Total dissolved iron concentrations in the overlying water samples of the upper estuary, Satilla 1 (SAT1) and Satilla 2 (SAT 2), were lower than the bulk river dissolved Fe(III) at the same salinity (Fig. 4.2). Inversely, total dissolved Fe(III) in the overlying waters of the lower estuary

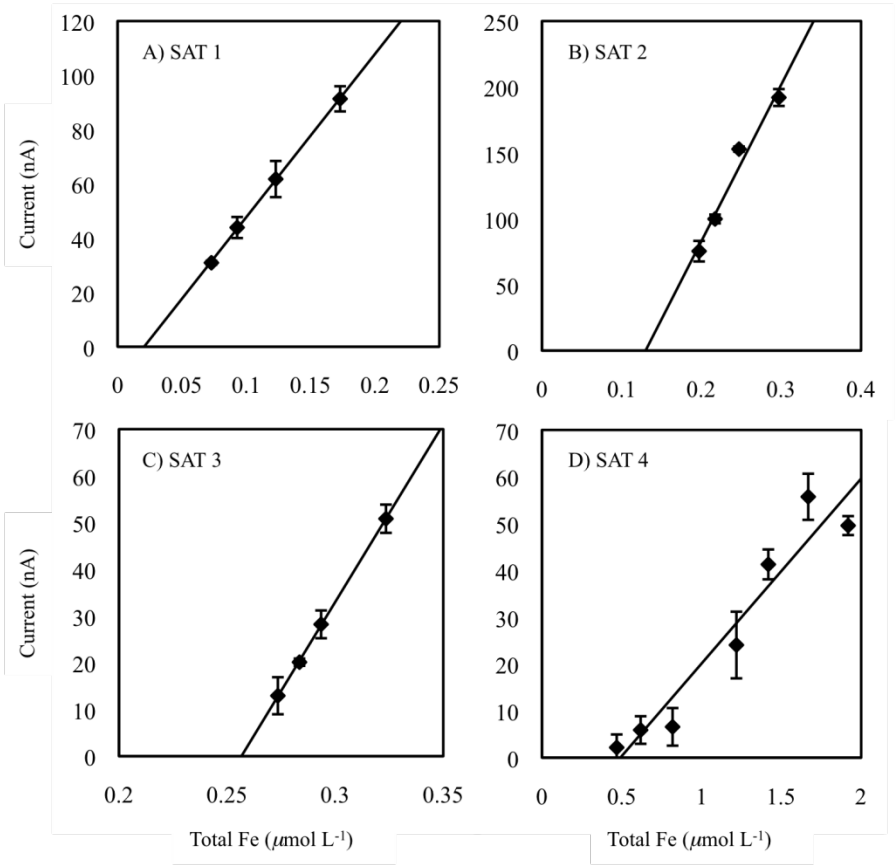

Figure 4.3 – CLE-ACSV titrations of overlying waters with the competitive ligand 1N2N. Current intensities of the Fe(III)-1N2N complex as a function of total iron (sample Fe + added Fe) at each station. Lines represent the regression of the linear portion of the titration. [FeL] is determined from the x-intercept and corrected for the dilution factor. (A) SAT 1 overlying waters were diluted 100 times and (B-D) SAT 2-4 overlying waters were diluted 20 times prior to CLE titration. Error bars represent the standard deviation of triplicate measurements.

(SAT 3 and SAT 4) were 3 to 8 times higher than the bulk river iron concentrations at the same salinity. In addition to total dissolved Fe(III) measurements, CLE-ACSV titrations were conducted on 20 to 100 times diluted overlying water samples of each core during the January 2008 cruise. Titration curves clearly revealed the presence of organic-Fe(III) complexes in the overlying waters at each station (Fig. 4.3) in increasing concentrations from the upper river to the lower estuary (Table 4.2). In contrast to the total dissolved

iron concentration, the fraction of organic-Fe(III) complexes correlated strongly with salinity: At low salinity (7 g kg^{-1}), 52 ± 22% of the total dissolved iron was under the form of organic complexes, while at high salinity (20 g kg^{-1}), 104 ± 32% of the total dissolved iron was complexed by organic ligands (Table 4.2).

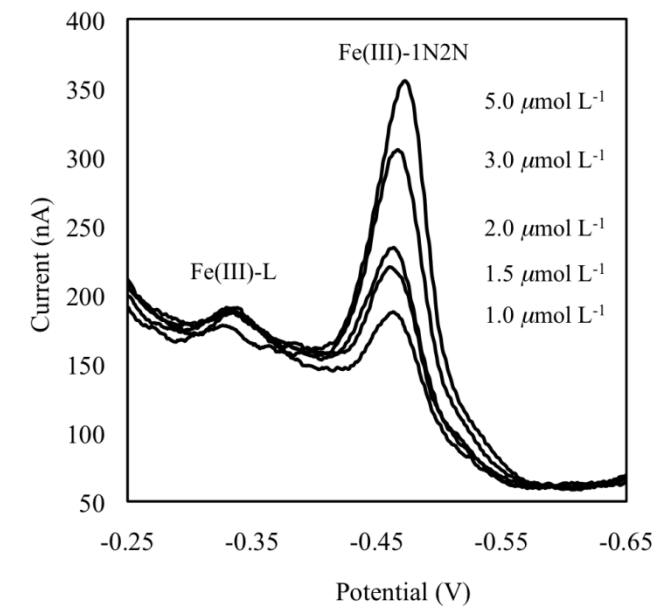

Figure 4.4 – Voltammetric scans from CLE titrations of SAT 3 sediment porewaters in the presence of excess 1N2N. A natural organic-Fe(III) complex is observed at -0.33 V in addition to the Fe(III)-1N2N competitive ligand complex detected at -0.48 V. As the current intensities of this unknown complex does not vary during the titration, it is likely less labile than the natural organic-Fe(III) complexes determined by the CLE titrations.

4.4.3 CLE-ACSV of sediment porewaters

CLE-ACSV titrations of porewaters from SAT 3 collected during low flow conditions displayed a voltammetric signal for natural organic-Fe(III) complexes at -0.34 volts in addition to the Fe(III)-1N2N complex observed at -0.48 volts (Fig. 4.4). The current intensities of these unknown complexes did not vary significantly during the

titrations, suggesting that they represent non 1N2N-exchangeable organic-Fe(III) complexes. As their electrochemical signals were sufficiently separated from those of the Fe(III)-1N2N complex, they did not interfere with the CLE titrations. Porewater samples from SAT2 during the low flow conditions of July 2007 were analyzed by CLE-ACSV titrations with 1N2N. In most samples, the current of the Fe(III)-1N2N complex reached a plateau at high Fe(III) additions during the titrations (Fig. 4.5), indicating that the 1N2N ligand was saturated at high Fe(III) additions. As a result, only the linear portion of the titration curve was considered in the calculations of the concentrations of the 1N2N- exchangeable organic-Fe(III) complexes. The Ruzic linearizations, used to calculate the total ligand concentration and the conditional stability constant at each depth in the sediment, typically produced linear curves except for the data at 1 cm depth (Fig. 4.6) likely due to the proportionally low dissolved Fe(III) concentration at that depth. Measurements of total dissolved iron and dissolved Fe(II) by the ferrozine technique revealed that both dissolved Fe(II) and Fe(III) increased with depth in the sediment; however, the concentration of dissolved Fe(II) reached a maximum of 0.32 ± 0.05 mmol L^{-1} at 5.2 cm while that of dissolved Fe(III) reached a maximum of 0.92 ± 0.05 mmol L^{-1} at 5.9 cm at SAT 3 (Fig 4.7A). The depth profile of dissolved Fe(III) mirrored that of soluble organic-Fe(III) complexes measured directly with Au-Hg voltammetric microelectrodes which provided the highest current intensities (542 ± 51 nA) in the deepest portion of the core between 5.9 and 8.0 cm. Similarly, the concentrations of natural organic-Fe(III) complexes measured from the CLE-ACSV titrations (Fig. 4.7B) closely matched the depth profile of dissolved Fe(III) and reached a maximum concentration of 1.18 ± 0.22 mmol L^{-1} at 6.6 cm. The concentrations of total natural

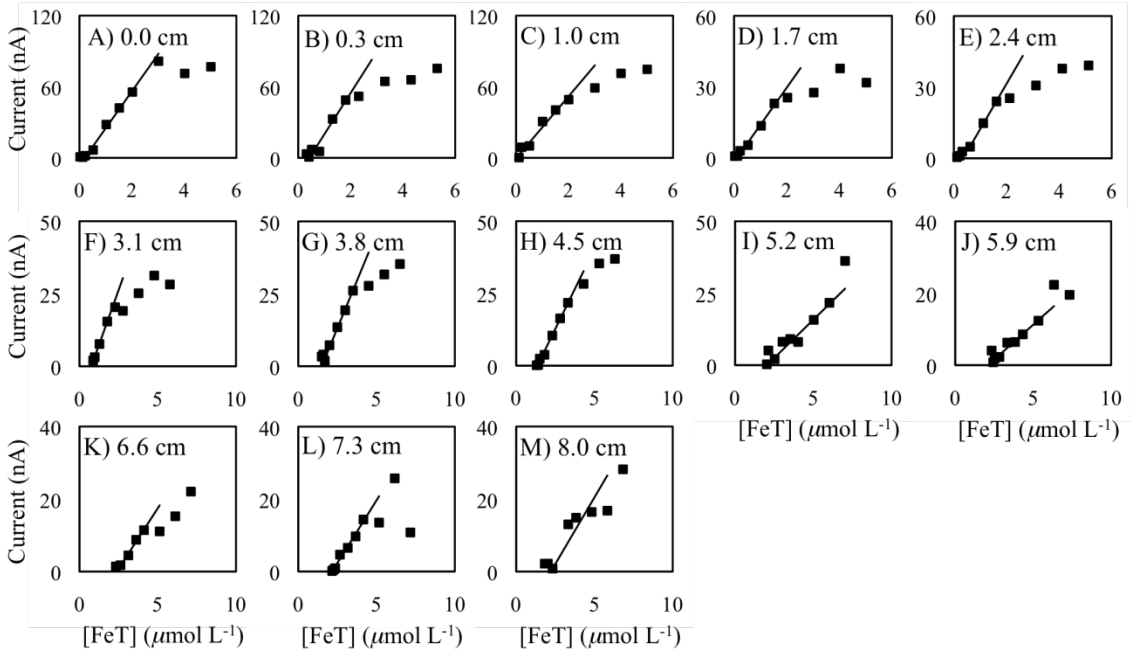

Figure 4.5– CLE titrations of sediment porewaters collected at SAT 2 in July 2007. (A) Overlying water and (B-M) porewater samples, extracted at 0.7 cm increments, were diluted 500 times prior to CLE titration. The linear regression of the titration data is used to determine the [FeL] from the x-intercept.

ligand, [L_T], determined by the Ruzic linearizations exceeded the organic-Fe(III) concentrations at all depths and reached a maximum of 3.5 ± 0.5 mmol L^{-1} at 6.6 cm. Finally, the conditional stability constants, Log K_{FeL}, calculated from the Ruzic linearizations displayed no discernable trend with depth and varied between 20.8 and 21.9 with an average value of 21.5 ± 0.6 across the depth profile (Fig. 4.7). These values are similar to other conditional stability constants measured in open ocean surface waters (Rue and Bruland 1995; Wu and Luther 1995).

4.4.4 Sediment profiles and flux of Fe(III)

A total of twenty sediment cores were collected between July 2007 and January 2008 along the Satilla River transect. Sediment cores were characterized by oxygen penetration depths that did not exceed 0.1-0.3 cm (Meiggs and Taillefert, in press). In

general, soluble Fe(III) concentrations were low at the surface of the sediment, rose until a maximum was reached within the first few centimeters of the sediment, and then either fell or remained at their maximum value (Fig. 4.8). Simultaneously, soluble Fe(III) concentrations in the porewaters generally decreased from the freshwater stations to the mouth of the estuary. Consistently high soluble Fe(III) concentrations, ranging between 295 and 749 μmol L^{-1}, were measured at the upriver station, SAT 1 (Fig. 4.8), while concentrations ranging between 71 and 997 μmol L^{-1}, the highest measured over the course of this study, were observed at SAT 2. Soluble Fe(III) concentrations between 95 and 292 μmol L^{-1} were produced in the porewaters of the middle station, SAT 3, while no

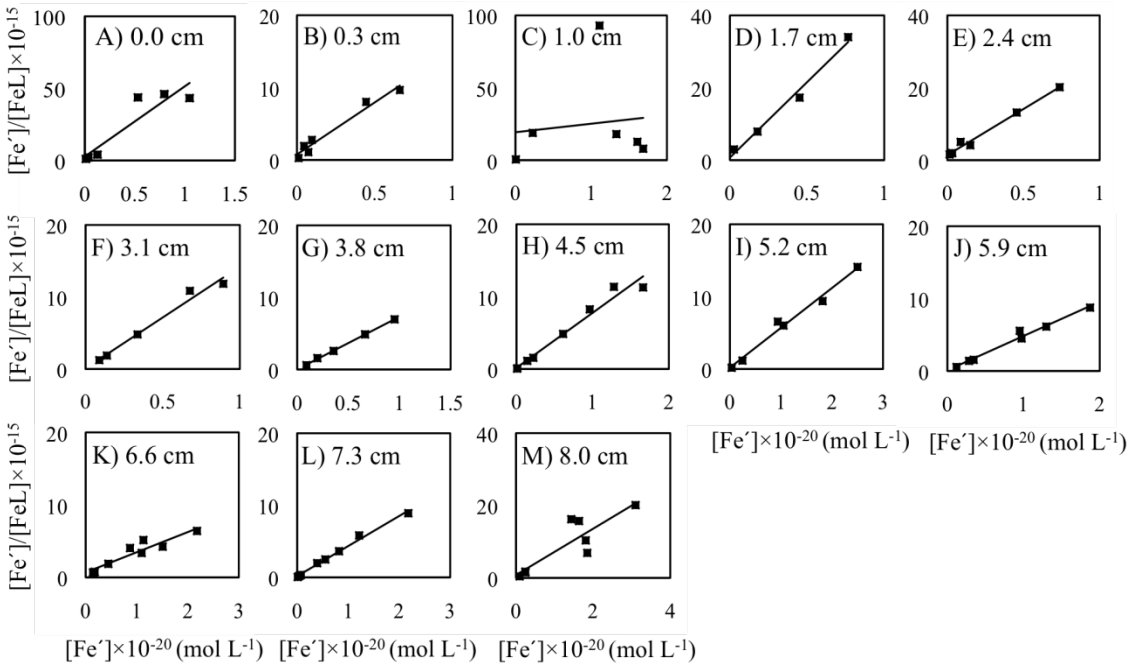

Figure 4.6 – Ruzic linearizations of the CLE titrations of sediment porewaters collected at SAT 2 in July 2007. Total ligand concentration, [L_T], and conditional stability constants (Log K) of the Fe(III)-ligand complex in the (A) overlying water and (B-M) sediment porewaters were calculated from the slope and y-intercept of the linear regression.

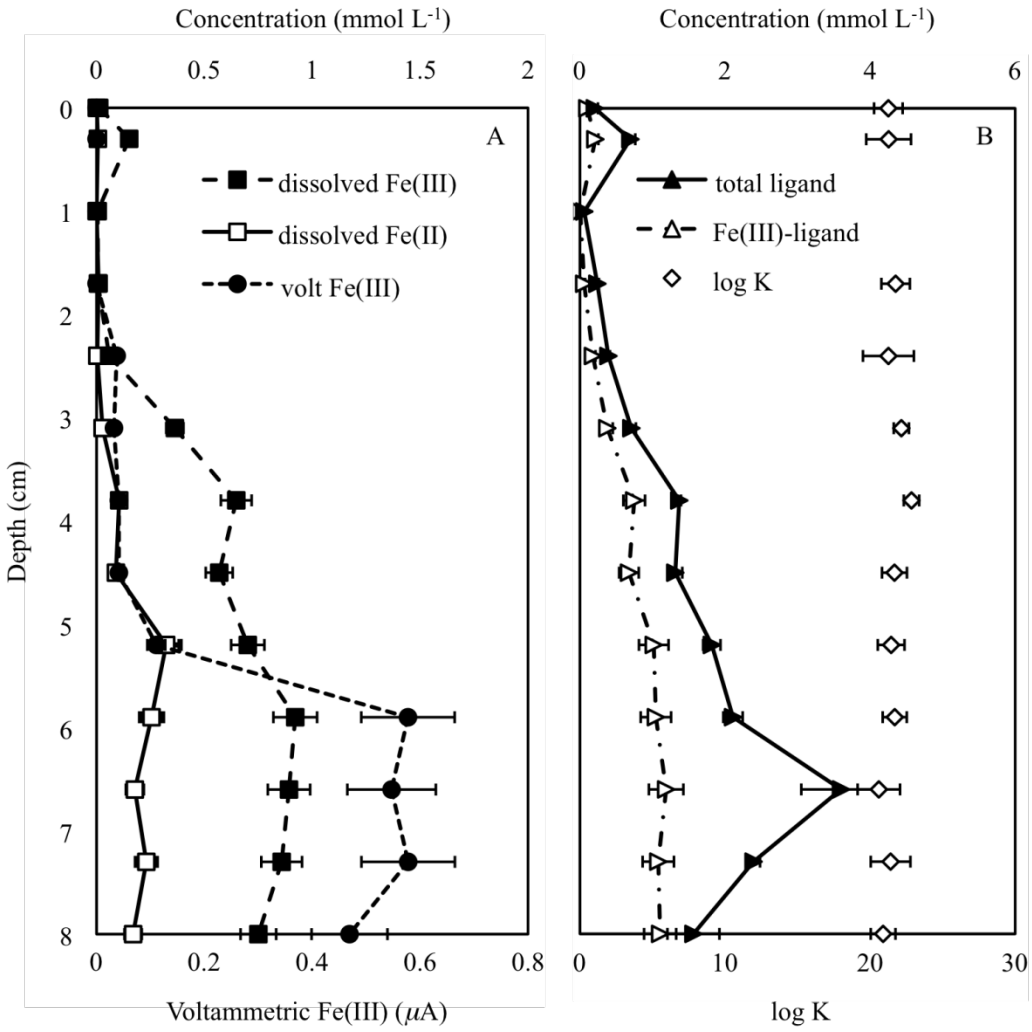

Figure 4.7 – (A) Porewater profiles of dissolved Fe(III) (closed squares), dissolved Fe(II) (open squares), and voltammetric (Volt) Fe(III) (closed circles) from sediments collected at SAT 2 in July 2007. (B) Total ligand [L_T] (closed triangles), Fe(III)-ligand [FeL] (open triangles), and conditional stability constant, Log K (open diamonds) determined by CLE-ACSV.

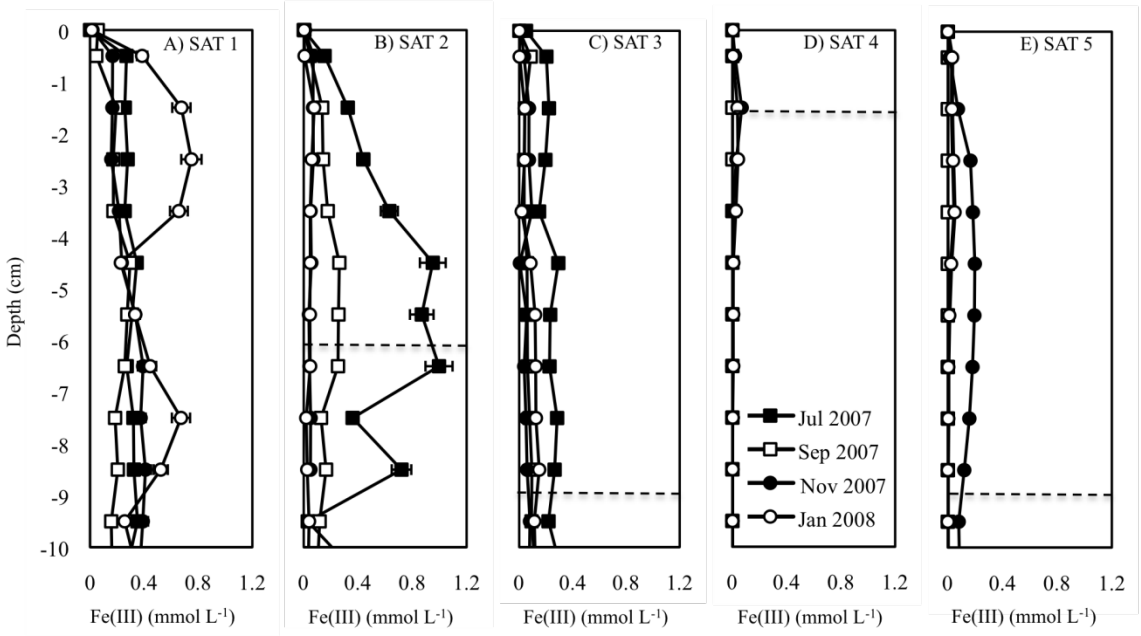

Figure 4.8 – Dissolved Fe(III) in sediment porewater profiles of (A) SAT 1, (B) SAT 2, (C) SAT 3, (D) SAT 4, and (E) SAT 5 between July 2007 and January 2008. The highest concentrations of porewater Fe(III) were measured at SAT 1 and SAT 2. Intermediate concentrations of Fe(III) were found in SAT 3 porewaters during each sampling trip, while Fe(III) was below detection limit at both SAT 4 and SAT 5 during the July and September samplings. Dashed lines represent the onset depths of dissolved sulfide in each profile. Error bars represent instrument error for triplicate measurements.

soluble ferric iron (minimum detection limit ~ 5 μmol L^{-1}) was observed during the summer months at the two estuarine stations, SAT 4 and Satilla 5 (SAT 5), and maximum concentrations between 70 and 195 μmol L^{-1} were observed during the rest of the year. Depth profiles of the main redox species obtained with Au-Hg voltammetric microelectrodes did not reveal any dissolved sulfides nor $FeS_{(aq)}$ complexes, proposed to form during the precipitation of $FeS_{(s)}$ (Tercier-Waeber and Taillefert 2008), at SAT 1 at any time during the four cruises (Meiggs and Taillefert 2011). In addition, sulfide concentrations were generally low at all stations (< 50 μmol L^{-1}) except for SAT4 where they reached 2.25 mM during the summer and fall only (Meiggs and Taillefert, in press).

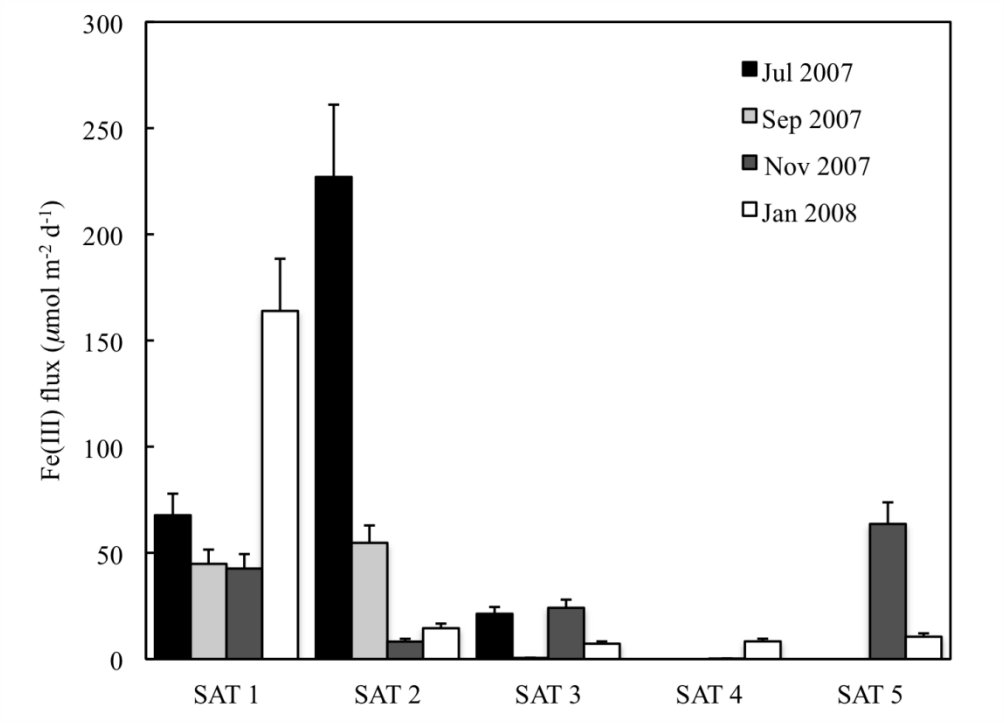

Figure 4.9 – Diffusive flux of dissolved Fe(III) from the sediments of the Satilla River Estuary calculated from the top 3.5 cm of the depth profiles (Fig. 3) using Fick's first law. Salinity increases from SAT 1 to SAT 5. Error bars represent the standard deviation from the linear regression used to calculate the fluxes.

Finally, sulfides were only found below the depths where dissolved iron was detected, typically deeper than 6-9 cm depending on the station and season, except at SAT 4 where the onset of sulfides was found as close as 1.5 cm from the sediment-water interface during the summer (Fig. 4.8). The diffusive flux of dissolved Fe(III), calculated from the sediment porewater profiles, was highest in the upper estuary stations and in general decreased with salinity (Fig. 4.9). In addition, the upper estuary stations, SAT 1 and SAT 2, displayed the highest average fluxes during the four sampling periods (62 ± 39 and 59 ± 69 μmol m^{-2} d^{-1}) and the highest individual fluxes (127 ± 19 and 177 ± 27 μmol m^{-2} d^{-1}) compared to the other stations at each sampling period. In contrast, the average flux at SAT 3 (10 ± 7.6 μmol m^{-2} d^{-1}) and SAT 4 (1.7 ± 2.8 μmol m^{-2} d^{-1}) decreased as salinity

increased. SAT 4, the most sulfidic station (Meiggs and Taillefert, in press), did not produce any dissolved Fe(III) flux during the summer (Fig. 4.9) and displayed the lowest concentrations of dissolved Fe(III) in the estuary (Fig. 4.8). In contrast, the average flux of dissolved Fe(III) at SAT 5 (14 ± 21 μmol m^{-2} d^{-1}) was highly variable, including no flux observed during the summer and the highest fluxes (50 ± 7 μmol m^{-2} d^{-1}) determined during the November sampling (Fig. 4.9).

4.5 Discussion

The Satilla River Estuary provides a unique environment to study the interaction of high dissolved iron, high DOC, and low pH riverine waters with seawater (Perdue et al. 1976). The black water Satilla River carries a large amount of unstable material at seawater ionic strength and pH, leading to flocculation and precipitation in the estuary (Windom et al. 1971; Beck et al. 1974). The high rate of sedimentation observed in the Satilla River Estuary leads to the formation of unconsolidated sediments and stimulates microbial respiration (Alber et al. 2003). In this study, the speciation of dissolved iron in the sediments and overlying waters along the salinity gradient of this estuary was determined using a combination of spectrophotometric and voltammetric techniques. Voltammetric measurements included direct qualitative determination of organic-Fe(III) complexes using Au-Hg microelectrodes and, for the first time, indirect quantification of the same complexes using CLE-ACSV. Together with total dissolved iron measurements in the water column, these data were used to investigate whether these stable Fe(III) complexes diffuse across the sediment-water interface and contribute to the export of iron to the continental shelf in two different river discharge regimes.

4.5.1 Loss of iron and change in speciation during estuarine mixing

The loss of dissolved iron from riverine waters during their interaction with seawater is well documented (Boyle et al. 1977). In the Satilla River Estuary this characteristic loss of dissolved iron is observed over a 30 km transect (Fig. 4.2). The loss of dissolved iron is consistent with both conservative mixing between fresh and marine waters and non-conservative flocculation and precipitation observed in other estuaries (Boyle et al. 1977; Dai and Martin 1995; Buck et al. 2007). Estuarine waters with S > 15 g kg^{-1} over the two sampling periods display a relatively linear loss of iron as salinity increases, which suggests simple seawater dilution as the primary action that decrease iron concentrations in the water column. This linear loss of iron is similar to the loss of soluble iron (< 3 nm) observed during estuarine mixing in other estuaries (Dai and Martin 1995). In turn, the upper estuary (S < 15 g kg^{-1}) reveals less consistent agreement between dissolved iron in the surface and bottom waters and between normal and low flow conditions. The high variability and rapid loss of dissolved iron are likely indicative of flocculation and precipitation, leading to the high rates of sedimentation previously observed in this estuary (Alber et al. 2003). Higher dissolved iron in the bottom waters during normal flow conditions (average of 60 m^3 s^{-1}) can either be explained by the resuspension of colloidal material (< 200 nm) generated by river flow or by the increased flux of dissolved iron from the sediment, as higher dissolved Fe(III) fluxes from the sediment were observed during this period than in the low flow conditions (Fig. 4.9). The speciation of dissolved iron in the overlying waters along the salinity gradient helps better understand the processes affecting the loss of dissolved iron in the Satilla River

Estuary. Unlike the surface and bottom waters (Fig. 4.2), no discernable trend was observed between total dissolved iron in the overlying waters and the salinity of the site (Table 4.2). In turn, the fraction of dissolved iron exchangeable by 1N2N was highly correlated to the salinity suggesting the aggregation and precipitation of iron oxide removes most of the colloidal Fe(III) at high salinity, while the fraction of dissolved Fe(III) complexed by organic ligands is persistent in solution. These findings are consistent with open ocean studies that have demonstrated the importance of organic ligands in maintaining Fe(III) in solution in seawater (Hunter and Boyd 2007) and suggest that dissolved organic-Fe(III) complexes may fuel primary productivity in the Satilla River Estuary and the continental shelf.

4.5.2 Diffusive flux of Fe(III) from estuarine sediments

The speciation of dissolved iron was investigated in sediment porewaters to better assess the role of the sediment as source of soluble organic-Fe(III) complexes to the overlying waters. As for the solubility of Fe(III) in seawater (Millero 1998; Hunter and Boyd 2007), the solubility of Fe(III) in porewaters appears to be controlled by the concentration of organic ligands. The concentration of total dissolved iron is always lower than the total ligand concentration (Fig. 4.7), suggesting excess ligand is present in the porewaters. The maximum concentrations of organic ligand at 6.5 cm (Fig. 4.7B) and soluble Fe(III) in some of the porewaters (Fig. 4.8) suggest the local production of ligand and remobilization of organic-Fe(III) complexes in these areas may be important processes in the sediments of the Satilla River Estuary. In contrast to the overlying waters (Table 4.2), colloids were not detected in the sediment porewaters, as concentrations of total dissolved Fe(III) and organic-Fe(III) complexes determined by

CLE-ACSV were comparable across the depth profile (Fig. 4.7). The large concentrations of dissolved Fe(III) found (Fig. 4.8) well below the maximum depth of oxygen penetration in these sediments (Meiggs and Taillefert, in press) suggest oxygen may not be responsible for the production of these ferric iron complexes. Alternately, ferrous iron could be oxidized by manganese or iron oxides (Postma 1985) or by nitrate-reducing Fe-oxidizing bacteria (Roden 2004) and form, in the presence of organic ligands, soluble organic-Fe(III) complexes at depth. To our knowledge, however, the effect of organic ligands on metal oxide-catalyzed oxidation of ferrous iron has yet to be demonstrated, and the presence of nitrate-reducing Fe-oxidizing bacteria requires nitrate, which is scarce in Satilla River sediments (Jahnke et al. 2003). Dissolved Fe(III) in the Satilla River Estuary is strongly associated with DOM (Perdue et al. 1976) and these complexes aggregate and settle to the sediment during estuarine mixing. Once deposited in the sediments, soluble Fe(III) complexes may be released into the porewaters through reequilibration of the particles with the surrounding porewaters, especially if organic ligands are produced as catabolites from the microbial degradation of DOM (Marschner and Kalbitz 2003). Finally, dissimilatory Fe(III) reducing bacteria (DIRB) may provide an alternative source of soluble organic-Fe(III) complexes in anoxic sediments. DIRB have been proposed to produce soluble organic-Fe(III) complexes either directly or indirectly in aqueous sediments (Brendel and Luther 1995). Recently, the DIRB *Shewanella oneidensis* and *Shewanella putrefaciens* have been demonstrated to produce soluble organic-Fe(III) complexes as intermediates in the reduction of solid Fe(III) oxides (Taillefert et al. 2007; Jones et al. 2010) that are not siderophores (Fennessey et al. 2010). These organisms produce an organic ligand that non-reductively dissolves Fe(III) oxides

as an intermediate step in the respiration of Fe(III). It is therefore possible that iron reducing organisms present in Satilla River Estuary sediments employ similar strategies.

The diffusive flux of soluble organic-Fe(III) complexes from the sediments of the Satilla River Estuary is highly variable both spatially and temporally. The highest fluxes from the sediments (177 ± 27 μmol m^{-2} d^{-1}) are similar in magnitude to the Fe(II) flux (289 μmol m^{-2} d^{-1}) measured in shelf sediment from low oxygen upwelling zones (Elrod et al. 2004). However, the stability of the organic-Fe(III) complexes in oxic waters should allow for greater transport than Fe(II) which is rapidly oxidized and hydrolyzed at circumneutral pH (Millero et al. 1995). The absence of colloids and the high concentration of iron binding ligand observed in the porewaters of the upper Satilla River Estuary (Fig. 4.7) suggest that the majority of ferrous iron eventually oxidized in the upper Satilla River Estuary would remain in solution under the form of organic-Fe(III) complexes as previously demonstrated (Taillefert et al. 2000). These findings suggest that organic-Fe(III) complexes comprise the majority of the flux of dissolved Fe(III) across the sediment-water interface. In turn, the flux of dissolved Fe(III) from these estuarine sediments may be underestimated as it was determined in sediment cores. Unfortunately, core collection suppresses advective forces, which typically change the shape of the depth profiles compared to in situ measurements (Taillefert et al. 2007; Meiggs and Taillefert, in press). Indeed, advective forces, either from river flow (Huettel et al. 1998) or submarine groundwater discharge (Moore 1996), contribute to the mobility of dissolved species from Satilla River sediments (Jahnke et al. 2003; Meiggs and Taillefert, in press) and could enhance the flux of iron to the overlying waters by resuspension of colloids and nanoparticles (Raiswell et al. 2006). The highest fluxes of

soluble Fe(III) measured in the upper estuary (SAT 1 and SAT 2) are associated with muddy sediments, presumably due to the high sedimentation rates (0.4 cm yr^{-1}) (Alber et al. 2003) from the flocculation of organic and inorganic colloids at these stations that is enhanced in low flow conditions (Meiggs and Taillefert, in press). More than 80% of the total riverine dissolved iron is lost by a salinity of 20 g kg^{-1} through flocculation and precipitation (Fig. 4.2), providing a source of iron to the upper estuary sediments. Increased delivery of mineral constituents to estuarine sediments induces higher microbial iron reduction activity (Meiggs and Taillefert, in press) leading to high benthic fluxes of dissolved iron to the overlying waters (Fig. 4.9). The total iron and organic content of the next two stations, SAT 3 and SAT 4, are typically lower than the upstream sites and are characterized by higher proportion of sandy sediments of marine origin. In turn these sediments produce the lowest total fluxes of dissolved Fe(III) of all the stations. Finally, the most saline station, SAT 5, displays greater mud content then the middle stations (Table 4.1) and higher dissolved Fe(III) than SAT 4, leading to larger fluxes of dissolved Fe(III) to the overlying waters (Fig. 4.9). As salinity increases, total iron in sediments decreases and sulfate reduction contributes to anaerobic microbial respiration processes in these sediments (Meiggs and Taillefert, in press). Dissolved sulfides produced during sulfate reduction are good reductants of dissolved Fe(III) (Taillefert et al. 2000), form stable iron sulfide minerals, and thus limit the presence of dissolved Fe(III) at these stations. As a result, the flux of dissolved Fe(III) from the sediment must be controlled by the rate of deposition of iron and organic compounds (Meiggs and Taillefert, in press) as well as the intensity of sulfate reduction. These findings suggest that the pelagic-benthic coupling of iron through sedimentation,

reduction and oxidation, and flux across the sediment-water interface is an important component of the iron cycle in estuaries that may also result in a net production of iron to the overlying waters.

4.5.3 Importance of organic-rich rivers on the flux of iron to the continental shelf

The total flux of organic-Fe(III) complexes in the Satilla River Estuary was determined from the average dissolved Fe(III) fluxes along each section of the river, assuming the majority of dissolved Fe(III) is under the form of organic-Fe(III) complexes (Table 4.3). The estuary was divided in to five sections each represented by a sediment core collected from the station within the section. Sediment surface areas were calculated from the average river width through each section along the river. The sediment flux for each section of the estuary was determined by multiplying the diffusive flux measured at each station by the sediment surface area of the river section. The total estuarine sediment flux for a given sampling period was determined as the sum of the fluxes in the five river sections (Table 4.3). The total flux of organic-Fe(III) complexes from the sediment at each section of the estuary ranged between 7.8×10^4 and 6.0×10^5 moles soluble organic-Fe(III) yr^{-1}. The upper sections of the estuary consistently produced the highest sedimentary Fe(III) fluxes (Table 4.3), however, the relatively small sediment surface area diminished the contribution of these stations to the total estuarine flux. In addition, the total flux of organic-Fe(III) complexes from the sediment was nearly three times as high during the low flow (6.0×10^5 moles soluble organic-Fe(III) yr^{-1} in November 2007) than in the normal flow (2.2×10^5 moles soluble organic-Fe(III) yr^{-1} in January 2008) conditions. To better understand the importance of the flux of sediment-derived organic-Fe(III) complexes on the total flux of dissolved iron to the ocean, the

Table 4.3 - Total Satilla River Estuary sediment flux of soluble organic-Fe(III) complexes to the overlying water

Date	Station	River discharge (m^3 s^{-1})	Station flux (μmol $m^{-2}d^{-1}$)	Surface area (km^2)	Soluble Fe (III) flux (10^5 mol yr^{-1})
July 2007	SAT 1	0.76	67.7 ± 10.2	1.2	0.30 ± 0.04
	SAT 2	0.76	227 ± 34	4	3.31 ± 0.40
	SAT 3	0.76	21.3 ± 3.2	7.5	0.58 ± 0.09
	SAT 4	0.76	0 ± 0	19	0 ± 0
	SAT 5	0.76	0 ± 0	29	0 ± 0
	Total				4.2 ± 0.5
September 2007	SAT 1	19.82	44.8 ± 6.7	1.2	0.20 ± 0.03
	SAT 2	19.82	54.7 ± 8.2	4	0.80 ± 0.12
	SAT 3	19.82	0 ± 0	7.5	0.01 ± 0.01
	SAT 4	19.82	0 ± 0	19	0 ± 0
	SAT 5	19.82	0 ± 0	29	0 ± 0
	Total				1.0 ± 0.1
November 2007	SAT 1	4.25	42.6 ± 6.4	1.2	0.19 ± 0.03
	SAT 2	4.25	8.2 ± 1.2	4	0.12 ± 0.02
	SAT 3	4.25	24.1 ± 3.6	7.5	0.66 ± 0.10
	SAT 4	4.25	0.2 ± 0.1	19	0.01 ± 0.01
	SAT 5	4.25	63.6 ± 9.5	29	6.74 ± 1.01
	Total				7.7 ± 1.0
January 2008	SAT 1	59.47	163.9 ± 24.6	1.2	0.72 ± 0.11
	SAT 2	59.47	14.5 ± 2.2	4	0.21 ± 0.03
	SAT 3	59.47	7.2 ± 1.1	7.5	0.20 ± 0.03
	SAT 4	59.47	8.3 ± 1.2	19	0.58 ± 0.09
	SAT 5	59.47	10.5 ± 1.6	29	1.11 ± 0.17
	Total				2.8 ± 0.2

total riverine flux of iron was calculated by multiplying the concentration of dissolved iron in the water column at the mouth of the estuary in November 2007 (low flow conditions) and January 2008 (normal discharge) by the total river discharge. Using these calculations, it is estimated that 4.5 x 10^4 mol Fe yr^{-1} is transported to the continental shelf from the Satilla River Estuary during low flow conditions while the flux from the sediments was estimated at 6.0 x 10^5 mol Fe yr^{-1}. The difference between sediment flux and total river flux indicates that 8% of the sediment-derived organic-Fe(III) reaches the ocean during low flow conditions and suggests that sediment-derived organic-Fe(III) may be consumed during primary production in the estuary or

reprecipitated downriver. During normal flow conditions, however, the Satilla River Estuary provides a flux of 3.5 x 10^5 mol Fe yr^{-1} to the continental shelf, while 2.2 x 10^5 mol Fe yr^{-1} is supplied by the sediments. In these conditions sediment-derived Fe(III) contributes to nearly all of the total Fe(III) flux to the ocean, most likely because the combination of high turbidity and shorter residence times in the estuary associated with higher discharge prevents biological uptake and minimize reprecipitation downriver. The total flux of dissolved iron is small when compared to the world wide riverine flux of iron (1.5 x 10^9 mol Fe yr^{-1}). The concentration of dissolved iron in the Satilla River Estuary (189 – 336 nmol L^{-1}), however, is 5 to 8 times higher than the average concentration in the major world rivers (40 nmol L^{-1}) (Martin and Meybeck 1979), suggesting the Satilla River and other blackwater rivers like it are underrepresented in world average river flux calculations.

4.6 Acknowledgements

We thank the captain and crew of the R/V *Savannah* for their generous support on the Satilla River cruises. Deidre Meiggs, Gwendolyn Bristow, Patrick Wilson, Kathleen Salome, W. Holmes Merritt, Jason Peart, Hong Wu, and Hui Lin assisted with shipboard sampling and analysis. This research was supported by the National Science Foundation Faculty Early Career Development (CAREER) Program (Ocean Sciences 0239376).

CHAPTER 5

SHEWANELLA ONEIDENSIS MR-1 MUTANTS SELECTED FOR THEIR INABILITY TO PRODUCE SOLUBLE ORGANIC-FE(III) ARE UNABLE TO RESPIRE FE(III) AS ANAEROBIC ELECTRON ACCEPTOR

This is a reprint of an article whose final and definitive form has been published in Environmental Microbiology, authored by Jones, M. E.; Fennessey, C. M.; DiChristina, T. J.; and Taillefert, M. entitled *Shewanella oneidensis* MR-1 mutants selected for their inability to produce soluble organic-Fe(III) are unable to respire Fe(III) as anaerobic electron acceptor.

5.1 Abstract

Recent voltammetric analyses indicate that *Shewanella putrefaciens* strain 200 produces soluble organic-Fe(III) during anaerobic respiration of sparingly soluble Fe(III) oxides. Results of the present study expand the range of *Shewanella* species capable of producing soluble organic-Fe(III) to include *S. oneidensis* MR-1. Soluble organic-Fe(III) was produced by *S. oneidensis* cultures incubated anaerobically with Fe(III) oxides, or with Fe(III) oxides and the alternate electron acceptor fumarate, but not in the presence of O_2, nitrate or trimethylamine-*N*-oxide. Chemical mutagenesis procedures were combined with a novel MicroElectrode Screening Array (MESA) to identify four (designated Sol) mutants with impaired ability to produce soluble organic-Fe(III) during anaerobic

respiration of Fe(III) oxides. Two of the Sol mutants were deficient in anaerobic growth on both soluble Fe(III)-citrate and Fe(III) oxide, yet retained the ability to grow on a suite of seven alternate electron acceptors. The rates of soluble organic-Fe(III) production were proportional to the rates of iron reduction by the *S. oneidensis* wild-type and Sol mutant strains, and all four Sol mutants retained wild-type siderophore production capability. Results of this study indicate that the production of soluble organic-Fe(III) may be an important intermediate step in the anaerobic respiration of both soluble and sparingly soluble forms of Fe(III) by *S. oneidensis*.

5.2 Introduction

Dissimilatory iron reducing bacteria (DIRB) impact a variety of important environmental processes, including biogeochemical cycling of carbon and iron, bioremediation of organic and inorganic contaminants, and generation of electricity in microbial fuel cells (Nealson and Saffarini 1994; Lovley et al. 2004; Logan et al. 2006; Gralnick and Newman 2007). SSU rRNA analyses indicate that DIRB are deeply rooted and scattered throughout the domains *Archaea* and *Bacteria* (Weber et al. 2006), an indication that dissimilatory iron reduction may have been one of the first respiratory processes to have evolved on early earth (Vargas et al. 1998; Schulze-Makuch et al. 2005). DIRB play integral roles in remineralization of organic matter in redox-stratified, aqueous environments (Thamdrup 2000; Kostka et al. 2002; Koretsky et al. 2003) and in remobilization of iron in iron-limited oceans (Elrod et al. 2004; Severmann et al. 2006; Gerringa et al. 2007). Some DIRB degrade hazardous organics in contaminated ground water (Lovley et al. 1989; Zachara et al. 1998) or work in concert with fermenting bacteria to decompose recalcitrant organic compounds (Watson et al. 2005). Metal,

metalloid, and radionuclide solubility is also altered by DIRB activity in natural and contaminated environments (Lovley et al., 1991; DiChristina et al., 2005) and DIRB-catalyzed, reductive precipitation (immobilization) of radionuclides has been proposed as a alternate remediation strategy in radionuclide-contaminated environments.

At circumneutral pH, Fe(III) is sparingly soluble and is typically found in the form of crystalline and poorly ordered oxyhydroxides (Zinder et al. 1986). Consequently, neutrophilic DIRB are postulated to employ a variety of novel respiratory pathways not found in other bacteria that respire soluble electron acceptors such as O_2, NO_3^-, SO_4^{2-}, and CO_2 (DiChristina et al., 2005; Weber et al., 2006). Several alternate pathways for respiration of sparingly soluble Fe(III) oxides have been proposed, including: 1) a direct enzymatic pathway in which terminal Fe(III) reductases, localized on the outer membrane or on electroactive nanowires, contact and deliver electrons directly to the Fe(III) oxide surface (Myers and Myers, 1992; DiChristina et al., 2002; Reguera et al., 2005; Gorby et al., 2006; Shi et al., 2006); 2) a two-step electron shuttling pathway in which endogenous or exogenous electron shuttles are first reduced by DIRB followed by chemical reduction of the Fe(III) oxide by the reduced electron shuttle in a second (abiotic) electron transfer reaction (Newman and Kolter, 2000; Coates et al., 2002; Hernandez et al., 2004; Marsili et al., 2008); and 3) a two-step Fe(III) chelation (solubilization) pathway in which solid Fe(III) oxides are first non-reductively dissolved by endogenous organic ligands prior to the DIRB-catalyzed reduction of the soluble organic-Fe(III) complexes (Arnold et al., 1988; Lovley and Woodward, 1996; Taillefert et al., 2002). Cells adjacent to the mineral surface are postulated to employ the direct enzymatic pathways, while cells at a distance may rely on the electron shuttling or Fe(III)

solubilization pathways. For the latter two pathways, the energetic cost of synthesizing extracellular, electron transfer components must be offset by faster reduction rates, increased energy production, or increased access to electron acceptors (Taillefert et al., 2007; Marsili et al., 2008). Thus, the recycling of Fe(III)-chelating compounds or electron shuttles between the cell and mineral surfaces may minimize the energetic costs associated with DIRB biosynthesis and provide advantages over other respiratory pathways.

Evidence for Fe(III) solubilization in the environment includes the voltammetric detection of high concentrations of soluble organic-Fe(III) in porewaters of redox stratified sediments (Brendel and Luther 1995; Taillefert et al. 2000b; Taillefert et al. 2002). Voltammetric analyses demonstrate that soluble organic-Fe(III) is readily formed at circumneutral pH in both laboratory and field experiments, an indication that Fe(III) solubilization may be an important first step in the microbial reduction of Fe(III) oxides (Taillefert et al. 2000a; Carey and Taillefert 2005; Crowe et al. 2007; Marsili et al. 2008). In laboratory cultures, soluble organic-Fe(III) enhances the rate and/or extent of DIRB-catalyzed Fe(III) reduction (Arnold et al. 1988; Dollhopf et al. 2000; Nevin and Lovley 2002; Taillefert et al. 2007). Soluble organic-Fe(III) is also reduced more rapidly than Fe(III) oxides by purified outer membrane *c*-type cytochromes of the gram-negative DIRB *Shewanella oneidensis* MR-1, a metal respiring member of the γ-proteobacteria (Myers and Myers, 2003; Shi et al., 2006; Xiong et al., 2006). As the outer membrane *c*-type cytochromes of *Shewanella* are postulated to act as terminal Fe(III) reductases during anaerobic Fe(III) respiration (Dichristina et al. 2005; Fredrickson and Zachara

2008), the production of soluble organic-Fe(III) may therefore enhance the overall Fe(III) respiratory activity of *Shewanella* (Taillefert et al. 2007).

In addition to soluble and sparingly soluble forms of Fe(III), *S. oneidensis* also respires a wide variety of alternate terminal electron acceptors, including oxygen (O_2), nitrate (NO_3^-), nitrite (NO_2^-), manganese oxides (Mn(III,IV)), trimethylamine-*N*-oxide (TMAO), sulfite (SO_3^{2-}), thiosulfate ($S_2O_3^{2-}$), elemental sulfur (S(0)), uranium [U(VI)], technetium(Tc(VII)), fumarate, anthraquinone 2,6-disulphonate (AQDS), and potentially several others (Myers and Nealson 1988; Nealson and Saffarini 1994; Venkateswaran et al. 1999; Wade and Dichristina 2000; Payne and Dichristina 2006). The suite of electron acceptors respired by *S. oneidensis* spans nearly the entire range of redox potentials encountered in the environment. Recent voltammetric analyses have demonstrated that *S. putrefaciens* strain 200 produces soluble organic-Fe(III) during anaerobic respiration of Fe(III) oxides as electron acceptor (Taillefert et al. 2007). The production of soluble organic-Fe(III) during anaerobic Fe(III) respiration by *S. oneidensis* has yet to be examined.

The main objectives of the present study were to 1) determine if *S. oneidensis* was capable of producing soluble organic-Fe(III) during anaerobic respiration of Fe(III) oxides, 2) develop a voltammetric-based, mutant screening technique for rapid identification of *S. oneidensis* (designated Sol) mutants unable to produce soluble organic-Fe(III) during anaerobic respiration of Fe(III) oxides, 3) test the Sol mutants for siderophore production activity and for anaerobic growth on a variety of alternate, anaerobic electron acceptors, including soluble and sparingly soluble forms of Fe(III), and 4) compare the rates of soluble organic Fe(III) production to the rates of Fe(II)

production to determine if soluble organic Fe(III) production is a potential rate-limiting step in the overall Fe(III) respiratory activity of *S. oneidensis*.

5.3 Methods

5.3.1 Bacterial strains, cultivation conditions and mutagenesis procedures

S. oneidensis MR-1 (ATCC no. 700550) was originally isolated from Oneida Lake, NY (Myers and Nealson 1988). Anaerobic respiratory mutant strain T121 (only capable of aerobic growth) isolated via transposon mutagenesis of *S. putrefaciens* 200R (Saffarini et al. 1994) was used as a negative control strain for anaerobic respiration. All *Shewanella* strains were cultured on previously described *Shewanella* growth medium (Dichristina and Delong 1994).

Previously described chemical (ethyl methanesulfonate; EMS) mutagenesis procedures were used to generate a set of randomly mutagenized *S. oneidensis* strains (Burnes et al. 1998; Dichristina and Delong 1994; Taratus et al. 2000; Wade and Dichristina 2000; Payne and Dichristina 2006). Liquid cultures of MR-1 were grown aerobically to late log phase, harvested by centrifugation, washed, and suspended in PM-2 buffer (70 mM Na_2HPO_4, 30 mM NaH_2PO_4, 1 mM $MgSO_4$, and 200 μM $MnSO_4$). EMS was added to a final concentration of 19 μL mL^{-1}, and the cell suspension was incubated with gentle mixing for 1 hour to achieve 90% kill. Surviving cells were plated on LB agar and incubated aerobically for 1 day at 30 °C. A total of 3840 colonies arising from EMS-mutagenized cells were subsequently tested for soluble organic-Fe(III) production during anaerobic respiration of 2L-ferrihydrite.

5.3.2 Preparation of 2L-ferrihydrite

All solutions were prepared with ACS or trace metal grade chemicals in autoclaved 18 MΩ-water (Milli-Q). 2L-ferrihydrite was prepared by dissolving 54 g of $FeCl_3 \cdot 6H_20$ into 500 mL sterile H_20. Fe(III) oxides were precipitated by raising the pH to 7.0 by the addition of 10 N NaOH (Schwertmann and Cornell 2000). The resulting 0.4 M mixture was stored in the dark until needed. Just before use, the desired volume was centrifuged and the supernatant decanted. The precipitated iron oxides were then washed three times with sterile H_2O and used as a 0.4 M suspension of 2L-ferrihydrite.

5.3.3 Construction of a Microelectrode Screening Array (MESA)

A Microelectrode Screening Array (MESA) for voltammetric detection of soluble organic-Fe(III) complexes was constructed to screen large numbers of mutants in the individual 300 uL wells of a 96-well tray (8 x 12 matrix). MESA consists of an electrode holder with eight removable 100 μm diameter gold-mercury (Au/Hg) amalgam working electrodes and eight permanent 0.5 mm diameter Ag/AgCl reference and 0.5 mm diameter platinum counter electrodes mounted on a manual micromanipulator (Narishige). A machined aluminum tray holder with raised stops corresponding to the distance between the rows of the 96-well trays facilitated deployment of the tray from one row to another for screening (Fig 5.1a). The array of eight counter electrodes (Fig. 5.1b) was fabricated by soldering eight one inch pieces of 0.5 mm platinum wire together every 0.8 cm along a 8 cm piece of striped stranded coaxial cable such that the distance between each wire was equal to the distance between the wells of a 300 μL 96-well tray. A similar array of reference electrodes was fabricated from 0.5 mm silver wire. The counter and reference arrays were placed 0.7 cm apart in a 12 cm x 1 cm x 2 cm mold

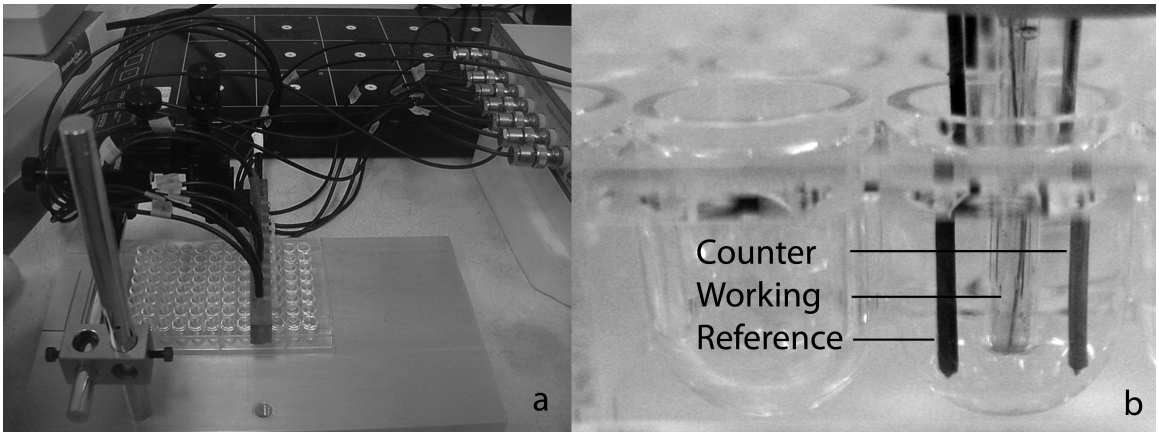

Figure 5.1 - Microelectrode screening array (MESA) developed to identify Sol mutants. An array of eight Au/Hg voltammetric microelectrodes was used to analyze each row of a 96-well tray. A computer-controlled multiplexer automatically switched between working electrodes during each analysis. (A) View of MESA in a 96-well tray. (B) Interconnected platinum counter (left) and Ag/AgCl reference (right) electrodes are fixed within the resin body, while Au/Hg working electrodes (center) can be removed for polishing and storage.

such that 2 cm of the unstripped coaxial cables were within the mold and 2 cm of the wires were outside the mold. The mold was filled with epoxy resin and eight 5/32 inch holes were drilled between the counter and reference to receive the 3/16 inch PEEK™ tubing sheath of the working electrodes. Tapped holes were added to secure working electrodes with setscrews. The Ag/AgCl reference electrodes were conditioned by applying +9 volts for 30 seconds between the reference and counter electrodes in a 3 M KCl solution. Au/Hg working electrodes were fabricated by soldering a one inch length of 100 um gold wire to the end of stranded coaxial cable. The gold wire and exposed copper wire were threaded into a 1.0 mm outer diameter glass tube. The joint between the glass tube and coaxial cable was covered by a one inch piece of 3/16 inch PEEK™ tubing sheath for reinforcement and mounting in the array body. The glass end was filled with epoxy until excess epoxy was observed from all joints. After drying, the tip was sanded with 400 grit sandpaper. BNC connectors were added and electrodes were

polished, plated and conditioned as previously described (Brendel and Luther 1995). Microelectrodes were first tested for quality using O_2, then calibrated with Mn^{2+}. Minor differences in electrode construction, polishing, and mercury plating generally result in electrodes that vary in mercury size, geometry, and analyte sensitivity (Osteryoung and Osteryoung, 1985; Brendel and Luther, 1995). Current intensities of each electrode were therefore normalized by multiplying the measured analyte intensity by the current intensity ratio of a Mn^{2+} standard for a given electrode to the average Mn^{2+} current intensity for the eight electrodes in the array (Eq.1):

$$I_{normalized} = I_{measured} \cdot \frac{I_{standard}}{average(I_{standard})} \qquad \text{(Eq. 5.1)}$$

where $I_{normalized}$ is the normalized current intensity, $I_{measured}$ is the measured current intensity of the analyte of interest, $I_{standard}$ is the current intensity of a 200 uM Mn^{2+} standard, and $average(I_{standard})$ is the average current intensity of the Mn^{2+} standard for the eight electrodes of the array. A Model DLK-100 potentiostat with DLK-MUX-1 eight channel electrode multiplexer (Analytical Instruments Systems, Inc.) was used for all voltammetric measurements. Working electrodes were controlled by the computer-operated DLK-MUX-1 multiplexer, while the reference and counter electrodes shared respective leads between each cell and the DLK-100A potentiostat. All voltammetric potentials are reported versus the Ag/AgCl reference electrode.

5.3.4 Detection of *S. oneidensis* (designated Sol) mutants unable to produce soluble organic-Fe(III)

Single colonies arising from EMS-mutagenized cells were transferred to individual wells of a 96-well tray containing 32 mM 2L-ferrihydrite in *Shewanella*

growth medium. Each tray included one row of wild-type *S. oneidensis* and an abiotic control row with cells omitted. Inoculated trays were incubated in a Coy anaerobic chamber (atmosphere consisting of 85% N_2, 10% CO_2, 5% H_2) at 30 °C for 30-36 hrs prior to voltammetric analysis. Each well of a row contained an individual working electrode and shared reference and counter electrodes. MESA was lowered into a row of the 96-well tray and the sequence started to automatically measure voltammetric signals across the individual wells of a row. At the end of a sequence, MESA was lifted, the tray moved to the next stop of the base plate, and MESA was lowered into the next row of eight wells. This procedure was repeated for each of the 12 rows of a tray. Analysis time for all 96 wells was approximately 2 hours. Voltammetric conditions used in triplicate measurements included: a conditioning step for 10 sec at -0.9 V to reduce any Fe(III) species on the electrode surface prior to a subsequent measurement, a deposition step for 10 sec at -0.1 V to concentrate Fe(III) species at the electrode surface, a scan rate of 200 mV s^{-1} from -0.1 to -1.8 V to cover the ranges of Fe(III) and Fe(II) reduction potentials, and a pulse height of 0.05 V (Taillefert et al. 2000b). Voltammograms were integrated using the program VOLTINT in Matlab™ (Bristow and Taillefert 2008). Mutant colonies displaying aberrant voltammetric responses were rescreened in triplicate and subsequently confirmed for Sol mutant phenotypes in individual batch reactor incubations.

5.3.5 Confirmation of Sol mutant phenotypes in batch reactor incubations

Wild-type *S. oneidensis* MR-1 and the putative Sol mutant strains were incubated in 100 mL PEEK™ batch reactors containing *Shewanella* growth medium supplemented with 32 mM 2L-ferrihydrite as electron acceptor and 20 mM sodium lactate as electron

donor. Reactors were inoculated with cells at a final concentration of 2 x 10^7 cells mL^{-1} and incubated in a Coy chamber under anaerobic conditions (85% N_2, 10% CO_2, 5% H_2) with gentle stirring. For experiments with competing electron acceptors, O_2 was introduced via constant bubbling with compressed air, or 15 mM nitrate, 25 mM trimethylamine oxide (TMAO), or 10 mM fumarate were added from filter-sterilized stock solutions. Two 200 µL aliquots were removed every six to eight hours for ancillary analyses. The first 200 µL aliquot was added to 1 mL 0.5 M HCl to extract adsorbed Fe^{2+} (Lovley and Phillips 1986) and analyzed for total Fe^{2+} via the Ferrozine colorimetric method (Stookey 1970). The second was transferred to a well of a 300 µL 96-well tray for voltammetric analysis as described above. Initial rates of organic-Fe(III) production were determined by linear regression of the increase in organic-Fe(III) current intensities for 24 hours (disregarding any initial lag period). Initial rates of Fe(III) reduction were determined by linear regression of the total Fe(II) production rate during the period of soluble organic-Fe(III) production. All rates were normalized to cellular protein content determined via previously described procedures (Dichristina and Delong 1994).

5.3.6 Siderophore detection with Chrome Azurol S (CAS)

Siderophores were detected during growth on liquid or solid *Shewanella* growth media via application of CAS-based techniques. CAS screening plates were prepared using a modified version of a previously described procedure (Schwyn and Neilands 1987). Blue CAS (Sigma Aldrich) agar was prepared by adding 60.5 mg of CAS dye dissolved in 50 mL water to 10mL acidic solution of $FeCl_3$ (1 mM $FeCl_3$, 10 mM HCl). This mixture was slowly added to a solution of surfactant hexadecyltrimethyl amine (HDTMA) (Sigma Aldrich) (72.9 mg dissolved in 40 mL H2O), and the resulting

solution was autoclaved, cooled to 55ºC and added to 900 mL sterile *Shewanella* growth media supplemented with 1.5% w/v agar (CAS agar). CAS shuttling solution was prepared as previously described (Schwyn and Neilands 1987). Siderophore production by *S. oneidensis* wild-type and Sol mutants was monitored by patching colonies onto CAS agar plates, incubating aerobically for 24 hours or anaerobically for 48 hours (atmosphere of 85% N_2, 10% CO_2, 5% H_2), and visually scoring the colony periphery for yellow halos. Siderophore production was also monitored during aerobic growth in liquid *Shewanella* growth medium with lactate as electron donor. Liquid culture aliquots of 0.5 mL were centrifuged for 1 min (12,000 *g*), and the resulting supernatant was mixed with 0.5 mL CAS shuttling solution and allowed to incubate for 3 hours. Samples were subsequently measured spectrophotometrically at 630 nm to determine siderophore production. Absorbance readings are recorded as the absorbance of the CAS-treated sample divided by the absorbance of CAS-treated uninnoculated growth medium.

5.3.7 Determination of overall respiratory capability of *S. oneidensis* and Sol mutants

S. oneidensis wild-type and Sol mutants were inoculated in liquid *Shewanella* growth medium (final concentration of 10^7 cells mL^{-1}) amended with either 18 mM lactate or 60 mM formate as electron donor and either saturated O_2, 15 mM nitrate, 50 mM dimethylsulfoxide (DMSO), 25 mM trimethylamine-*N*-oxide (TMAO), 10 mM fumarate, 10 mM thiosulfate, 50 mM Fe(III)-citrate, or 20 mM 2L-ferrihydrite as electron acceptor. For growth with O_2 as electron acceptor, compressed air was vigorously bubbled through the flasks. Anaerobic conditions were maintained by continuous sparging with N_2 (g). Cell growth was monitored by absorbance measurements at 600 nm

over time. Nitrite (NO_2^-) concentrations in nitrate-grown cultures, were monitored by 250-fold aliquot dilution in a solution consisting of 9.6 mM sulfanilic acid, 96 mM $KHSO_4$, and 3.2 mM N,N-ethylenediamine (Montgomery and Dymock 1962). Samples were held in the dark for 15 minutes prior to absorbance measurements at 510 nm. Fe(III) reduction was determined from total Fe(II) production over time monitored by the Ferrozine technique (Stookey 1970) after extraction with HCl (Lovley and Phillips 1986). Cell growth was monitored by direct cell counts via epifluorescence microscopy. Acridine orange-stained cells were counted (Carl Zeiss AxioImager Z1 Microscope) according to previously described procedures (Lovley and Phillips 1988).

5.4 Results

Soluble organic-Fe(III) was produced by *S. oneidensis* liquid cultures incubated anaerobically with 2L-ferrihydrite, or with 2L-ferrihyrite and the alternate electron acceptor fumarate, but not in the presence of O_2, NO_3^-, or TMAO (Fig. 5.2). Anaerobic abiotic control incubations indicate that soluble organic-Fe(III) was not produced by interaction with lactate or any other component of the *Shewanella* growth medium (data not shown). Voltammetric signals indicative of soluble organic-Fe(III) were detected after an initial lag phase (16 h) and reached a maxima of 252 ± 17 nA for 2L-ferrihydrite alone. In turn, the incubation containing 2L-ferrihydrite and the alternate electron acceptor fumarate produced a soluble organic-Fe(III) signal after 8 hours which reached a maximum of 425 ± 10 nA at 52 hours. The rates of soluble organic-Fe(III) production in incubations of 2L-ferrihydrite with fumarate and the 2L-ferrihydrite alone were not significantly different, suggesting that the same solubilization process was involved in

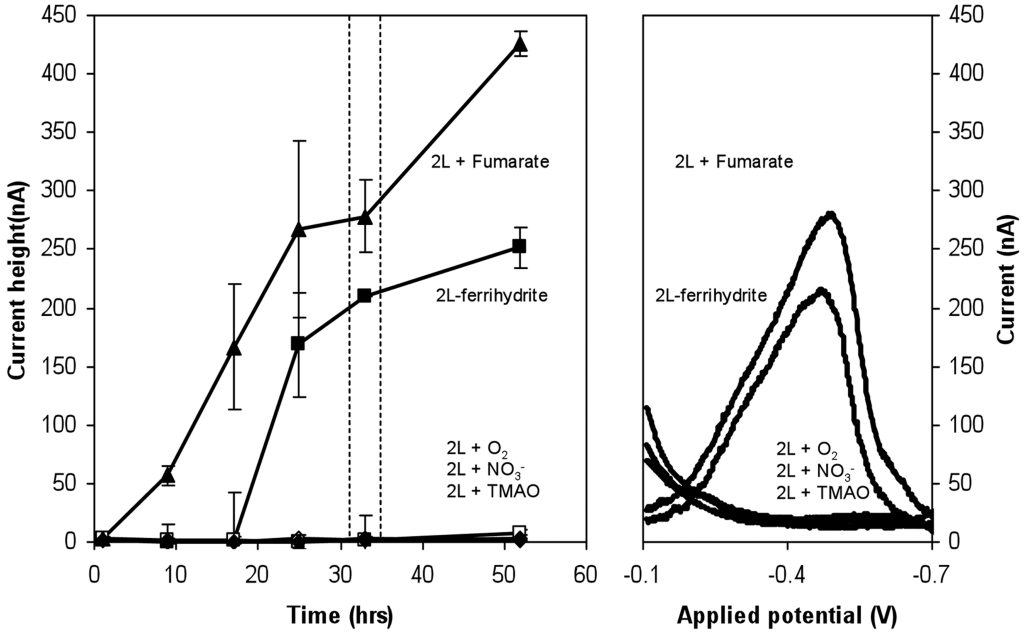

Figure 5.2 - Production of soluble organic-Fe(III) by wild-type *S. oneidensis* incubated anaerobically with lactate as electron donor and 2L-ferrihydrite as electron acceptor or with 2L-ferrihydrite in the presence of alternate electron acceptors O_2, NO_3^-, TMAO, and fumarate. 2L-ferrihydrite (■), O_2 + 2L-ferrihydrite (□), NO_3^-,+ 2L-ferrihydrite (◆), TMAO + 2L-ferrihydrite (◇), fumarate + 2L-ferrihydrite (▲).

these incubations. No voltammetric signal was observed after 52 hours in incubations containing 2L-ferrihydrite and the alternate electron acceptors O_2, NO_3^-, or TMAO.

A mercury-gold (Hg/Au) MicroElectrode Screening Array (MESA) was constructed to identify EMS-mutagenized strains of *S. oneidensis* for their inability to produce soluble organic-Fe(III) during anaerobic incubation with 2L-ferrihydrite (Fig. 5.1). The voltammograms resulting from wild-type *S. oneidensis* cultures incubated in 96-well trays were identical to those observed with single electrode systems for dissolved oxygen and Mn^{2+} standards in 0.25 M NaCl (data not shown). Initially, rows of EMS-mutagenized strains were alternated with rows of 0.25 M NaCl blanks to wash the electrodes and check for inadvertent transfer of cells between rows. Control experiments

with wild-type *S. oneidensis* indicated that inadvertent transfer was not a problem (data not shown), and the washing step was omitted in subsequent Sol mutant screening experiments. The first row of a tray contained wild-type *S. oneidensis* to ensure that conditions for wild-type organic-Fe(III) production were maintained during the 36 h anaerobic incubation period. The next row of the tray contained *Shewanella* growth medium with cells omitted (abiotic control). Finally, the last ten rows of the tray contained mutagenized cells.

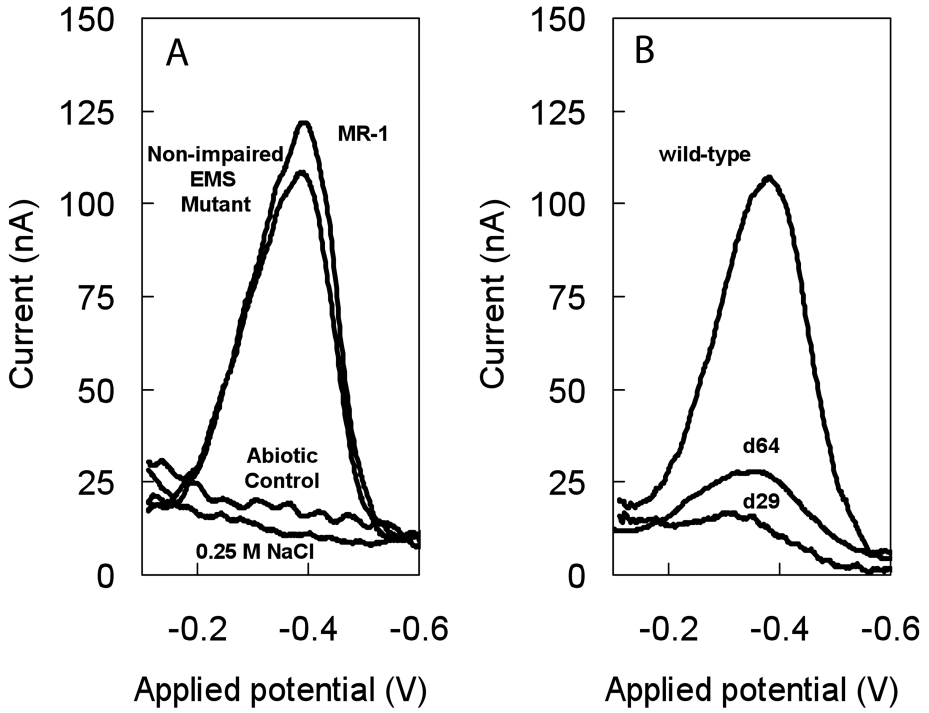

Figure 5.3 - Voltammetric signals obtained from liquid cultures of wild-type *S. oneidensis* and a randomly selected, non-impaired EMS mutant (A) and Sol mutants d29, d64, H1, and B7 (B) incubated anaerobically in *Shewanella* growth medium supplemented with lactate as electron donor and 2L-ferrrihydrite as electron acceptor.

A total of 3840 EMS mutants were screened via MESA for the ability to produce soluble organic-Fe(III). Four putative Sol mutants (designated d29, d64, H1, and B7) were identified with impaired soluble organic-Fe(III) production activity (defined as

<50% wild-type activity) (Fig.3b). Wild-type *S. oneidensis* produced current intensities of 88.2 (± 31.9) nA, while the 3836 non-impaired, EMS-mutagenized strains produced current intensities of 102.7 (± 34.2) nA (abiotic controls produced current intensities <2% of wild-type *S. oneidensis*) (Table 5.1). Current intensities increased with time as cultures were in the growth phase. As a consequence, non-impaired mutants, analyzed last during screening, generally produced higher current intensities than wild-type *S. oneidensis*.

Table 5.1 - Average current intensities of soluble organic-Fe(III) production measured by MESA in the presence of wild-type *S. oneidensis* and Sol mutants d29, d64, H1, and B7 compared to other non-impaired EMS mutants

Sample	Current (nA)*	% wild-type	S.D.**	n
Wild-type MR-1	88.2	-	31.9	384
Abiotic control***	1.9	2%	3.4	384
Sol mutant d29	24.2	27%	4.3	5
Sol mutant d64	14.6	17%	1.8	5
Sol mutant H1	40.4	46%	5.0	5
Sol mutant B7	9.0	10%	1.6	5
All other non-impaired EMS mutants****	102.7	116%	34.2	3836

*Current intensities were normalized to a 200 uM Mn(II) standard.
**Standard deviations of the average current intensities are reported for n measurements.
*** Incubation of 2L-ferrihydrite with cells omitted.
**** Average current intensities of the remaining 3,836 mutants screened.

To confirm the Sol mutant phenotype, each of the four Sol mutants was incubated individually in *Shewanella* growth medium amended with 2L-ferrihydrite. Soluble organic-Fe(III) was observed in wild-type *S. oneidensis* incubations by 18 hours and reach steady state value of 350 nA after 60 hours (Fig. 5.4a). The Sol mutants d29 and H1 produced organic-Fe(III) signals late in the experiment reaching maximum current

intensities of 200 nA and 125 nA. No significant organic-Fe(III) signals were produced by the Sol mutants d64 or B7. Fe(III) reduction in wild-type *S. oneidensis* incubations reach a maximum of 20 mM Fe(II) (Fig. 5.4b). Sol mutants d29, H1, and d64 produced maximums of 10 mM, 14 mM, and 2.5 mM Fe(II). The Sol mutant B7 produced no Fe(II) over the course of the experiment.

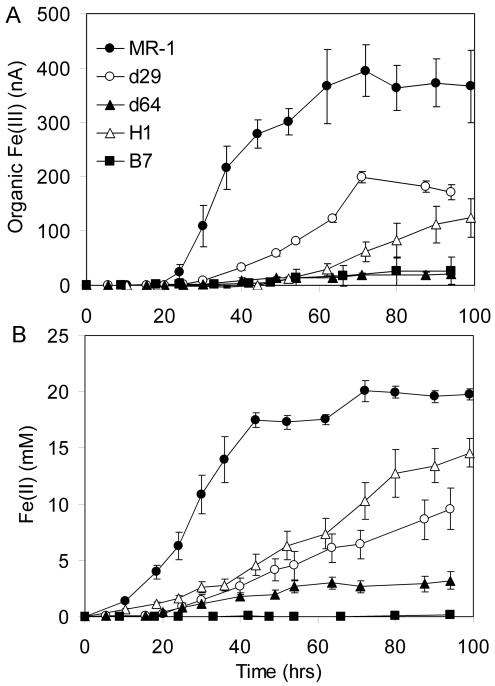

Figure 5.4 - Anaerobic incubations of wild-type *S. oneidensis* (MR-1) and Sol mutants d29, d64, H1, and B7 in batch reactors amended with lactate as electron donor and 2L-ferrihydrite as electron acceptor: production of soluble organic-Fe(III) (A) and total Fe(II) (B) as a function of time. Error bars represent standard deviations calculated from three parallel yet independent anaerobic incubations. *S. oneidensis* MR-1 (●) and Sol mutants: d29 (○), d64 (▲), H1, (△), and B7 (■).

Wild-type *S. oneidensis* produced soluble organic-Fe(III) at an initial rate of 21.5 nA L mg protein^{-1} hr^{-1}, while all Sol mutants produced soluble organic Fe(III) at rates lower than the wild-type strain (% of wild-type rate in parentheses): d29 (35%), d64 (3%), H1 (25%), and B7 (1%) (Table 5.2). Wild-type *S. oneidensis* produced Fe(II) at a

rate of 855 mmol mg protein^{-1} hr^{-1}, while all Sol mutants produced Fe(II) at rates lower than the wild-type strain (% of wild-type rate in parentheses): d29 (32%), d64 (9%), H1 (58%), and B7 (1%) (Table 5.2). The initial rates of Fe(III) reduction and organic-Fe(III) production were highly correlated with a R^2 greater than 0.8 and a slope of 24 (± 4) nA organic-Fe(III) mM^{-1} Fe(II) (Fig. 5.5).

Table 5.2 - Rates of production of soluble organic-Fe(III) and Fe(II) by *S. oneidensis* wild-type and Sol mutants

Strain	Soluble organic-Fe(III) production		Fe(II) production	
	Rate (nA L mg protein^{-1} hr^{-1})	% wild-type	Rate (mmol mg protein^{-1} hr^{-1})	% wild-type
Wild-type MR-1	21.5 ± 3.5	-	855 ± 74	-
Sol mutant d29	7.5 ± 1.9	35 ± 11	275 ± 28	32 ± 4
Sol mutant d64	0.6 ± 0.2	3 ± 1.6	78 ± 20	9 ± 2.5
Sol mutant H1	5.3 ± 2.9	25 ± 15	500 ± 114	58 ± 14
Sol mutant B7	0.2 ± 0.1	1 ± 1.0	13 ± 5	1 ± 0.4

The overall respiratory activity of the EMS mutants was tested on combinations of two electron donors and nine electron acceptors (Table 5.3). Sol mutants d29 and d64 grew at wild-type rates on O_2, NO_3^-, NO_2^-, DMSO, TMAO, fumarate, and $S_2O_3^{2-}$ as electron acceptor (S 5.1), yet were unable to grow at wild-type rates on either 2L-ferrihydrite (Fig. 5.6) or Fe(III) citrate (Fig. 5.7), regardless of electron donor. Sol mutants H1 and B7 displayed growth deficiencies on 2L-ferrihydrite (Fig. 5.6) and Fe(III) citrate (Fig. 5.7) and nearly the entire spectrum of anaerobic electron acceptors (except for B7, which retained NO_3^-, NO_2^-, and $S_2O_3^{2-}$ respiratory capability).

Table 5.3 Respiratory capabilities* of *S. oneidensis* wild-type, anaerobic respiratory mutant T121, and Sol mutants with impaired organic-FeIII) production activity

	O_2		NO_3^-		NO_2^-		DMSO		TMAO		Fumarate		$S_2O_3^{2-}$		Fe(III)-Cit		Fe(III)-Ox	
Strains	L	F	L	F	L	F	L	F	L	F	L	F	L	F	L	F	L	F
Wild-type MR-1	+	+	+	+	+	+	+	+	+	+	+	+	+	+	+	+	+	+
T121	+	+	-	-	-	-	-	-	-	-	-	-	-	-	-	-	-	-
Sol mutant d29	+	+	+	+	+	+	+	+	+	+	+	+	+	+	-	-	-	-
Sol mutant d64	+	+	+	+	+	+	+	+	+	+	+	+	+	+	-	-	-	-
Sol mutant H1	+	+	-	-	-	-	-	-	-	+	-	-	-	-	-	-	-	-
Sol mutant B7	+	+	+	+	+	+	-	-	-	+	-	-	+	+	-	-	-	-

*Respiratory capability: +, >50% wild-type growth rate; -, <50% wild-type growth rate
Electron donors: L = lactate, F = formate; Electron acceptors: O_2 = oxygen, NO_3^- = nitrate, NO_2^- = nitrite, DMSO = dimethyl sulfoxide,
TMAO = trimethylamine oxide, $S_2O_3^{2-}$ = thiosulfate, Fe(III)-Cit = ferric citrate, Fe(III)-Ox = 2L-ferrihydrite.

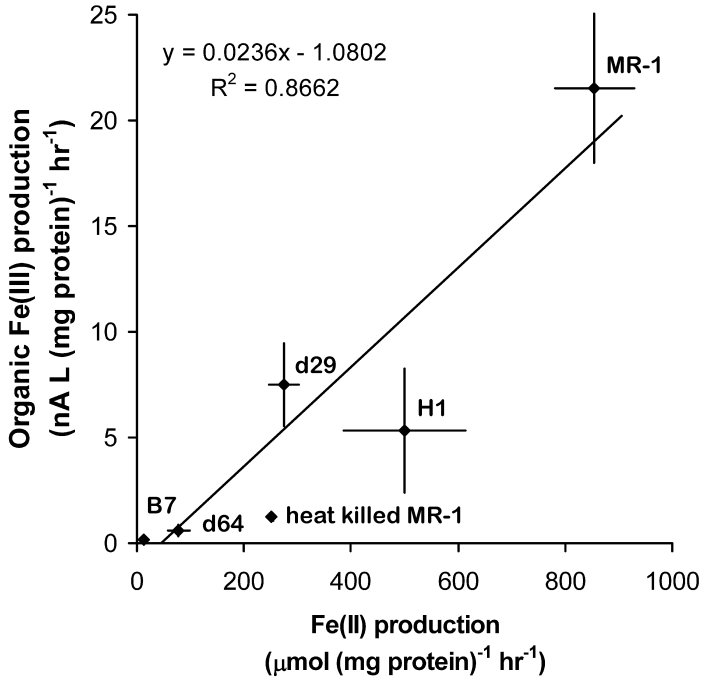

Figure 5.5 - Correlation between initial rates of organic-Fe(III) production and initial rates of Fe(III) reduction by wild-type *S. oneidensis* and Sol mutants d29, d64, H1, and B7 incubated anaerobically with lactate as electron donor and 2L-ferrihydrite as electron acceptor.

Chrome azurol S (CAS) was used to determine if the Sol mutants were impaired in siderophore production activity. Measurement of siderophore production activity during cell growth in aerobic liquid cultures indicated that the Sol mutants produced

siderophores at wild-type rates (Fig. 5.8) with the exception of H1 that produced siderophore at 50% of the wild-type rate. On CAS infused agar, under aerobic and anaerobic (S 5.2) conditions, all four Sol mutants produced a yellow halo in the colony periphery that was similar in size to that produced by wild-type *S. oneidensis*, an indication that the Sol mutants retained siderophore production activity.

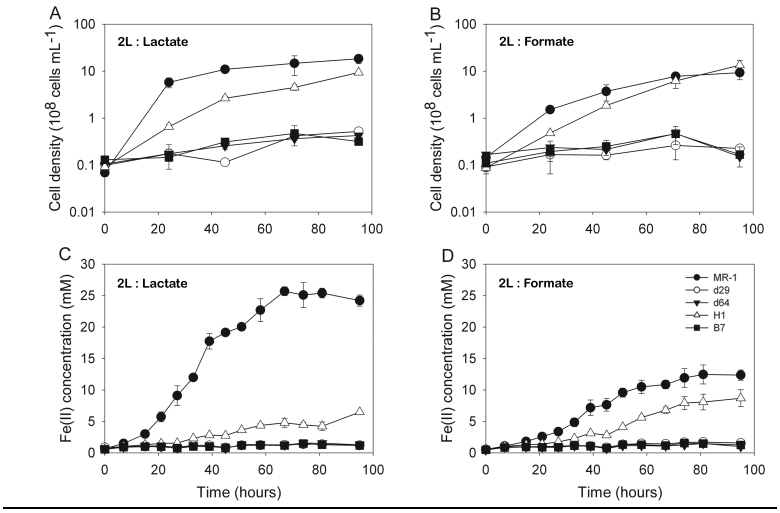

Figure 5.6 - Anaerobic incubations of wild-type *S. oneidensis* (MR-1) and Sol mutants d29, d64, H1, and B7 in batch reactors amended with lactate or formate as electron donor and 2L-ferrihydrite as electron acceptor: cell density as a function of time with lactate (A) or formate (B) as electron donor, Fe(II) concentration as a function of time with lactate (C) or formate (D) as electron donor. *S. oneidensis* MR-1 (●) and Sol mutants: d29 (○), d64 (▲), H1, (△), and B7 (■).

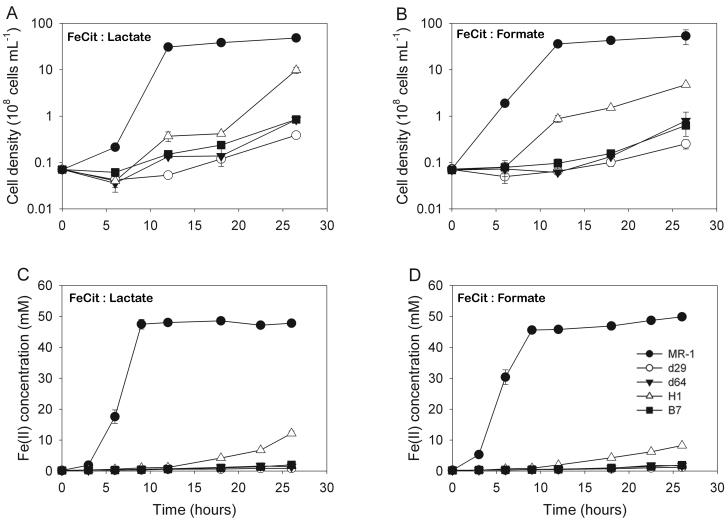

Figure 5.7 - Anaerobic incubations of wild-type *S. oneidensis* (MR-1) and Sol mutants d29, d64, H1, and B7 in batch reactors amended with lactate or formate as electron donor and Fe(III)-Citrate as electron acceptor: cell density as a function of time with lactate (A) or formate (B) as electron donor, Fe(II) concentration as a function of time with lactate (C) or formate (D) as electron donor. *S. oneidensis* MR-1 (●) and Sol mutants: d29 (○), d64 (▲), H1, (△), and B7 (■).

5.5 Discussion

The use of Au/Hg voltammetric microelectrodes in studies of bacterial respiratory processes is a relatively new application (Dollhopf et al. 2000; Taillefert et al. 2007). These devices have been used to follow iron and manganese reduction in batch reactors incubated with *Shewanella* species (Dollhopf et al. 2000), including the production of soluble organic-Fe(III) as an intermediate in the reduction of Fe(III) oxides (Taillefert et al. 2007). Results of the present study expand the range of *Shewanella* species capable of producing soluble organic-Fe(III) to include *S. oneidensis* MR-1. In addition, this study is the first to apply Au/Hg voltammetric microelectrodes as a screening technique to identify mutants with impaired ability to produce soluble organic-Fe(III).

Fe(III) respiratory pathways that include an initial step of non-reductive Fe(III) dissolution may provide several advantages over direct contact pathways, including raising the reduction potential of the electron acceptor to conserve more energy (Taillefert et al. 2007; Zinder et al. 1986); lowering the activation energy of the intermediate to increase reduction rates (Taillefert et al. 2007; Wang et al. 2008); binding Fe(II) products to prevent passivation of Fe(III) mineral surfaces by Fe(II) adsorption (Royer et al. 2004; Roden 2006); or providing a bioavailable electron acceptor that may interact with periplasmic- or inner membrane-localized Fe(III) reductases (Furrer and Stumm 1986; Duckworth and Martin 2001). This study reveals that, soluble organic-Fe(III) is produced by *S. oneidensis* cultures incubated anaerobically with Fe(III) oxides, or with Fe(III) oxides and the alternate electron acceptor fumarate, but not in the presence of O_2, NO_3^-, or TMAO. These results suggest that soluble organic-Fe(III) production by *S. oneidensis* MR-1 may be regulated by the redox potential of terminal electron acceptors. Soluble organic-Fe(III) is produced when grown on terminal electron acceptors with reduction potentials (E_o) around +0.05 V, the reduction potential of fumarate and 2L-ferrihydrite, but is not produced in the presence of electron acceptors with E_o values greater than +0.15 V (TMAO). Such a correlation was recently reported for *c*-type cytochrome maturation (CCM)-dependent metal respiration by *S. putrefaciens* 200 (Dale et al., 2007). A conserved histidine in cytochrome *c* maturation permease CcmB was required for anaerobic growth below a threshold E_o value of +0.36 V (NO_3^- /NO_2^- couple). Additional research will be required to determine if soluble organic-Fe(III) production by *S. oneidensis* is also regulated by E_o of the electron acceptor.

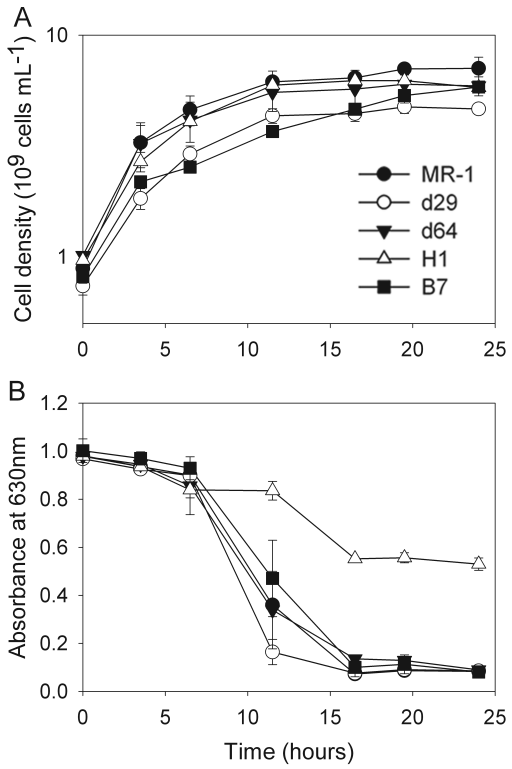

Figure 5.8 - Siderophore production during growth under aerobic conditions by wild-type *S. oneidensis* (MR-1) and Sol mutants d29, d64, H1, and B7 in batch reactors with lactate as electron donor: cell density as a function of time (A) and absorbance at 630 nm of CAS-treated samples to monitor siderophore production (B). Decrease in absorbance of CAS complex at 630 nm is indicative of siderophore production. *S. oneidensis* MR-1 (●) and Sol mutants: d29 (○), d64 (▲), H1, (△), and B7 (■).

The newly developed MESA is able to measure small sample volumes (less than 100 uL) rapidly (2 hours per tray containing 96 mutagenized strains) and could be applied to multivariate analysis of biological and/or chemical reactions involving voltammetrically active species such as O_2, Fe^{2+}, Mn^{2+}, ΣH_2S, Cu^{2+}, Cd^{2+}, Pb^{2+}, and Zn^{2+}. Chemical mutagenesis procedures were combined with MESA to screen 3840 EMS-mutagenized strains for production of soluble organic-Fe(III). Four Sol mutants (designated d29, d64, H1, and B7) were identified with impaired ability to produce soluble organic-Fe(III) during anaerobic incubation with Fe(III) oxides (Fig. 5.4).

The Fe(III)-chelating ligand has not been characterized but may originate from a variety of sources, including siderophores produced for Fe(III) assimilation, organic compounds resulting from cell lysis, or endogenous ligands specifically produced for Fe(III) respiration. While the typical binding strength of siderophores may make them inappropriate for respiratory processes, the biochemical reactions involved in Fe(III) assimilation (Wandersman and Delepelaire 2004) are similar to those proposed for Fe(III) solubilization and respiration (Dichristina et al. 2005). Both mechanisms include the biosynthesis of Fe(III)-chelating ligands, export of the ligands from the cell, solubilization of extracellular Fe(III) substrates, and reduction of the solublized Fe(III) via intracellular (assimilatory) or outer membrane-localized (dissimilatory) Fe(III) reductases. In the case of siderophores, however, the reductase destabilizes the Fe(III)-siderophore complex to facilitate iron removal for subsequent biochemical reactions, while the respiratory Fe(III) reductase is hypothesized to be the final step of the Fe(III)-reducing, electron transport chain (DiChristina et al., 2005; Shi et al., 2006). The siderophore production activity of three of the Sol mutants (d29, d64, and B7) is identical to wild-type *S. oneidensis* during aerobic growth (Fig. 5.8), an indication that these Sol mutants are not impaired in siderophore biosynthesis. The 50% siderophore production observed by the Sol mutant H1 suggests the mutation is not in the siderophore production pathway but a general impairment to the metabolic pathway. The positive signal for siderophore production on CAS infused agar by the Sol mutants under anaerobic conditions (S 5.2) is attributed to the removal of CAS-bound Fe(III) by the chelating ligand produced during anaerobic respiration of Fe(III) as no other electron acceptor is present in these incubations. Inadvertent cell lysis is also a possible source of Fe(III)-

binding organic ligands including flavins, quinones, organic acids, organo-phosphates, and cytochromes (Hirst et al., 1999; Myers and Myers, 2004; von Canstein et al., 2008). However, soluble organic-Fe(III) is not produced by *S. oneidensis* cultures grown in the presence of 2L-ferrihydrite and the alternate electron acceptors O_2, NO_3^-, or TMAO. Soluble organic-Fe(III) complexes are also not produced by heat-killed, wild-type *S. oneidensis* cultures incubated anaerobically with 2L-ferrihydrite (Fig. 5.5). These results suggest that cell lysis products or respiration by-products are not significant sources of the voltammetric signal associated with soluble organic-Fe(III) production during anaerobic respiration of 2L-ferrihydrite.

Although the voltammetric current response should be proportional to the concentration of soluble organic-Fe(III) complexes, the exact concentration of soluble organic-Fe(III) can not be determined as unknown Fe(III)-ligand complexes can not be

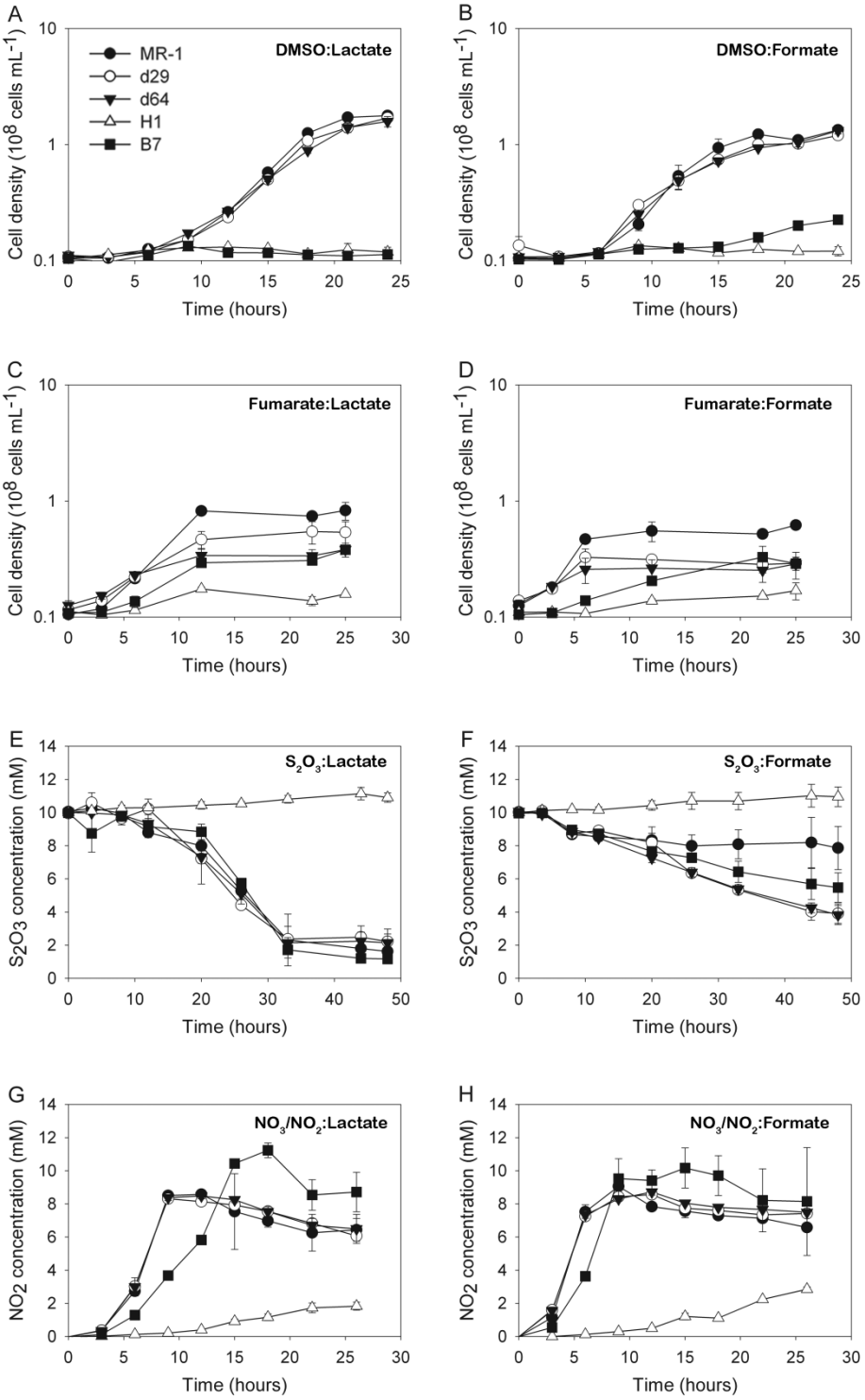
A
DMSO:Lactate
MR-1
d29
d64
H1
B7
Cell density (10^8 cells mL^{-1})
Time (hours)
B
DMSO:Formate
C
Fumarate:Lactate
D
Fumarate:Formate
E
S_2O_3:Lactate
S_2O_3 concentration (mM)
F
S_2O_3:Formate
G
NO_3/NO_2:Lactate
NO_2 concentration (mM)
H
NO_3/NO_2:Formate

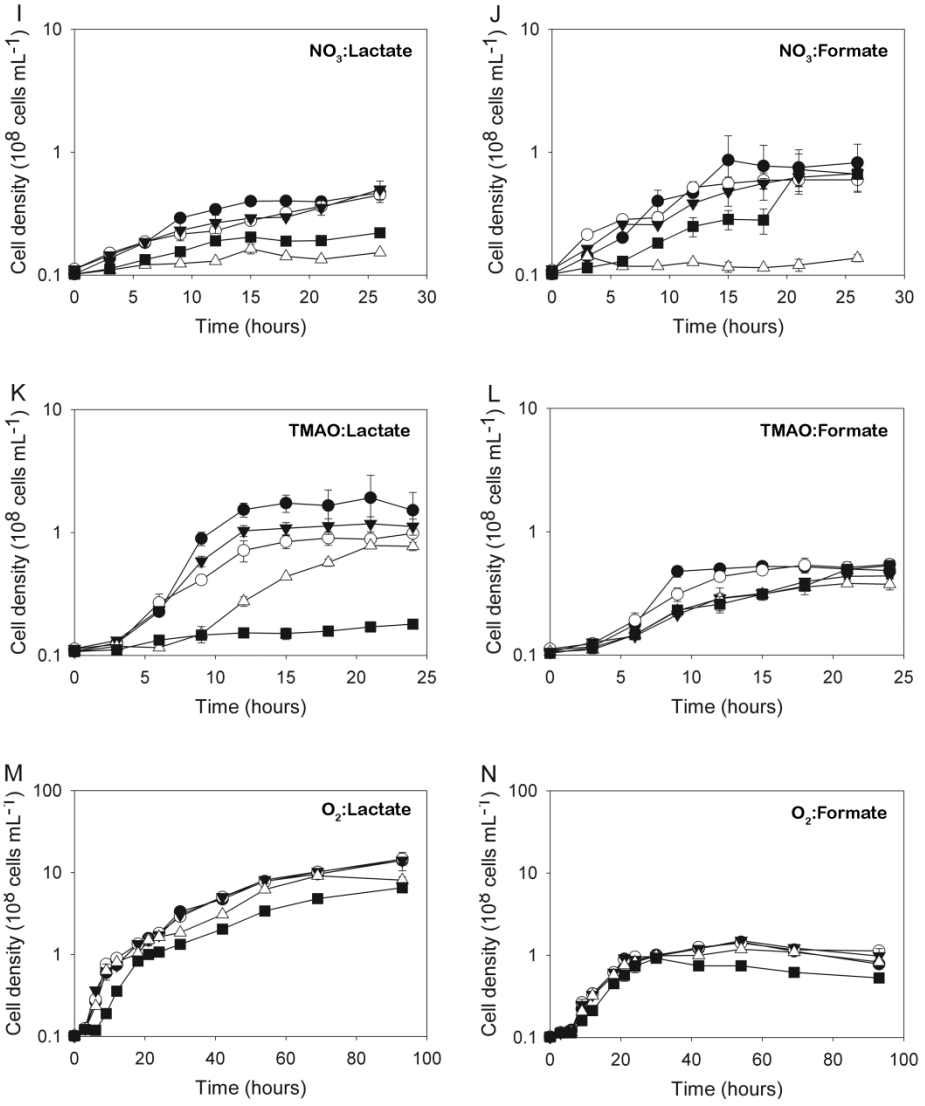

Figure 5.9 - Respiratory capability of wild-type *S. oneidensis* (MR-1) and Sol mutants d29, d64, H1, and B7 on a set of alternate electron donors and acceptors. Cell density as a function of time with DMSO as electron acceptor and either lactate (A) or formate (B) as electron donor. Cell density as a function of time with fumarate as electron acceptor and either lactate (C) or formate (D) as electron donor. $S_2O_3^{2-}$ concentration as a function of time with $S_2O_3^{2-}$ as electron acceptor and either lactate (E) or formate (F) as electron donor. NO_2^- concentration as a function of time with NO_3^- as electron acceptor and either lactate (G) or formate (H) as electron donor. Cell density as a function of time with NO_3 as electron acceptor and either lactate (I) or formate (J) as electron donor. Cell density as a function of time with TMAO as electron acceptor and either lactate (K) or formate (L) as electron donor. Cell density as a function of time with O_2 as electron acceptor with either lactate (M) or formate (N) as electron donor. *S. oneidensis* MR-1 (●) and Sol mutants: d29 (○), d64 (▲), H1, (△), and B7 (■).

directly quantified by voltammetry (Taillefert et al. 2000a). The initial rate of soluble organic-Fe(III) production (21.5 nA L mg protein^{-1} hr^{-1}), however, correlates strongly (R^2 = 0.8) with the initial rate of Fe(II) production (855 mmol mg protein^{-1} hr^{-1}) by the *S. oneidensis* wild-type (24 nA soluble organic-Fe(III) per mM Fe(II)) and Sol mutant strains (Fig. 5). This finding suggests that respiration of Fe(III) oxides proceeds via a non-reductive, Fe(III) solubilization step prior to reduction of the produced, soluble organic-Fe(III) complex. While other pathways can not be ruled out, soluble organic-Fe(III) is reduced at rates up to 20 times faster than sparingly soluble Fe(III) substrates (Arnold et al. 1988; Lovley and Woodward 1996). If another respiration pathway were to precede the solubilization of Fe(III) oxides, the more favorable soluble Fe(III) reduction should rapidly overtake a slower pathway to become the dominant mechanism of Fe(III) reduction. The energetic cost of ligand biosynthesis, however, must be offset by greater energetic return though the Fe(III)-solubilization pathway. For instance, it has been suggested the energy spent to synthesize Fe(III)-binding ligands may be recovered by increased rates of electron transfer to Fe(III) in biofilms (Marsili et al. 2008). A group of cells working in concert to cycle ligands intercellularly may also maximize the advantages of solubilization while minimizing the biosynthetic cost of ligand production.

The four Sol mutants were tested for growth on combinations of two electron donors (lactate or formate) and nine electron acceptors (O_2, NO_3^-, NO_2^-, DMSO, $S_2O_3^{2-}$, TMAO, fumarate, soluble Fe(III)-citrate or Fe(III)-oxide) (Table 3, S1). Two of the four Sol mutants (H1 and B7) display anaerobic growth deficiencies on a broad spectrum of

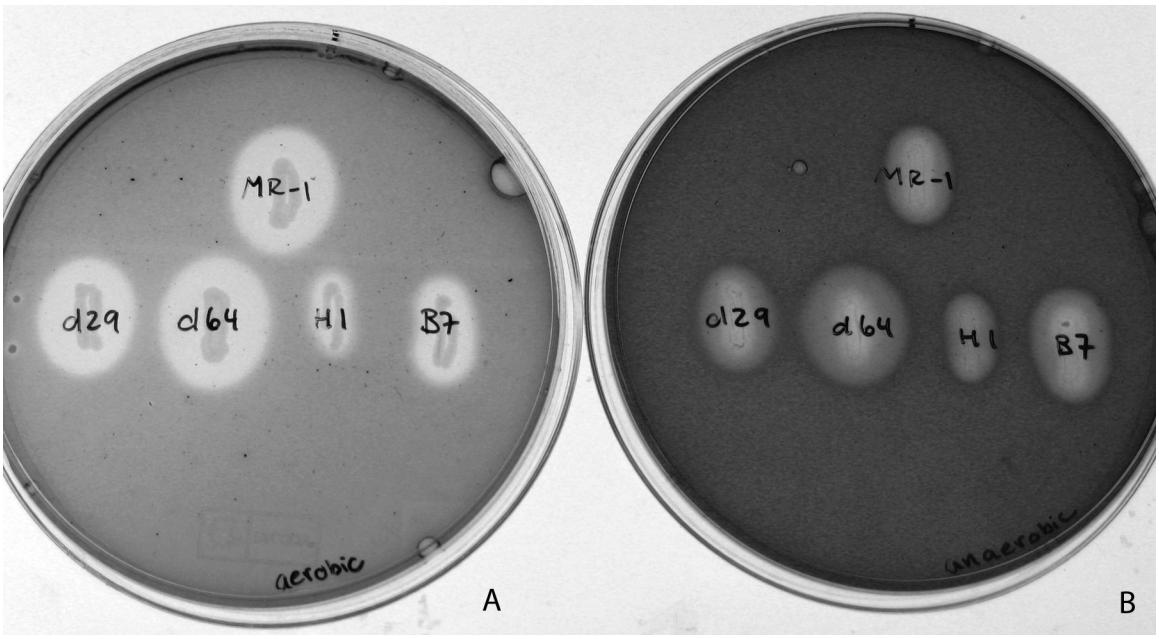

Figure 5.10 - Chrome Azurol-S (CAS) plates incubated aerobically (A) and anaerobically (B) for 24-36 hours with wild-type *S. oneidensis* and Sol mutants d29, d64, H1, and B7. Note yellow halo surrounding colonies indicative of production of an Fe(III)-chelating ligand.

electron acceptors (regardless of electron donor). The pleiotropic respiratory deficiencies displayed by Sol mutants H1 and B7 are identical to those displayed by other *S. oneidensis* and *S. putrefaciens* respiratory mutants previously identified for their inability to respire Fe(III), Mn(IV), U(VI), Se(IV) or Tc(VII) (DiChristina and Delong, 1994; Burnes et al., 1998; Taratus et al., 2000; Wade and DiChristina, 2000; Payne and DiChristina, 2006). Such mutants are postulated to contain mutations in regulatory components required for anaerobic gene expression (Saffarini et al. 1994). Sol mutants d29 and d64, on the other hand, are unable to respire or grow with 2L-ferrihydrite (Fig. 5.6) or soluble Fe(III)-citrate (Fig. 5.7), yet retain the ability to respire the remaining seven alternate electron acceptors (regardless of electron donor). The lack of growth, soluble organic-Fe(III) production, and iron reduction capability suggest that at least one

component of the soluble organic-Fe(III) production system is a part of the Fe(III) respiratory pathway of *S. oneidensis* and indicate that the production of soluble organic-Fe(III) may be an important intermediate step in the anaerobic respiration of both soluble and sparingly soluble forms of Fe(III) by *S. oneidensis*. The formation of endogenous organic-Fe(III) by *S. oneidensis* when provided a soluble Fe(III) substrate suggests the endogenous ligand is not only required for solubilization of solid Fe(III) but is also required for soluble Fe(III) respiration. These results suggest that a ligand exchange reaction between endogenous and exogenous organic ligands (e.g., citrate) is required for soluble Fe(III) respiration. Current work is focused on genetic complementation analysis of the Sol mutants to identify the genes required for production of soluble organic-Fe(III) during anaerobic Fe(III) respiration by *S. oneidensis*.

5.6Acknowledgements

We would like to thank Jordon Beckler, Justin Burns, Patrick Wilson, Porntawee Aphivantrakul, Ewelina Kieley, and Lindsey Miller for their help during this project. This work was supported by the National Science Foundation (OCE-0433941) and a REU supplement (EAR-0525438).

CHAPTER 6

CHARACTERIZATION OF ORGANIC-FE(III) COMPLEXES BY COMPLETITIVE LIGAND EQUILIBATION PRODUCED DURING REDUCTION OF FE(III) BY *SHEWANELLA ONEIDENSIS* MR-1

6.1 Abstract

The facultative anaerobes *Shewanella putrefaciens* 200 and *Shewanella oneidensis* MR-1 produce organic-Fe(III) complexes during dissimilatory iron reduction (DIR), suggesting that *Shewanella* employs the non-reductively dissolve iron oxides to transfer electrons to this terminal electron acceptor. Unfortunately, the concentration of these complexes cannot be determined directly without knowing the organic ligand involved. In such conditions, competitive ligand equilibration adsorptive cathodic stripping voltammetry (CLE-ACSV) has been used to determine the concentrations of iron-binding ligands, the concentration of organic-Fe(III) complexes, and the conditional stability constants of these complexes in open ocean waters, estuaries, and recently coastal sediments. In this study, the production of organic-Fe(III) complexes by the wild-type and known iron reduction mutants of *S. oneidensis* is investigated to gain more insights on the mechanism of production of the endogenous organic ligand. Results reveal that the the type-II secretion system is required for both the solubilization of Fe(III) and Fe(III) reduction. In turn, the outer membrane c-type cytochromes MtrC and OmcA are not required for Fe(III) solubilization but are necessary for Fe(III) reduction.

The production of endogenous organic ligands for the solubilization of Fe(III) is enhanced by the addition of organic substrates (fumarate or yeast extract) to microbial incubations. The organic ligands can be cycled 12 to 50 times between the cell and mineral surface helping to offset the energetic cost of ligand synthesis. Together these results suggest the chelation pathway for the DIR of iron oxides involves endogenous production of organic ligands, followed by the solubilization of Fe(III), and the reduction of the organic-Fe(III) complex.

6.2 Introduction

6.2.1 Dissimilatory iron reduction

Dissimilatory iron reducing bacteria (DIRB) constitute an important class of microorganisms in terrestrial environments as they are able to respire a suite of sparingly soluble iron oxides, including 2L-ferrihydrite, goethite, and hematite (Arnold et al. 1986; Roden and Zachara 1996; Lovley 1997), that regulate the distribution and mobility of toxic metals and radionuclides (Nealson and Saffarini 1994; Lovley et al. 2004; Gralnick and Newman 2007). In addition, dissimilatory iron reduction (DIR) is a deeply rooted process throughout the domains of *Archaea* and *Bacteria* and may represent one of the first respiratory processes on Early Earth, prior to the oxygenation of the atmosphere by oxygenic photosynthesis (Vargas et al. 1998; Weber et al. 2006). At that time Fe(III) was a soluble electron acceptor with a redox potential rivaling oxygen (+0.76 V). As a result of the rise in pH associated with the onset of oxygenic photosynthesis, however, the solubility of Fe(III) diminished, exposing DIRB to the unique challenge of having to transfer electrons to a solid terminal electron acceptor.

The mechanism of electron transfer to solid iron oxides remains poorly constrained, and three mechanisms have been proposed to explain the different observations made during growth on ferric iron as substrate: 1) the direct contact between a terminal reductase on the cell surface and the mineral (Myers and Myers 1992; DiChristina et al. 2002); 2) nanowire appendages or pili that conduct electrons from the cell to the mineral (Reguera et al. 2005; Gorby et al. 2006); and 3) electron shuttling compounds that are reduced by the cell and then chemically reoxidized by iron oxide (Newman and Kolter 2000; Coates et al. 2002). These pathways are also theorized to be involved in the transfer of electrons in microbial fuel cells (Logan et al. 2006).

Several proteins involved in the transfer of electrons to the outer membrane have been identified in *Shewanella* species. First, the type-II secretion system appears to be required for DIR, as deletion of the GspD multimeric channel protein inhibits reduction of Fe(III) and Mn(IV), presumably due to the inability to secrete components of the terminal reductase to the outer membrane (DiChristina et al. 2002). Second, a MtrABC trans outer-membrane protein complex has been identified and proposed to deliver electrons from the periplasm to the mineral surface. In this complex, MtrB is a β-barrel porin spanning across the outer membrane (Ross et al. 2007; Hartshorne et al. 2009). The decaheme cytochrome MtrA is associated with MtrB on the periplasmic side of the outer membrane (Ross et al. 2007; Hartshorne et al. 2009), while the decaheme cytochrome MtrC, located on the outside of the outer membrane, has been theorized to be the terminal reductase in dissimilatory iron reduction (Myers and Myers 1992). Finally, the outer membrane decaheme OmcA is a homolog of MtrC that may be able to accept electrons

from the MtrABC complex (Shi et al. 2006). Deletion of these proteins has been demonstrated to disrupt DIR; however, the terminal reductase has yet to be isolated.

In addition to these three mechanisms, a solubilization pathway has been proposed to be involved in the reduction of sparingly soluble iron oxides. In this mechanism, organic ligands produced by the organism, non-reductively dissolve iron oxide minerals and produce soluble organic-Fe(III) complexes that are respired by the organism (Taillefert et al. 2007). Several lines of evidence suggest that the anaerobic respiration of iron oxides may require a solubilization step. First, organic-Fe(III) complexes have been observed by voltammetry with gold amalgam microelectrodes in the zones of iron reduction in porewaters of redox stratified sediments (Brendel and Luther 1995; Taillefert et al. 2000a; Taillefert et al. 2002, Chapter 4 of this thesis), suggesting that they may be produced by a wide variety of metal-reducing bacteria. Second, soluble forms of Fe(III) are reduced more rapidly than solid iron oxides (Arnold et al. 1988), thus providing a distinct advantage over the direct contact and electron shuttling pathways. Third, a similar mechanism is involved in iron assimilation, suggesting that organisms acquiring iron have evolved similarly. Finally, the facultative anaerobes *Shewanella oneidensis* MR-1 and *Shewanella putrefaciens* produce organic-Fe(III) during DIR (Taillefert et al. 2007; Chapter 5 of this thesis).

Much of the previous work investigating the production of organic-Fe(III) complexes during dissimilatory iron reduction has used gold amalgam voltammetric microelectrodes to detect these complexes (Taillefert et al. 2007; Chapter 5 of this thesis). Unfortunately, the sensitivity of these electrodes depends on the composition of the organic ligand such that the concentration of organic-Fe(III) complexes can only be

determined with these electrodes if the ligand is identified (Taillefert et al. 2000). As the change in current intensity measured at the electrode is proportional to the concentration of these complexes, assuming the same ligands are produced during the incubations, changes in the concentrations of organic-Fe(III) complexes measured by microelectrodes are typically reported in current intensity units (Taillefert et al. 2007, Chapter 5 of this thesis). To fully understand the biological relevance of the solubilization pathway versus the other proposed pathways, the concentration of organic ligand produced by the organism needs to be determined. Knowing the concentration of the organic-Fe(III) complexes will help relate the biogeochemical significance of microbially produced ligands in sediments on the geochemical cycling of iron (Chapter 4 of this thesis). In addition, quantifying these complexes is necessary to determine the energetics of the reduction of the organic-Fe(III) complex at the terminal reductase (Taillefert et al. 2007). Finally, quantifying these complexes should provide insights into the eventual recycling or sharing of these endogenous ligands between cells.

Competitive ligand equilibration adsorptive cathodic stripping voltammetry (CLE-ACSV) has been used to characterize unknown organic ligands in the open ocean (Rue and Bruland 1995; Wu and Luther 1995), estuaries (Buck et al. 2007; Gerringa et al. 2007) and, recently, sediment pore waters (Chapter 4 of this thesis). This technique requires addition of a competitive ligand to determine the concentration of natural ligand and the concentration and conditional stability constant of the Fe(III)-ligand complex during titrations with Fe(III).

The main objectives of the present study were to 1) determine if known iron reduction mutants of *S. oneidensis* that display iron reduction deficiencies also are

impaired in their ability to produce organic-Fe(III) complexes, 2) develop a CLE-ACSV technique for the characterization of organic ligands produced during DIR, 3) compare the organic ligand production of wild-type and reduction mutants to determine the role of organic-Fe(III) complexes in DIR, 4) evaluate the incubation conditions that enhance or suppress organic-Fe(III) production, and 5) modify the proposed model of Fe(III) respiration by *Shewanella* species that involves the dissolution of Fe(III) oxides.

6.3 Materials and Methods

6.3.1 Bacterial strains, cultivation, and mutagenesis

All solutions were prepared with ACS or trace metal grade reagents in >18.3 MΩ-water (Milli-Q). The facultative anaerobe *Shewanella oneidensis* MR-1 was the primary strain used for microbial incubations in the present study. Both random and target mutagenesis of *S. oneidensis* MR-1 were used to identify the proteins involved in dissimilatory iron reduction. Four Sol mutants (d29, d64, H1, and B7), of approximately 4000 random ethyl methanesulfonate (EMS) mutants screened using the MESA technique (Chapter 5 of this thesis), were selected for their inability to produce soluble organic-Fe(III). Genes encoding the proteins GspD, OmcA, MtrA, MtrB, and MtrC were deleted in-frame from the *S. oneidensis* MR-1 genome as described previously (Burns and DiChristina 2009). Additionally, a double deletion mutant of the genes encoding OmcA and MtrC was prepared. All biological mutations and genetic manipulations were preformed by the DiChristina Laboratory in the School of Biology at the Georgia Institute of Technology.

Microbial incubations were performed as single or triplicate incubations in autoclaved 100 mL serum bottles sealed with septa and crimped caps. Incubations and

sampling were carried out in an anaerobic chamber (Coy, 95% nitrogen 5% hydrogen) at 30 ^{0}C that contains multiple magnetic stirring plates to ensure complete mixing of the slurries. Less than 10% of the total incubation volume was removed over the course of each experiment. In all incubations, 2 x 10^{7} cells ml^{-1} of cells from late log phase cultures were inoculated with 18 mM lactate as electron donor and carbon source. Microbial incubations were carried out either in defined salts (M1) or *Shewanella* growth media (WL) and amended with 32 mM of either 2L-ferrihydrite, goethite, or hematite, as electron acceptor, prepared according to well-established methods (Schwertzmann and Cornell 2000). In some cases 10 mM fumarate was added at the beginning of the incubations as an alternate electron acceptor in addition to the Fe(III) oxide. Two 200 µl aliquots were removed every 6–8 h for ancillary analyses. The first 200 µl aliquot was added to 1 ml of 3 M HCl to extract adsorbed Fe^{2+} (Lovley and Phillips, 1986) and analyzed for total Fe^{2+} via the ferrozine colorimetric method (Stookey, 1970). The second aliquot was transferred to a well of a 300 µl 96-well tray for voltammetric analysis using the MESA system described in Chapter 2 and 5 of this thesis. Initial rates of organic-Fe(III) production were determined by linear regression of the increase in organic-Fe(III) current intensities for 24 h (disregarding any initial lag period). Initial rates of Fe(III) reduction were determined by linear regression of the total Fe(II) production rate during the period of soluble organic-Fe(III) production.

6.3.2 Direct titration of *S. oneidensis* supernatant by EDTA

To determine the viability of CLE-ACSV titrations of the *Shewanella* supernatants, the iron species present in the incubation supernatants were titrated with ethylenediaminetetraacetic acid (EDTA). The supernatant of the *S. oneidensis* incubation

was filtered through 0.2 μm, polyethersulfone syringe filters (Millipore) after 100 hours. In an anaerobic chamber, the filtrate was diluted 10x with a degassed buffer containing 10 mM piperazine-1,4-bis(2-ethanesulfonic acid (PIPES) in 0.2 M NaCl. The diluted samples were divided between 10 sealable centrifuge tubes with concentrations of EDTA varying from 0 to 100 μM. The centrifuge tubes were sealed inside the anaerobic chamber and allowed to equilibrate in the dark for one hour. The samples were then removed from the anaerobic chamber and analyzed by square wave voltammetry with a hanging mercury drop electrode (Metrohm VA-663) connected to a computer-controlled potentiostat (Autolab PG STAT 12). Samples from the titrations were analyzed using a scan rate of 200 mV sec^{-1} from -0.1 V to -1.7 V after a 10 second deposition at -0.1 V. In total, five replicates were obtained per sample. Data from voltammetric scans were integrated using VOLTINT, a semi-automated integration software implemented in Matlab (Bristow and Taillefert 2008).

6.3.3 Reverse CLE-ACSV procedure

Reverse CLE-ACSV was used to determine the Fe(III) ligand concentration and the conditional stability constant in single microbial cultures. Samples were taken daily and filtered through 0.2 μm, polyethersulfone syringe filters (Millipore). Total dissolved iron was determined by the ferrozine technique (Stokey 1970). Ten aliquots were diluted 100 fold with a buffer containing 10 mM piperazine-1,4-bis(2-ethanesulfonic acid (PIPES) in 0.2 M NaCl. Iron contamination in the 0.1 M piperazine-1,4-bis(2-ethanesulfonic acid (PIPES) stock solutions was avoided by equilibrating 1 g of Chelex 100 with 500 mL of 0.1 M PIPES stock at pH 7 for 1 hour with periodic mixing. The pH of the PIPES-Chelex 100 mixture was raised with sodium hydroxide pellets until the

desired pH was obtained, at which point the mixture was allowed to equilibrate for 30 minutes with periodic mixing. The pH was tested again and adjusted if necessary. Chelex 100 was removed from the PIPES stock solution through a trace metal cleaned fritted glass funnel. Buffered samples were titrated with increasing concentrations of the competitive ligand 1-nitroso-2-napthol (NN) from 0.1 μM to 100 mM from stock solutions of NN prepared in methanol then diluted by 50% with deionized water (>18.3 MΩ, Milli-Q). In some cases where little iron was present, 0.5 to 50 μM of $FeCl_3$ was added to the diluted samples prior to the competitive ligand additions. Samples were allowed to equilibrate in the dark for 4 hours prior to analysis by hanging mercury drop electrode (Metrohm VA-663) connected to a computer-controlled potentiostat (Autolab PG STAT 12). Voltammetric scans were performed by differential pulse polarography at a stationary mercury drop electrode after 3 min purge with nitrogen gas to remove oxygen. A 10 s deposition at -0.1 V was followed by a 3 s equilibration time. Scans were run from -0.2 V to -0.7 V with a step voltage was 7.5 mV and a modulation amplitude of 100 mV with a scan rate of 25 mV s^{-1}. The current height of the Fe(III)-NN complex was measured at -0.48 V vs. Ag/AgCl. Data from the voltammetric scans were integrated using VOLTINT, a semi-automated integration software implemented in Matlab (Bristow and Taillefert 2008).

6.3.3 Reverse CLE-ACSV theory

Reverse CLE-ACSV titrations are similar to the forward CLE-ACSV titrations described in Chapter 4 of this thesis except that the concentration of competitive ligand is increased instead of the concentration of total Fe(III) (Nuester and van den Berg, 2005). This technique is explained in detail in the Methods chapter of this thesis (Chapter 2).

Briefly, the concentration of free [Fe^{3+}] decreases during the titration with the addition of the competitive ligand, making this titration the reverse of the forward titration. The iron species present in reverse CLE-ACSV are described by the mass balance equation:

$$[Fe_T] = [FeL] + [Fe´] + [FeNN] \qquad \text{(Eq. 6.1)}$$

where [Fe_T] is the concentration of total dissolved Fe(III), [FeL] is the concentration of the natural organic-Fe(III) complex exchangeable with the competitive ligand NN, [Fe'] is the concentration of inorganic and 'free' hydrated Fe(III), and [FeNN] is the concentration of the Fe(III)-NN complex measured electrochemically.

This method presents two main advantages over forward CLE-ACSV titrations. First, reverse CLE-ACSV titrations feature a much larger detection window than forward CLE-ACSV titrations, extending the typical two decade detection window to five decades. Second, this technique does not require the determination of the sensitivity of the Fe(III)-NN complex to the mercury electrode. Instead, the relative current response of the titration, or the ratio of the current intensity to the maximum current intensity observed during the titration, is evaluated by the equation:

$$X = \frac{i}{i_{max}} = \frac{[FeNN]}{[Fe_T]} \qquad \text{(Eq. 6.2)}$$

where X is the relative current response, i is the current intensity for a given titration point, and i_{max} is the maximum observed current intensity for the titration. This ratio is equivalent to the ratio of concentration of [FeNN] to the [Fe_T], assuming all the Fe(III) in

the system is titratable by the competitive ligand. The concentration of 'free' iron, [Fe^{3+}], is determined at each titration point from the X ratio, the total iron in the system, [Fe_T], and the side reaction coefficient for the formation of the FeNN complex, α_{FeNN}. The relationship is described by the equations:

$$[FeNN] = \alpha_{FeNN} \times [Fe^{3+}] \quad \text{(Eq. 6.3)}$$

and

$$[Fe^{3+}] = \frac{X \times [Fe_T]}{\alpha_{FeNN}} \quad \text{(Eq. 6.4)}$$

where α_{FeNN} is the side reaction coefficient for the complexation of the competitive ligand NN with free iron, Fe^{3+}, and $\alpha'_{Fe'}$, the side reaction coefficient for the complexation of free iron by inorganic species and is defined in the following equation:

$$\alpha'_{Fe} = \frac{[Fe']}{[Fe^{3+}]} = 1 + \Sigma(\beta'_{FeXi}[X]^i) \quad \text{(Eq. 6.5)}$$

where β'_{FeXi} is the stability constant for iron complexes with, *i*, major anions (X) in M1 growth media at pH 7 and was determined for the growth M1 growth media used in the microbial cultures by the thermodynamic calculation program Visual MINTEQ 3.0 (Gustafson 2005). Finally, the concentration of the natural ligand complex, [FeL], is determined by mass balance equation (6.1). Ruzic and Scatchard linearizations can be used to determine the conditional stability constant (K_{FeL}) and the total ligand concentration ([L_T]) from the slope and intercepts of the linearizations (Fig. 2.3 and Fig. 6.1).

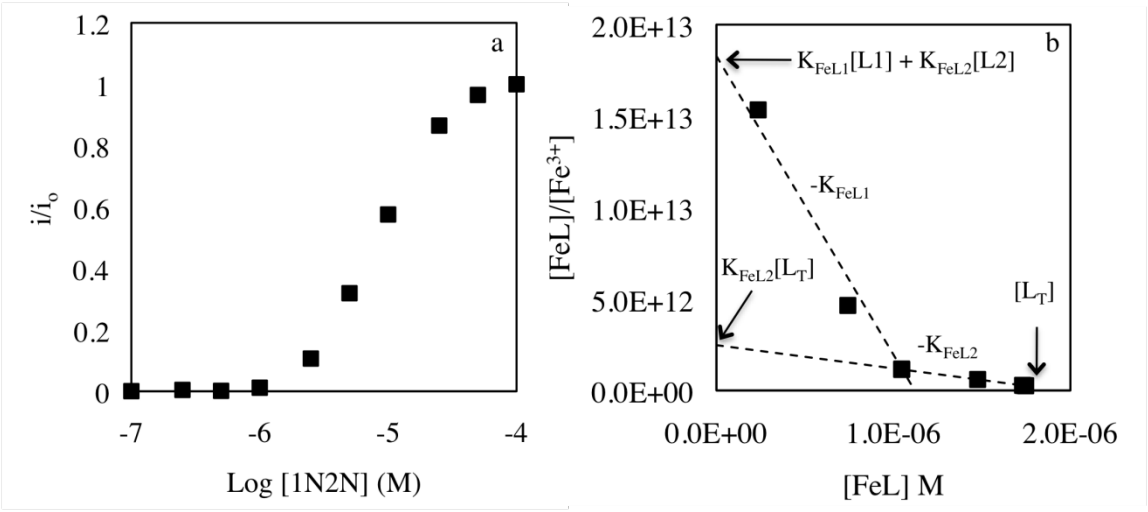

Figure 6.1 Reverse CLE-ACSV titration of the supernatant from a *ΔmtrC S. oneidensis* mutant after 42 hours incubation with goethite (A) and Scatchard linearization of the microbial culture supernatant (B). The titration displays the typical S-shaped curve of the reverse CLE-ACSV titration when represented against the log of the competitive ligand concentration. The Scatchard linearization exhibits a two-ligand behavior.

6.4 Results

6.4.1 Production of organic-Fe(III) complexes by mutants of *S. oneidensis*

Soluble organic-Fe(III) complexes were produced by *S. oneidensis* during incubation with 2L-ferrihydrite in the presence of lactate as electron donor (Fig. 6.2). Organic-Fe(III) complexes were detected in the wild-type strain after 16 hours and increased to a maximum of 244 nA at 90 hours. The reduction of Fe(III) by the wild-type was nearly linear and increased from 16 hours throughout the course of the incubation to a maximum of 11.8 mM Fe(II). The *ΔomcA* mutant not only produced as much organic-Fe(III) as the wild-type, with a maximum of 268 nA at 90 hours, it also reduced Fe(III) at near wild-type rates producing a maximum of 14.2 mM after 100 hours. The production of organic-Fe(III) by the outer-membrane decaheme deletion mutant *ΔmtrC* was much

slower than the wild-type, yet matched the maximum measured current after 93 hours. In turn, *ΔmtrC*, by reducing only 4.2 mM of Fe(III) after 100 hours, was significantly less efficient than the wild-type. The outer-membrane β-barrel protein deletion mutant *ΔmtrB* produced 96 nA of organic-Fe(III) after 100 hours, much less than the organic-Fe(III) produced by *ΔmtrC* mutant. Conversely, 5.2 mM of Fe(III) was reduced by *ΔmtrB* during the course of the incubation, exceeding the concentration produced by the *ΔmtrC* mutant. The type-II secretion deletion mutant *ΔgspD* was less efficient than all the other

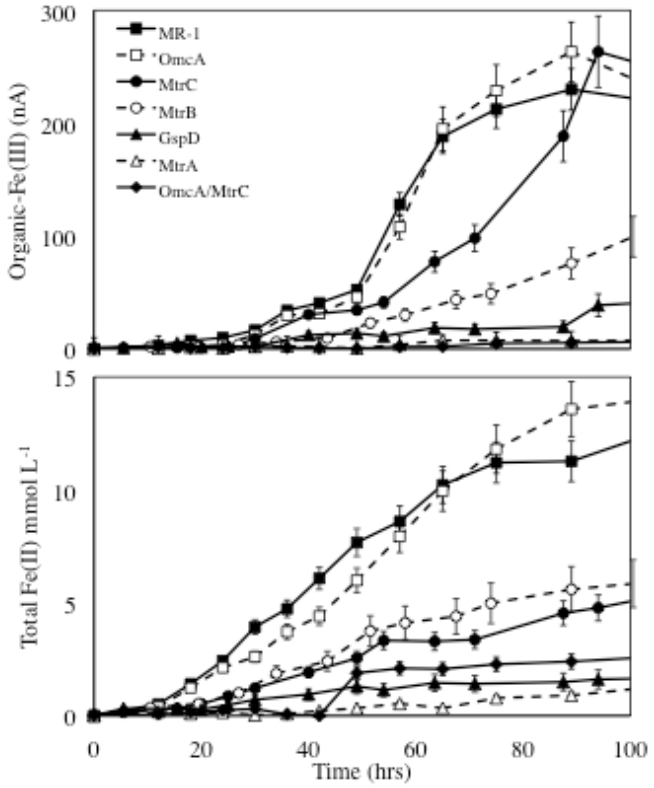

Figure 6.2 – Anaerobic incubations of wild type *S. oneidensis* (MR-1), deletion mutants *ΔomcA*, *ΔmtrC*, *ΔmtrB*, *ΔmtrA*, and *ΔgspD*, and the double deletion mutant *ΔomcA*/*ΔmtrC* in batch reactors amended with lactate as electron donor and 2L-ferrihydrite as electron acceptor and sole iron source in *Shewanella* growth media. Production of soluble organic-Fe(III) (A) and total Fe(II) (B) as a function of time. Error bars represent standard deviations from triplicate incubations.

mutants, producing only 29 nA of organic-Fe(III) during the incubation and reducing 1.2 mM of Fe(III) only. Finally, the outer-membrane bound periplasmic decaheme *ΔmtrA* and the double deletion mutant *ΔomcA/ΔmtrC* produced no detectable organic-Fe(III) after 100 hours and reduced 1.8 mM Fe(III) after 100 hours, while *ΔmtrA* only reduced 1.0 mM Fe(III) at the end of the experiment.

Initial rates of organic-Fe(III) production and Fe(III) reduction were calculated from the incubations without considering any phase lag. A linear trend was observed between the rates of production of organic-Fe(III) and the rates of reduction of Fe(III) (Fig. 6.3). The wild-type displayed the fastest rates of both organic-Fe(III) production and Fe(III) reduction. The *ΔomcA* mutant displayed only slightly lower organic-Fe(III) and Fe(III) reduction rates than the wild-type. In turn, a dramatic decrease in both rates was observed in the *ΔmtrC* and *ΔmtrB* mutants, which reached approximately 33% of the rates by the wild-type for organic-Fe(III) production and Fe(III) reduction. The rates of both soluble organic-Fe(III) production and Fe(III) reduction by *ΔgspD, ΔmtrA,* and *ΔomcA/ΔmtrC* were the lowest of all strains investigated.

6.4.2 Direct titration of *S. oneidensis* supernatant by EDTA

Cathodic square wave voltammetry of filtered supernatant from the incubation with *S. oneidensis* and 2L-ferrihydrite in growth media produced two voltammetric signals for organic-Fe(III) complexes at -0.35 V and Fe(II) at -1.4 V (Fig 6.4). When the supernatant was titrated with an increasing concentration of EDTA, the voltammetric

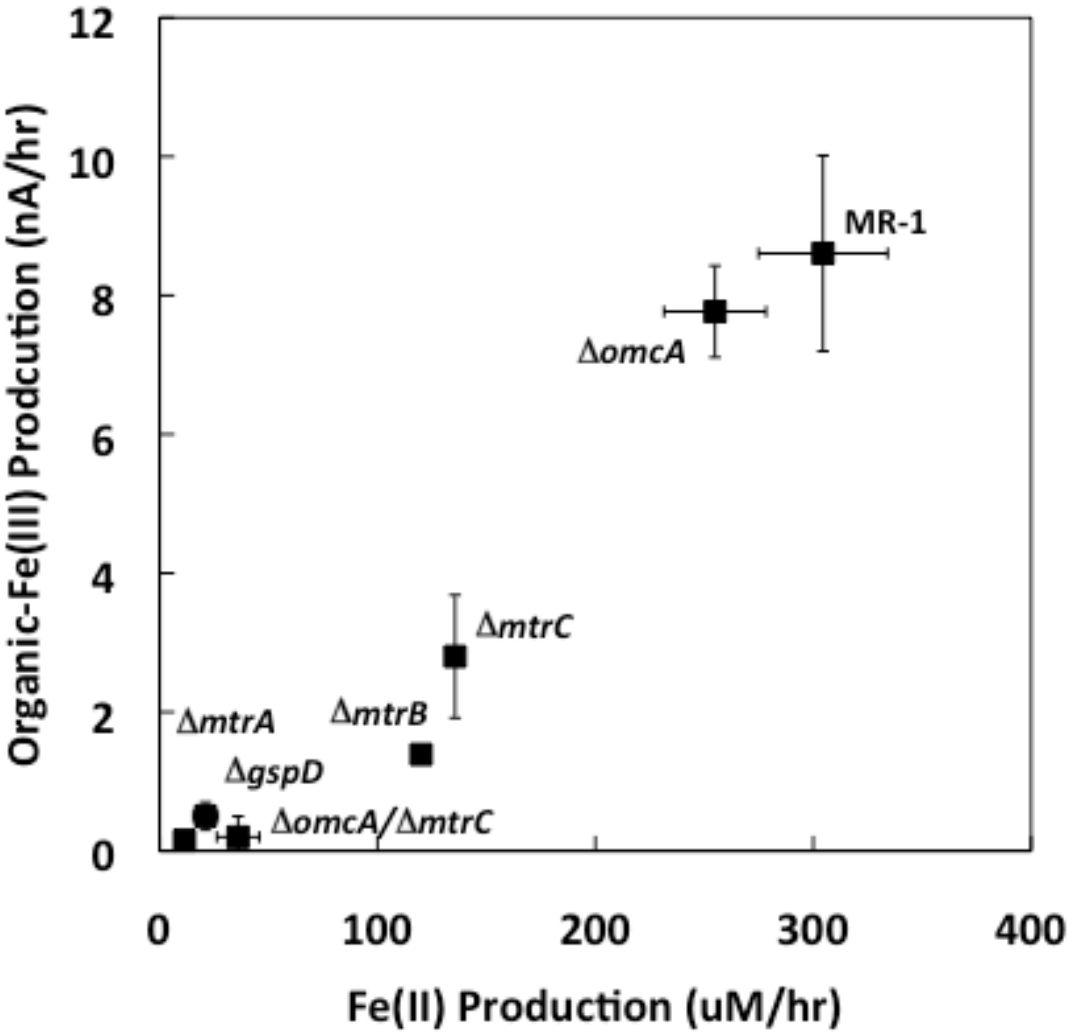

Figure 6.3 – Correlation between initial rates of organic-Fe(III) production and initial rates of iron oxide reduction by *S. oneidensis*, the deletion mutants *ΔomcA*, *ΔmtrC*, *ΔmtrB*, *ΔmtrA*, and *ΔgspD*, and the double deletion mutant *ΔomcA*/*ΔmtrC*. Incubations were conducted in growth media with lactate as electron donor and 2L-ferrihydrite as electron acceptor. Each data represents the average of triplicate incubations.

signals for organic-Fe(III) complexes and Fe(II) decreased consistently as a function of the increasing EDTA concentration. The decrease in the organic-Fe(III) and Fe(II) peak coincided with the increase in a voltammetric peak at -0.15 V that corresponds to a Fe(III)-EDTA complex (Shimizu et al. 2007). A representation of the log of the EDTA concentration versus the relative current response shows the simultaneous titration of organic-Fe(III) and Fe(II) by EDTA (inset of Fig. 6.4).

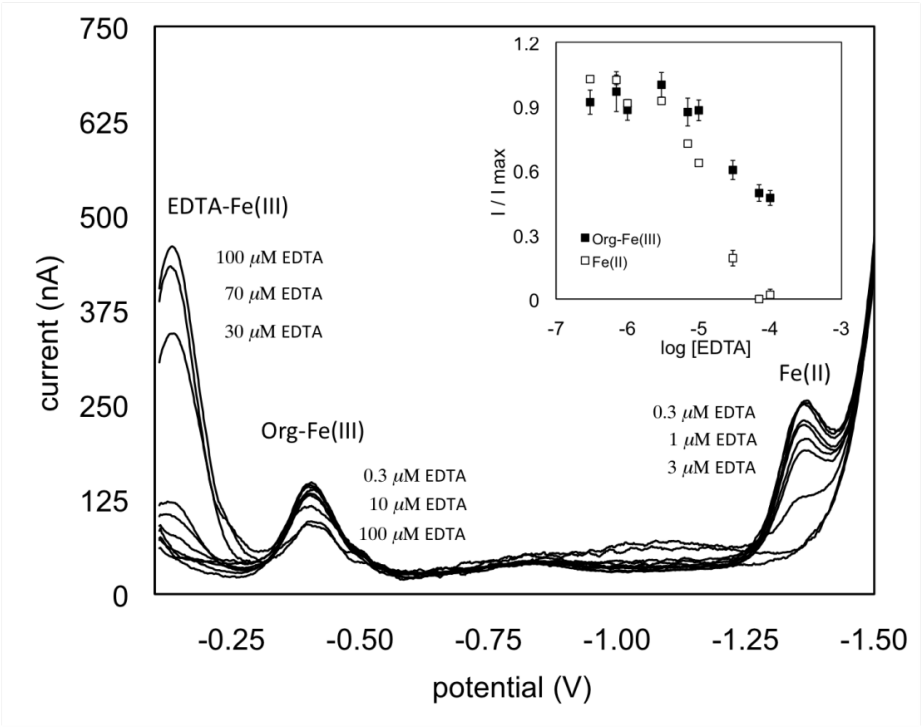

Figure 6.4 – Cathodic square wave voltammograms of the titration of filtered *S. oneidensis* supernatant with EDTA. A decrease in organic-Fe(III) complexes at -0.35 V and Fe(II) at -1.4 V is observed simultaneously with the production of the EDTA-Fe(III) complex at -0.15 V. Inset shows the relative current response (I/I_{max}) of each voltammetric signal as a function of the log of the EDTA concentration added during the titration.

6.4.3 Reverse CLE-ACSV titration of bacterial supernatant

S. oneidensis and the deletion mutants *ΔomcA*, *ΔmtrC*, and *ΔgspD* were incubated with goethite in M1 media (Fig 6.5). Reverse CLE-ACSV titrations of the filtered supernatant of incubations of *S. oneidensis* displayed an increase in the Fe(III)-NN signal as a function of added NN in all the MR-1, *ΔomcA,* and *ΔmtrC* titrations with maximum currents of approximately 40 nA, while a much lower Fe(III)-NN maximum of 15 nA was detected with the *ΔgspD* mutant (Fig. 6.6). The relative current response diagrams displayed the typical S-shaped curves observed in reverse CLE-ACSV titrations, with the notable exception of the four hour titration point in each of the titrations.

Ruzic and Scatchard linearizations of the reverse CLE-ACSV titrations displayed curvature indicative of multiple ligands within the detection window (Fig. 6.1). The results of the linearizations are summarized in Table 6.1. Ruzic linearizations for the MR-1 incubation showed a nearly constant ligand concentration with a $LogK_{FeL}$ from 18.2 to 20.4 over the course of the experiment. From the Scatchard linearizations, two ligands were identified, including a stronger L1 ligand (Log K_{FeL} 20.3 to 21.3) that decreased until none was detected after 66 hours, and a weaker L2 ligand (Log K_{FeL} 18.3 to 19.6) the was produced during the incubation and reached a maximum of 182 μmol L^{-1}. Unlike MR-1, the concentration of ligands produced by the MtrC deficient mutant increased throughout the incubations and formed Fe(III) complexes with a Log K_{FeL} of 18.3 to 20.8. The Scatchard linearization for this incubation displayed two ligands within the detection window, a strong ligand ($LogK_{FeL}$ 19.3 to 22.2) that increased through the first 42 hours before becoming undetectable and a weak ligand (Log K_{FeL} 18.0 to 20.4) that increased throughout the incubation to a final concentration of 257 μmol L^{-1}. The incubation with the OmcA deficient mutants produced similar results as the MtrC deficient mutants. The strong ligand (Log K_{FeL} 20.0 to 22.6) was produced in the first 42 hours then became undetectable. The weak ligand (Log K_{FeL} 18.2 to 19.4) continued to be produced throughout the incubation, reaching a maximum concentration of 223 μmol L^{-1} after 66 hours. The GspD mutant incubation produced little organic ligand compared to the others, with a maximum of 62 μmol L^{-1} (Log K_{FeL} 18.9) after 66 hours. The concentration of the weak ligand, L2, calculated from the Scatchard linearization increased over the course of the incubations of each of the strains investigated (Fig. 6.5C).

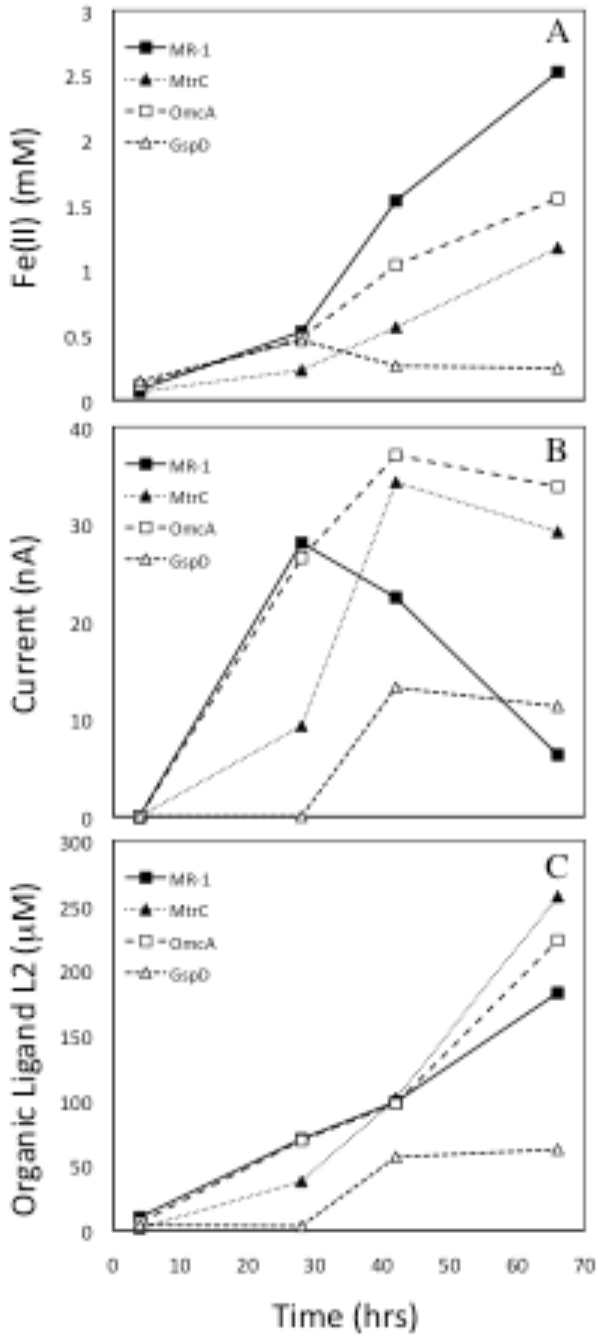

Figure 6.5 –Production of Fe(II) (A), organic-Fe(III) (B), and the L2 ligand (C) during single incubations of *S. oneidensis* and the deletion mutants *ΔomcA*, *ΔmtrC*, and *ΔgspD* in M1 media using goethite as electron acceptor and lactate as electron donor. Organic-Fe(III) complexes were produced then consumed in the MR-1 incubations. In turn, the *ΔmtrC* and *ΔomcA* mutants were unable to reduce the organic-Fe(III) as fast as MR-1 and lead to the build up of the organic-Fe(III) intermediate complexes in the supernatant of these incubations. The *ΔgspD* mutant was the only strain impaired in organic ligand production.

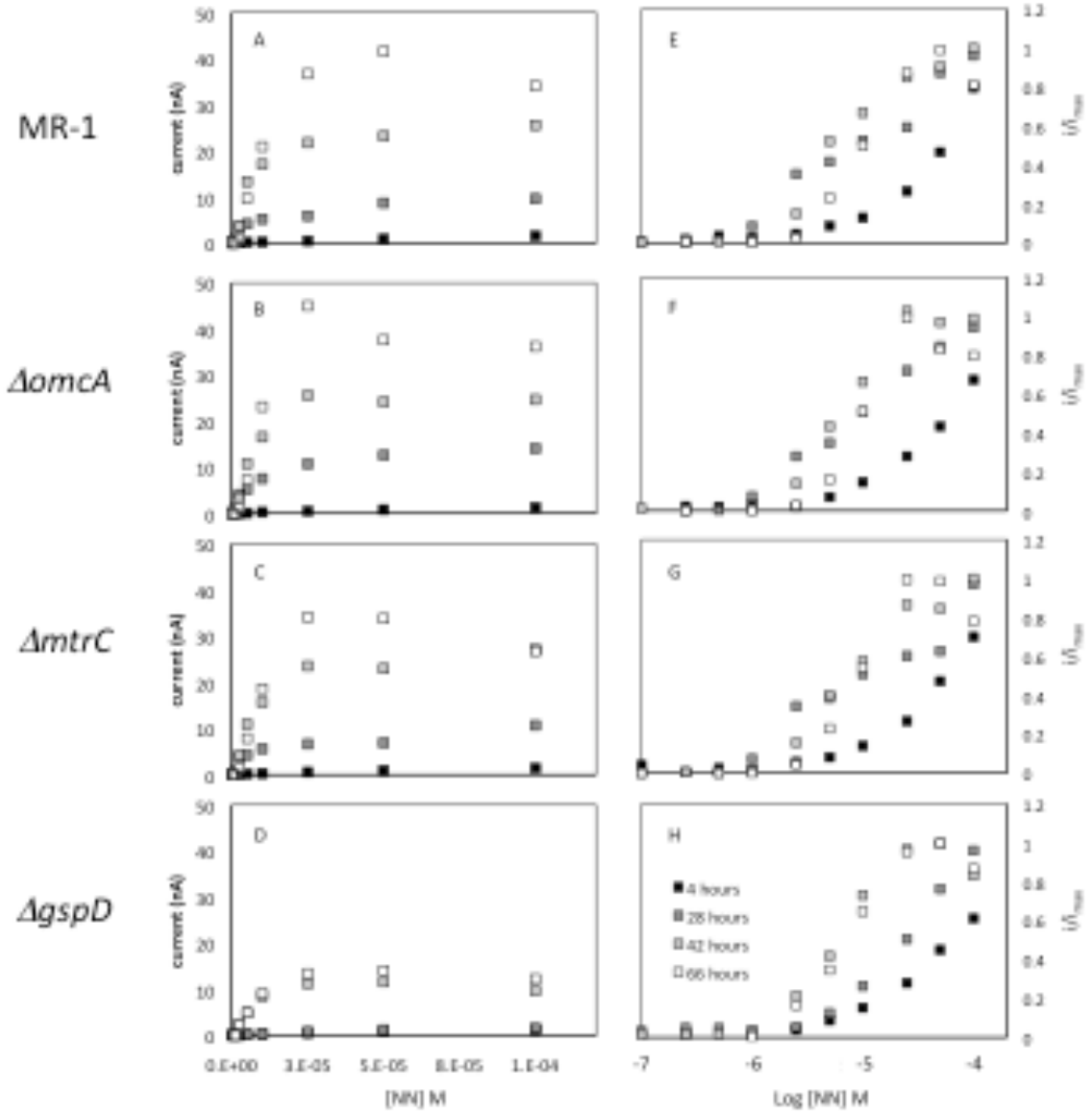

Figure 6.6 – Reverse CLE-ACSV titrations of filtered supernatants collected over the course of the microbial incubations of *S. oneidensis* (A.) and the deletion mutants *ΔomcA* (B), *ΔmtrC* (C), and *ΔgspD* (D). The left panel shows the increase in Fe(III)-NN signal current as a function of NN added, while the right panel shows the relative current response as a function of the log [NN] added.

Table 6.1 - Reverse CLE-ACSV Ruzic and Scatchard Linearizations. Scatchard Linearizations Provide Information on Strong, L1, and Weak, L2, Ligands. L2 Increases Over the Course of the Incubation.

			Ruzic linearization		Scatchard linearization			
	Time (hrs)	Fe(III) (μmol L-1)	[L_T] (μmol L-1)	Log KFeL	[L1] (μmol L-1)	Log KFeL1	[L2] (μmol L-1)	Log KFeL2
MR-1	4	105	103	20.4	94	21.3	10	19.6
	28	129	127	18.2	62	20.5	70	17.6
	42	127	126	18.6	40	20.3	99	18.3
	66	108	129	19.0	n.d.	n.d.	182	18.8
MtrC	4	13	13	20.8	12	22.2	1	20.4
	28	85	84	18.3	49	20.6	37	18.4
	42	175	181	18.5	102	19.3	101	18.0
	66	208	256	18.6	n.d.	n.d.	257	18.6
OmcA	4	12	12	20.5	10	22.6	6	19.4
	28	120	115	18.4	51	20.8	69	18.4
	42	149	149	18.6	50	20.0	97	18.2
	66	123	135	19.2	n.d.	n.d.	223	18.2
GspD	4	13	13	21.5	9	22.9	4	21.2
	28	14	13	20.8	10	21.4	3	20.7
	42	59	59	18.7	n.d.	n.d.	56	18.8
	66	60	55	19.0	n.d.	n.d.	62	18.9

n.d. = not detected

Simultaneously, the wild-type steadily reduced goethite and produced 2.6 mM of Fe(II) after 66 hours and generated a maximum of 29 nA of organic-Fe(III) complexes after 28 hours, followed by a decrease to just 6 nA at 66 hours. The *ΔomcA* mutant reduced goethite at a slower rate than the wild-type, and a maximum of 1.5 mM Fe(II) was produced after 66 hours. In turn, the voltammetric signals of the organic-Fe(III) complexes reached 38 nA and remained high through the end of the incubations. The *ΔmtrC* mutant displayed a similar behavior, producing 1.2 mM of Fe(II) and 33 nA of organic-Fe(III) complexes after 66 hours. In contrast, the type-II secretion mutant *ΔgspD* reduced little of the goethite (i.e. 0.4 mM) and produced little organic-Fe(III) complexes (i.e. 12 nA).

6.4.4 The effect of the addition of fumarate on the production of organic-Fe(III) complexes

The addition of 10 mM fumarate to 2L-ferrihydrite incubations of *S. oneidensis* and random Sol mutants selected for their inability to produce organic-Fe(III) (Chapter 5) in *Shewanella* growth media increased the rate of organic-Fe(III) production (Fig 6.7). In turn, the corresponding rate of Fe(III) reduction was not increased in the presence of fumarate. Yet, a linear correlation between the rate of organic-Fe(III) production and the rate of Fe(III) reduction is evident in the presence of fumarate. The ratio of the rate of

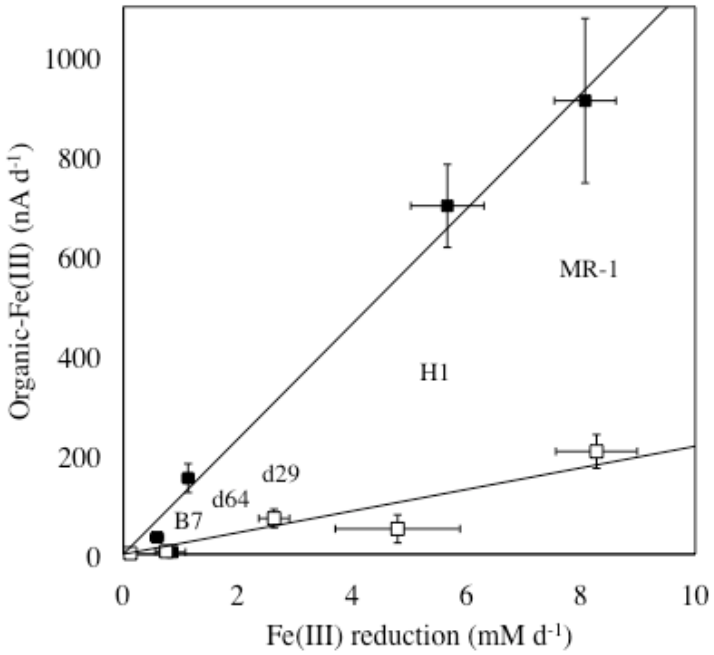

Figure 6.7 – Correlation between initial production rates of soluble organic-Fe(III) and Fe(III) reduction rates in incubations of *S. oneidensis* and the Sol mutants H1, d29, d64, and B7 on 2L-ferrihydrite with and without 10 mM fumarate. Fumarate increases the rate of organic-Fe(III) production in the wild-type and Sol mutants without corresponding increase in the rate of Fe(III) reduction. Each data represents the average of triplicate incubations.

organic-Fe(III) production to Fe(III) reduction increased (from 22:1 to 115:1) by more than five fold in the presence of fumarate.

Unlike the fumarate addition to 2L-ferrihydrite incubations, the addition of fumarate to incubations of *S. oneidensis* with hematite as terminal electron acceptor in *Shewanella* growth media displayed an increase in both the rates of organic-Fe(III) production and Fe(III) reduction by 3.5 times over non-fumarate incubations (Fig. 6.8). Similar incubations in M1 media produced different results. First, the fumarate-less

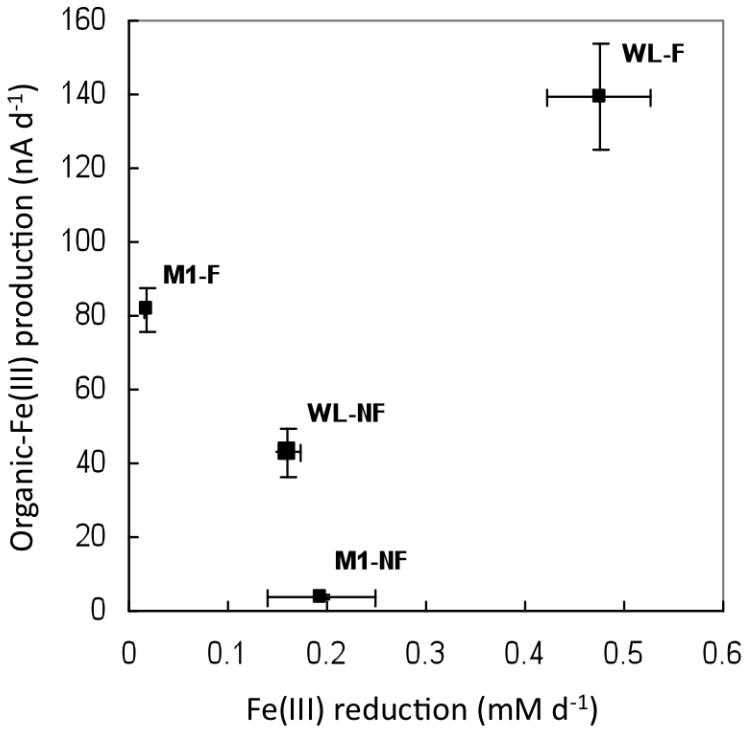

Figure 6.8 – Rates of organic-Fe(III) production and Fe(III) reduction by *S. oneidensis* in the presence (F) or absence (NF) of 10 mM fumarate in *Shewanella* growth (WL) or minimum (M1) media with hematite as electron acceptor and lactate as electron donor. Unlike similar incubations with 2L-ferrihydrite, the addition of fumarate to *Shewanella* growth media incubations generated a proportional increase in the rates of both organic-Fe(III) production and Fe(III) reduction. In M1 media, however, the rate of production of organic-Fe(III) remained low in the absence of fumarate while Fe(III) reduction was inhibited in the presence of 10 mM fumarate. Each data represents the average of triplicate incubations.

incubations did not produce any organic-Fe(III) complexes, while the rate of reduction of Fe(III) reached 0.2 mM d^{-1}, approximately the same as the incubation in *Shewanella* growth media but about 40 times slower than the equivalent incubation with 2L-ferrihydrite. In contrast the incubations in the presence of fumarate and hematite in M1 media produced 80 nA d^{-1} of organic-Fe(III) but did not reduce Fe(III).

6.5 Discussion

The mechanism of iron reduction by members of the genus *Shewanella* remains poorly constrained, and several mechanisms have been postulated to be involved in the dissimilatory reduction of iron oxides. In this study, the mechanism of solubilization of iron oxides by *S. oneidensis* was investigated using a combination of voltammetry with mercury amalgam microelectrodes and, for the first time, a reverse CLE-ACSV technique to determine the concentration of organic ligand and the conditional stability constant of the Fe(III)-ligand complex produced during respiration on iron oxides. In addition, proteins known to be involved in the transfer of electrons to iron oxides were deleted from *S. oneidensis* to investigate their involvement in the solubilization pathway.

The initial rates of organic-Fe(III) production and Fe(III) reduction by *S. oneidensis* and the in-frame deletion mutants *ΔomcA*, *ΔmtrC*, *ΔmtrB*, *ΔmtrA*, and *ΔgspD*, as well as the double deletion mutant *ΔomcA/ ΔmtrC* are highly correlated. These results suggest the reduction of iron oxides proceeds via production of an intermediate soluble organic-Fe(III) complex that is further reduced to Fe(II) as proposed recently (Taillefert et al., 2007). A similar result was observed with the random Sol mutants identified for their inability to produce organic-Fe(III) (Chapter 5 of this thesis).

Organic ligands are produced by the wild-type and the two outer-membrane decaheme cytochrome-deficient mutants *ΔmtrC* and *ΔomcA* even though the reduction capability of these mutants is less than the wild-type (Fig. 6.5). In addition, the rate of production of soluble organic-Fe(III) and the rate of reduction of Fe(III) by the *ΔmtrC* mutant are about half those of the wild-type and the *ΔomcA* mutant over the first 28 hours (Fig. 6.5), suggesting that the MtrC cytochrome is essential to the reduction of iron as already determined (Myers and Myers 1992). These findings suggest that these cytochromes are not involved in the solubilization pathway but are instead involved in the reduction of the soluble Fe(III) intermediates. These results complement the previous work conducted with these cytochrome-deficient mutants which only measured production of Fe(II) (Beliaev et al. 2001). In contrast, deletion of the genes involved in the production of both OmcA and MtrC completely inhibited iron solubilization and iron reduction, suggesting that these two proteins are central to the reduction of Fe(III) and the lack of these outer membrane c-type cytochromes inhibits the production and secretion of the organic ligand. The OmcA/MtrC double mutant has been shown to display Fe(III) reduction deficiency as well as electron transfer deficiency in unmediated microbial fuel cells (Gorby et al. 2006). Similarly, the deletion of the β-barrel protein MtrB resulted in a much lower rate of solubilization and a depressed reduction of iron oxides, indicating again that this protein is involved in the transfer of electrons to iron or the transfer of the organic ligand to the outer-membrane (Beliaev and Saffarini 1998). MtrB is presumed to form a transmembrane complex with MtrC and MtrA, providing a porin for the transfer of electrons from MtrA to MtrC through the outermembrane (Pitts et al. 2003). Alternatively, the β-barrel structure of the protein suggests MtrB could be involved in the

secretion of the ligand as a porin to transfer the ligand through the outer membrane. Finally, deletion of either MtrA or one of the components of the type-II secretion system (GspD) completely inhibited iron solubilization and reduction. MtrA is associated with the periplasmic side of the outer membrane and has been proposed to form a 1:1:1 complex with the outer membrane proteins MtrB and MtrC (Pitts et al. 2003; Ross et al., 2007). The strong impact of the deletion of this protein suggests either that the soluble organic-Fe(III) complex is reduced inside the periplasmic space or that this decaheme cytochrome is part of the electron transport chain to the soluble organic-Fe(III) compound, as proposed previously (Beliaev et al 2001). More importantly, the negative effect of deleting a central component of the type-II secretion system on both iron solubilization and reduction indicates that the type-II secretion system may be involved in the production or secretion of the organic ligand. The type–II protein secretion system is used to translocate exoproteins to the outer membrane of gram-negative bacteria (Pugsley 1993) and is required for the cell surface localization of the OmcA and MtrC proteins and has been previously show to be central to iron reduction (DiChristina et al. 2002). Additionally, the lack of organic ligand production in the *ΔgspD* mutant (Fig. 6.5) suggests the type II secretion apparatus is involved in the production and secretion of the ligand or the secretion of proteins required for ligand production.

The results of the reverse CLE-ACSV show the presence of two ligands a strong type L1 ligand and a weaker type L2 ligand. The L1 ligand with a log K of 20 to 22 is typically removed over the course of the experiment while the L2 ligand with a log K of 18 to 20 is produced during iron reduction. The conditional stability constants of the L2 organic-Fe(III) complexes are on the higher range of the observed effective stability

constants for iron reduction (Haas and DiChristina 2002). An organic ligand with a stability constant greater than 20 decreases reduction rates while reduction is completely inhibited in the presence of very strong ligands such as EDTA or siderophores (Log K > 25). The stability constant of an effective ligand for iron respiration must be weak enough to allow exchange with the reductase yet strong enough for the dissolution of iron oxide. Thus, for the non-reductive dissolution of iron oxide, either a strong ligand or a high ligand concentration is necessary to shift the equilibrium toward the dissolution of the iron oxideThe production of detectable amounts of dissolved Fe(III) during the incubations suggests that the dissolution rate is the rate limiting step in the respiration of iron oxides, and that the L2 ligand is in the optimal range for balancing iron oxide dissolution and organic-Fe(III) respiration.

Interestingly, the L2 ligand is produced in the wild type, *ΔomcA*, and *ΔmtrC* incubations, suggesting the outer membrane c-type cytochromes are not required for L2 ligand synthesis or secretion, while the lack of production by *ΔgspD* suggest the type-II secretion system is involved in the ligand production in one of three ways: 1) The type-II secretion system secretes the proteins for ligand transport across the outer membrane, 2) the type-II secretion system secretes a ligand synthase to the outer membrane, or 3) the type-II secretion apparatus is directly involved in the secretion of the organic ligand across the outer membrane. The type-II secretion system has only been shown to be involved in protein translocation (Pugsley 1993) such that secretion of the organic ligand would be a unique finding. The production rate and concentration of L2 organic ligands were similar between the wild type and the *ΔomcA* and *ΔmtrC* mutants strains (Fig. 6.5C); however, the solubilization of Fe(III) differed significantly. Organic-Fe(III)

production by the wild type is suggestive of the production and consumption of an intermediate species in the reduction reaction. The pattern of production of organic-Fe(III) complexes followed by consumption is consistent with and suggests the organic-Fe(III) complex is an intermediate in the reduction of iron oxides by *S. oneidensis MR-1*. The mutants deficient in the outer membrane c-type cytochromes (OmcA and MtrC) produce organic-Fe(III) complexes at the same rate as the wild-type after a phase lag (Fig 6.2 and 6.5), however, the rates of Fe(III) reduction are only half that of the wild-type, suggesting these proteins are involved in the reduction of Fe(III) but not the solubilization of Fe(III). As the rate of reduction is low in these mutant strains, the organic-Fe(III) intermediate is not consumed over the second half of the incubations (Fig 6.5B).

The production of endogenous iron-binding organic ligands for iron solubilization may represent a significant drawback as it likely required energy to synthesize the ligand. The energetic cost of ligand synthesis for the respiration of iron oxides, however, may be offset by the energetic gains provided by faster rates of reduction of soluble Fe(III), greater access to electron acceptors, and prevention of mineral passivation (Taillefert et al. 2007; Chapter 5 of this thesis). The cycling of the organic ligand between the cell and the mineral may further minimize the energy expended in ligand synthesis and secretion. If chelation is the only pathway employed during the respiration of Fe(III), 2.5 mmol L^{-1} of Fe(III) is reduced with only 0.2 mmol L^{-1} of organic ligand, suggesting that the ligand is cycled 12.5 times between the cell and the goethite mineral. If ligand production is the same for all iron oxides, it would suggest that 0.2 mmol L^{-1} of ligand can reduce 10 mmol L^{-1} of iron when provided with 2L-ferrihydrite. If this is the case the ligand may be

cycled up to 50 times during the reduction of the more easily dissolved 2L-ferrihydrite. This cycling of organic ligands between the cell and mineral minimizes the biosynthetic cost of ligand synthesis and lends credence to chelation as a viable respiratory pathway for the reduction of Fe(III).

Iron-binding organic ligands have been shown to increase (Arnold et al. 1986, Taillefert et al. 2007) or decrease (Haas and DiChristina 2002) the rates of iron reduction depending on the strength of the complex. Strong binding ligands such as siderophores are known to be produced by members on *Shewanella* (Vraspir and Butler, 2009) and are known to solubilize iron oxides (Hersman et al. 1995). The conditional stability constants of the complexes formed with these type ligands (>20) are typically beyond the range useful to *Shewanella* for respiratory purpose (Haas and DiChristina 2002), and the production of hydroxamate siderophores is not required for the respiration of iron oxides (Fennessey et al. 2010). This suggests the L1 ligand observed in the Scatchard linearization was not likely to be involved in the solubilization of Fe(III) and may be produced as a part of a separate cellular pathway not involved in DIR. Alternatively, the L2 ligand is within the range of ligand stability constants viable for respiration (Haas and DiChristina 2002).

The production of organic-Fe(III) complexes is highly dependent on the growth media used, the type of iron oxide reduced and the addition of fumarate to the *Shewanella* cultures. The addition of fumarate to 2L-ferrihydrite incubations of random mutants deficient in organic-Fe(III) production increased the rate of organic-Fe(III) production in all mutants tested except the B7 Sol mutant and the abiotic controls (Fig. 6.7). This increase in Fe(III) solubilization may result from the production of an unknown by

product of fumarate reduction that may provide an organic substrate involved in the biosynthesis of the microbial ligand. Malate, which can be formed by the enzymatic hydrolysis of fumarate, is known to increase the solubility and bioavailability of iron in soils (Jones et al. 1996). The hydrolysis of fumarate to malate is a known step within the citric acid cycle which creates a tridentate ligand (Maidigan and Martinko 2006) . The malate-Fe(III) complex produces an electrochemical signal at -0.33 V at circumneutral pH (Vukosav et al. 2010), suggesting production of malate in the presence of excess fumarate may enhance voltammetric organic-Fe(III) signals observed in these incubations. In either case the increase in solubilization is not accompanied by an increase in Fe(III) reduction, suggesting the maximum rate of reduction has already been achieved in the non-fumarate incubations. It is unknown if fumarate is reduced under these conditions, however, the reduction potential of 2L-ferrihydrite is similar to the reduction potential of fumarate, suggesting fumarate may be reduced concomitant with the reduction of 2L-ferrihydrite.

In contrast to the fumarate addition to 2L-ferrihydrite incubations the addition of fumarate to hematite incubations with *Shewanella* growth media (WL) increased the rate of organic-Fe(III) production as well as the rate of iron reduction. The rate of reduction of hematite was overall slower than the rate of reduction of 2L-ferrihydrite (Fig. 6.7. and Fig. 6.8) such that an increase in the rate of Fe(III) reduction would be excepted with an increase in the rate of Fe(III) solubilization. Fe(III) solubilization was not observed in otherwise identical incubations in minimal salts media (M1) even if the rate of Fe(III) reduction was similar to the incubations with the *Shewanella* <= italic growth media. These findings suggest the rate of hematite reduction is limited by the solubilization of

Fe(III) which is consistent with the low solubility of hematite, and may indicate direct contact is the preferred pathway for hematite reduction. In fumarate amended incubations with M1 media the reduction of fumarate was likely preferred to the reduction of hematite as the redox potential of fumarate was higher than hematite. The Fe(III) solubilization observed under these conditions must then be attributed to fumarate reduction products which may be strong enough to dissolve iron oxides.

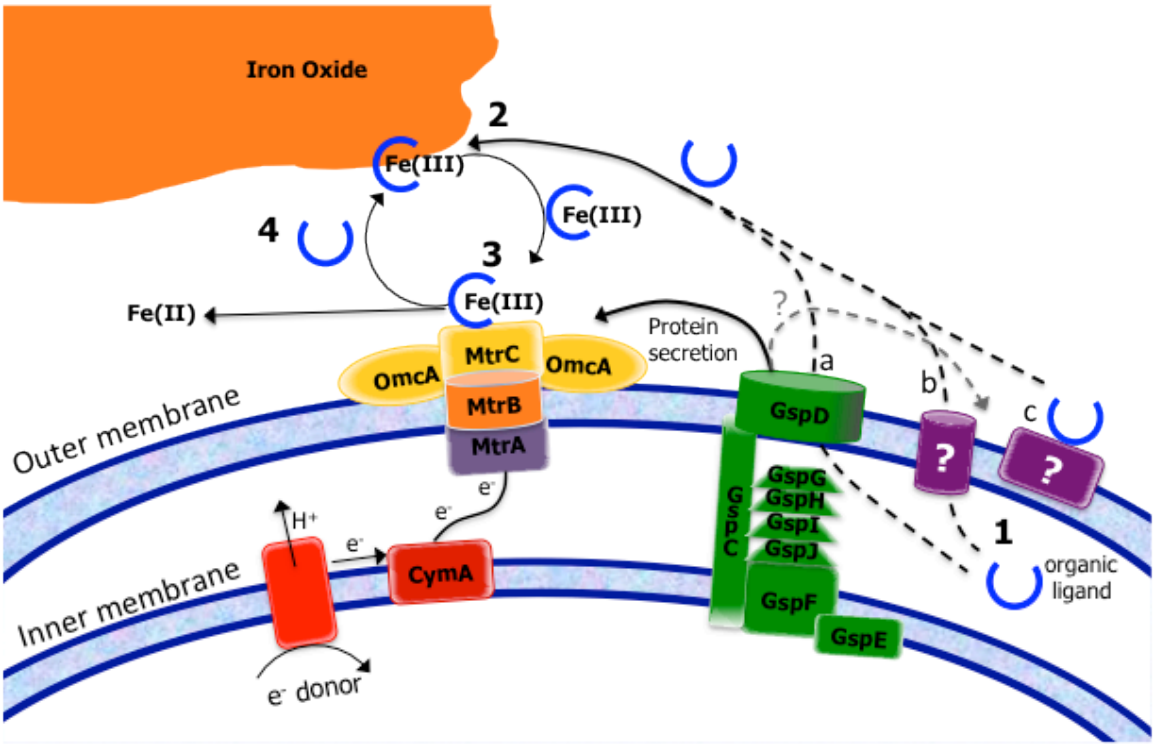

Figure 6.9 – Proposed chelation mechanism for the reduction of Fe(III) by *S. oneidensis* MR-1. Organic ligands, L, are produced at redox potentials < 0.1 V. The non-reductive dissolution of iron oxides produces the organic-Fe(III) complex, L-Fe(III). The organic-Fe(III) complex is reduced by *S. oneidensis* regenerating the organic ligand and producing Fe(II).

The reverse CLE-ACSV technique provides important new information about the mechanism of iron reduction by *S. oneidensis* MR-1. Combined with the voltammetric

organic-Fe(III) production determined from voltammetric microelectrodes, a mechanism for the non-reductive dissolution of iron oxides followed by the biological reduction of the organic-Fe(III) complexes can be proposed (Fig. 6.9). In the first step, iron-binding organic ligands are produced by *Shewanella* and secreted into the supernatant. In step two, these ligands non-reductively dissolve the iron oxide to form the organic-Fe(III) complexes detected with the voltammetric microelectrodes. In step three, the soluble organic-Fe(III) complexes are reduced to Fe(II) and the organic ligand is regenerated.

In summary, the facultative anaerobe *Shewanella oneidensis* MR-1 produces organic ligands for the solubilization of Fe(III) during the DIR of goethite that are cycled more than ten times between the cell and the mineral. This mechanism of respiration is in contrast to other extracellular electron transfer mechnisms that require direct contact between the iron oxide and the iron reductase or the use of electron shuttling compounds to respire iron oxides. While the outer membrane cytochromes, MtrC and OmcA, are important for the reduction of Fe(III) they are not involved in the production and secreation of organic ligands nor are they required for the solubilization of iron oxides. in turn, the type-II secreation system is critical to the production of iron binding organic ligands, subsequent solubilization of iron oxides, and the reduction of the soluble organic-Fe(III) complexes. Together with the recycling of the organic ligand, these results indicate the solubilization mechanism for iron reduction by dissimilatory iron reducing bacteria is a viable strategy to transfer electrons to iron oxides.

6.6 Acknowledgements

We would like to thank Dr. Thomas J. DiChristina from the School of Biology at Georgia Institute of Technology for providing the microbial strains and mutants analyzed here. Also we would like to thanks the members of the DiChristina Lab (Nadia, Christine, Seng, Justin) for the help in preparing microbial cultures.

CHAPTER 7

CONCLUSIONS

The bioavailability of iron is closely tied to its solubility throughout the environment, and has important implications for primary productivity in the oceans, the cycling of iron in sediments, and the immobilization of contaminants in soils and sediments. Hydrothermal vents have been proposed to represent a significant source of iron for primary productivity in the photic zone. Like other source of iron to the ocean, the bioavailability of iron released by hydrothermal vents depends on its residence time in solution. Organic ligands and sulfide nanoparticles are potential sources of long term stability for the iron fluxing from hydrothermal vents. Simultaneously, iron reduction in continental shelf sediments may generate a flux of iron across the sediment water interface. In upwelling zones, this iron flux may stimulate primary productivity in surface waters. In estuaries however, where 90% of riverine iron input is buried in the sediment as a result of flocculation and precipitation of iron oxides associated with seawater mixing, the diffusion of ferrous iron across the sediment-water interface generally results in the reprecipitation of iron oxides near the sediment surface. These sediments, however, may provide a source of dissolved iron to estuarine waters and the nearby continental shelf providing that ferric iron is stabilized in solution. Potential candidates for stabilizing ferric iron in solution include organic ligands, as a variety of natural organic ligands are well known to complex and solubilize ferric iron. Indeed in the past 15 years, the presence of such ferric iron complexes has become evident in a variety of sediments, and it has been proposed that iron-reducing bacteria may be able to generate such complexes during the dissimilatory reduction of iron oxides. The primary

objectives of this work were to test the hypotheses that hydrothermal vents and estuarine sediments provide a significant source of dissolved iron to the ocean under the form of stable organic-Fe(III) complexes and that iron-reducing bacteria may be partly responsible for the production of these complexes as intermediates during dissimilatory iron reduction.

In this study, the chemical composition of hydrothermal vent fluids from 9^0 North EPR and the speciation of trace metals between the particulate, colloidal, and truly dissolved fractions were investigated to determine the potential mechanisms involved in the preservation of metals in the dissolved phase. The interaction of hot, reduced, acidic vent fluids with cold, oxic, basic seawater creates dramatic gradients in which chemical and biological reactions occur, including the production of thiosulfate. The vents of 9° North are actively producing iron rich fluids that may provide a source of dissolved and colloidal iron to the pelagic zone. The highly colloidal nature of iron at some of the observed vents suggests small buoyant iron sulfide particles may provide a source of iron beyond the pelagic zone. The production of thiosulfate in hydrothermal vent fluids may be due to the oxidation of nanoparticles of pyrite by dissolved oxygen and may provide a source of reducible sulfur for carbon oxidation. Other trace metals that may also play a significant role in biochemical processes regulating primary productivity are also selectively released under the form of chloro complexes that may eventually be carried away by nanoparticulate sulfur species.

In a separate study, the production of soluble organic-Fe(III) complexes in estuarine sediments was measured and the flux of these complexes across the sediment-water interface quantified to establish the flux of dissolved iron to the nearby continental

shelf. The preservation of truly dissolved organic-Fe(III) complexes in the overlying waters as the pH and ionic strength increased from fresh to saline waters was observed over the course of four different cruises, and the sediment of this estuary was identified as the main source of these Fe(III) complexes. In a previous study, it was demonstrated that the high sedimentation rates in the estuary provide a source of iron oxides and organic material to the sediments. In these sediments, organic-Fe(III) complexes were formed in zones of microbial iron reduction, suggesting that they may be released by iron-reducing bacteria during the non-reductive dissolution of iron oxides. These soluble organic-Fe(III) complexes diffuse to the overlying water thereby providing a stable source of iron to the estuary and continental shelf. Total estuarine flux calculations show that up to 62% of the flux of iron from the estuary to the continental shelf may originate from estuarine sediments. The concentration of iron from the Satilla River is 5 to 8 times higher than the average concentration in major world rivers, suggesting the Satilla River and blackwater rivers like it are underrepresented in the world average river flux and may represent a more significant source of iron than previously suspected.

In the remaining of this dissertation, the production of soluble organic-Fe(III) complexes by DIRB was investigated using the model organism *Shewanella oneidensis* MR-1. This study demonstrated for the first time that *S. oneidensis* produces organic-Fe(III) complexes during dissimilatory iron reduction of iron oxides and these complexes are only produced at redox potentials less than 0.1 V. A novel microelectrode screening array (MESA) was developed to identify random mutants of *S. oneidensis* deficient in the production of organic-Fe(III) complexes. The mutants found to be deficient in organic-

Fe(III) production were also deficient in Fe(III) reduction suggesting these complexes are intermediate in the dissimilatory reduction of iron oxides.

The production of organic ligands by mutants previously described to be involved in the dissimilatory reduction of iron were investigated for their production of organic-Fe(III) complexes. The deletion mutants *ΔmtrA, ΔmtrB, ΔmtrC, ΔomcA, ΔgspD*, and *ΔmtrC/ΔomcA* all displayed deficiencies in the rates of Fe(III) reduction that corresponded to deficiencies in the rates of organic-Fe(III) production. A reverse CLE-ACSV technique was optimized to determine the concentration of organic ligand produced during the respiration of goethite. The results revealed that wild-type and c-type cytochrome mutants *ΔmtrC* and *ΔomcA* produce organic ligands that non-reductively solubilize goethite, while the type-II secretion mutant *ΔgspD* does not produce organic ligands over the same time frame. In the wild-type organism, the intermediate nature of these organic-Fe(III) complexes is evidenced by its consumption in the second part of the incubation, while in *ΔmtrC* and *ΔomcA* cultures, which are impaired in their ability to reduce iron, the intermediate organic-Fe(III) is not consumed significantly. It was also shown that the production of organic-Fe(III) complexes depends on the type of iron oxides and media used to grow the microorganisms. The addition of fumarate enhanced the rates of organic-Fe(III) production and Fe(III) reduction during hematite respiration by *S. oneidensis*. In turn, fumarate addition during 2L-ferrihydrite respiration showed an increase in organic-Fe(III) production rate without corresponding increase in reduction rates. These results suggest that the maximum rate of reduction was already reached with 2L-ferrihydrite due to the high reactivity of this terminal electron acceptor. From the findings of this thesis, a mechanism for the non-

reductive dissolution of iron oxides followed by the biological reduction of the organic-Fe(III) complexes can be proposed. In the first step, iron-binding organic ligands are produced by *Shewanella* and secreted into the supernatant. The biochemical pathway responsible for the production of the ligand remains unknown, but the Type-II secretion and MtrA may be involved by transferring proteins involved in the synthesis or transport of the ligand to the outer membrane. In step two, these ligands non-reductively dissolve iron oxides to form the organic-Fe(III) complex intermediates. The outer membrane c-type cytochromes MtrC and OmcA appear to be involved in Fe(III) reduction only, indicating that both the solubilization and reduction steps occur at the cell surface. In step three, soluble organic-Fe(III) complexes are reduced to Fe(II) and the organic ligand is regenerated. Evidence from the present experiments indicate the organic ligand for the solubilization of Fe(III) during the DIR of goethite may be cycled 12.5 times between the cell and the mineral. The production of organic-Fe(III) complexes by iron-reducing bacteria may present several advantages compared to a pathway requiring direct contact between the terminal reductase and the iron oxides. As the anaerobic respiration of soluble Fe(III) is fast, it may increase reduction rates and energy generation for the organism. Simultaneously, solubilization of ferric iron before reduction does not require the organism to be in direct contact with the iron oxide and may even allow respiration at a distance. Furthermore, the formation of a higher redox potential intermediate may reduce the activation energy for the formation of the reduction intermediate and thus increase iron respiration rates. Finally, the formation of the intermediate complexes may prevent the passivation of Fe(III) mineral surfaces by Fe(II) adsorption, which has been shown previously to limit iron-reducing activity. Together this research shows the

production of organic-Fe(III) complexes is an important component to the bioavailability of iron.

7.1 Recommendations for future research

Several questions have arisen from the present study, and suggestions for future research on the production and role of soluble organic-Fe(III) complexes are considered below. The detection limit of Fe in seawater samples needs to be several orders of magnitude lower to follow the distribution of organic-Fe(III) complexes beyond estuarine environments to the continental shelf. Flow injection analysis using highly reactive chemiluminescnce methods or measurements of total dissolved iron using a collision cell ICP-MS could be investigated as alternatives for analysis of low concentrations of iron.

CLE-ACSV analysis should be performed on Satilla River bulk water samples along a transect from low to high salinity. These samples would be a better representative of the organic-Fe(III) complexes that may be transported to the continential shelf. Especially useful would be the speciation of iron in river samples with salinities greater than 20 to quantify the speciation in the sediments and the estuary and determine the flux to the continental shelf directly. In the present study, the samples analyzed for total iron (<0.2 μm) in the high salinity waters were close to the limit of detection of the ferrozine method.

The organic-Fe(III) complex produced during dissimilatory iron reduction should be isolated and identified by mass spectrometry. This has been attempted before with little success. The organic compounds in the supernatant from cells grown on iron oxides in low organic media like M1 may be separated and concentrated from the bulk solution

by reverse solid phase extraction onto a C-18 cartridge. This concentrate may be compared to a similar sample prepared from nitrate grown cells to identify organic compounds specific to iron grown cells. This analysis will most likely require a 'soft' ionization technique such as Electro spray or field desorption ionization. This will require the assistance of a mass spectroscopist with interest in the project as the detection of the iron-ligand complex may be difficult.

Experiments need to be performed in environmentally relevant conditions to bring the great understanding of the laboratory work to the field. High organic content, high phosphate, and easily reducible iron oxides may be hindering the understanding of the processes involved in DIRB the environment by providing unrealistic results. High concentraions of these compounds may allow the organisms to use alternate pathways for the reduction of iron oxides that may not be available under environmentally relevent conditions.

Finally, the role of pH in the area surrounding the cells during dissimilatory iron reduction should be investigated. A small decrease in pH would correspond to an increase in the concentration soluble iron in solution and may be used to assist the non-reductive dissolution of iron oxides by the organic-ligand produced during dissimilatory iron reduction. Iron oxidizing bacteria have been show to decrease the pH surrounding their cells, presumably to slow the oxidation of Fe(II) and prevent encapsulation by the iron oxide oxidation by-product (Hegler et al. 2010). The pH surrounded the cell may be monitored by *in situ* fluorescence microscopy with pH sensitive dyes (Marcotte and Brouwer 2005)

APPENDIX A

This is a MATLAB program for the least squares optimization of revease ACSV-CLE

```
%Reverse CLE least squares optimization
%Matrix of X and ligand conc, X=imax/i
%first calc [Fe3+] at each [NN] using best guess for LT and KFeL
%new matrix of X, NN, and Fe3+
%least squares optimization, yeilds new LT and KFeL
%recalc [Fe3+] using new LT and KFeL
%repeat until no change in LT and KFeL
%starting information:
%1) data = matrix of X and [NN]
%2) FeT = total Fe, constant
%3) KFeNN = conditonal stability constant for FeNN complex, constant
%4) alphaFe = ratio of Fe' to Fe3+, constant
%5) KFeL = best initial guess of KFeL value
%6) LT = best inital guess of LT value

clear
global aFeNN aFe Fe3 NNin Xin Ksmall FeT;
data=load('MR1-66b.txt');%name of data matrix file
FeT=1.08E-06;%measured total Fe concentration mol/L
KFeL=1.7569e+17;%best initial guess of KFeL value
LT=3.9144e-05;%best inital guess of LT value
KFeNN=6.31e27;%conditonal stability constant for FeNN complex
logaFe=7.76;%log of the ratio of Fe' to Fe3+, side reaction coefficient
aFe=10^logaFe;%side reaction coefficient
Ksmall=KFeL/1e25;%divisor to make varibles in Eq have similar step sizes
NN=data(:,1);%Data input [NN] and current ratio X
S=1:10;%numbers current data "short"
L=1:0.1:10;%numbers interp data "long"
NNin=interp1(S,NN,L,'vchip');
logNN=log10(NN);
X=data(:,2);
Xin=interp1(S,X,L,'vchip');
aFeNN=KFeNN*NNin.^3;
%Calcuation of [Fe3+] vector
a=KFeL*aFe+KFeL*aFeNN;
b=aFe+aFeNN+KFeL*LT-KFeL*FeT;
```

```
c=-FeT;
Fe3=(-b+sqrt(b.^2-(4*a*c)))./(2*a);
%Vector of parameters of best guess, Po=initial parameters
Po=[LT,Ksmall];
LB=[];
UB=[];
options=optimset('Display','iter','LargeScale','off','DiffMinChange',1e-
20,'DiffMaxChange',10000,'TolX',1e-10,'TolFun',1e-
5,'MaxIter',5000,'MaxFunEvals',10000);
[P,RESNORM,RESIDUAL,EXITFLAG]=lsqnonlin('REVCLEFUN',Po,LB,UB,options)
pKFeL=P(:,2)*1e25
pLT=P(:,1)
Xplot=aFeNN./(aFe+aFeNN+((pKFeL*pLT)./((pKFeL*Fe3)+1)));
Xguess=aFeNN./(aFe+aFeNN+((KFeL*LT)./((KFeL*Fe3)+1)));
figure(1)
plot (logNN,X,'o',log10(NNin),Xin,log10(NNin),Xplot,log10(NNin),Xguess)
```

```
%REVCLEFUN.m
function F=REVCLEFUN(P)
global aFeNN aFe Fe3 Xin FeT;
%NN=data(:,1);
%X=data(:,2);
%KFeL=P(2);
Ksmall=P(2);
LT=P(1);
Xcal=aFeNN./(aFe+aFeNN+((1e25*Ksmall*LT)./((1e25*Ksmall*Fe3)+1)));
F=norm(Xcal-Xin,inf);
```

REFERENCES

Adams, D. K., and L. S. Mullineaux. 2008. Supply of gastropod larvae to hydrothermal vents reflects transport from local larval sources. Limnol. Oceanogr. **53:** 1945-1955.

Alber, M., C. R. Alexander, J. Blanton, A. Chalmers, and K. Gates. 2003. The Satilla River Estuary system: The current state of knowledge. Report for The Georgia Sea Grant College Program and The South Carolina Sea Grant Consortium. Retrieved from http://www.gcrc.uga.edu/PDFs/satilla_sok.pdf

Arnold, R. G., T. J. DiChristina, and M. R. Hoffmann. 1988. Reductive dissolution of Fe(III) oxides by *Pseudomonas* sp200. Biotechnol. Bioeng. 32: 1081-1096.

Badziong, W., and R. K. Thauer. 1978. Growth yields and growth rates of *Desulfovibrio vulgaris* (marburg) growing on hydrogen plus sulfate and hydrogen plus thiosulfate as sole energy sources. Archives of Microbiology **117:** 209-214.

Beck, K. C., J. H. Reuter, and E. M. Perdue. 1974. Organic and inorganic geochemistry of some coastal-plain river of Southeastern United States. Geochim. Cosmochim. Acta **38:** 341-364.

Beliaev, A. S., and D. A. Saffarini. 1998. *Shewanella putrefaciens* mtrB encodes an outer membrane protein required for Fe(III) and Mn(IV) reduction. J. Bacteriol. **180:** 6292-6297.

Beliaev, A. S., D. A. Saffarini, J. L. Mclaughlin, and D. Hunnicutt. 2001. MtrC, an outer membrane decahaem *c* cytochrome required for metal reduction in *Shewanella putrefaciens* MR-1. Mol. Microbiol. **39:** 722-730.

Bennett, S. A., E. P. Achterberg, D. P. Connelly, P. J. Statharn, G. R. Fones, and C. R. Gernian. 2008. The distribution and stabilization of dissolved Fe in deep-sea hydrothermal plumes. Earth Planet. Sci. Lett. **270:** 157-167.

Berelson, W. and others 2003. A time series of benthic flux measurements from Monterey Bay, CA. Continental Shelf Research **23:** 457-481.

Biber, M. V., M. D. Afonso, and W. Stumm. 1994. The coordination chemistry of weathering 4. Inhibition of the dissolution of oxide minerals. Geochim. Cosmochim. Acta **58:** 1999-2010.

Bischoff, J. L., and F. W. Dickson. 1975. Seawater-basalt interaction at 200 degrees C and 500 bars - Implications for origin of sea-floor heavy-metal deposits and regulation of seawater chemistry. Earth Planet. Sci. Lett. **25:** 385-397.

Blanton, J. O., H. Seim, C. Alexander, J. Amft, and G. Kineke. 2003. Transport of salt and suspended sediments in a curving channel of a coastal plain estuary: Satilla River, GA. Estuar. Coast. Shelf Sci. **57:** 993-1006.

Bond, D. R., and D. R. Lovley. 2005. Evidence for involvement of an electron shuttle in electricity generation by *Geothrix fermentans*. Appl. Environ. Microbiol. **71:** 2186-2189.

Boudreau, B. P. 1991. Modeling the sulfide-oxygen reaction and associated pH gradients in porewater Geochim. Cosmochim. Acta **55:** 145-159.

Boyd, P. W., D. S. Mackie, and K. A. Hunter. 2010. Aerosol iron deposition to the surface ocean - Modes of iron supply and biological responses. Mar. Chem. **120:** 128-143.

Breitbarth, E., E. P. Achterberg, M. V. Ardelan, A. R. Baker, E. Bucciarelli, F. Chever, P. L. Croot, S. Duggen, M. Gledhill, M. Hassellov, C. Hassler, L. J. Hoffmann, K. A. Hunter, D. A. Hutchins, J. Ingri, T. Jickells, M. C. Lohan, M. C. Nielsdottir, G. Sarthou, V. Schoemann, J. M. Trapp, D. R. Turner, and Y. Ye. 2010. Iron biogeochemistry across marine systems - progress from the past decade. Biogeosciences **7:** 1075-1097.

Brendel, P. J., and G. W. Luther. 1995. Development of a gold amalgam voltammetric microelectrode for the determination of dissolved Fe, Mn, O2 and S(-2) in porewaters of marine and freshwater sediments. Environ. Sci. Technol. **29:** 751-761.

Brittain, T., R. Blackmore, C. Greenwood, and A. J. Thomson. 1992. Bacterial nitrite-reducing enzymes. European Journal of Biochemistry **209:** 793-802.

Boyle, E. A., J. M. Edmond, and E. R. Sholkovitz. 1977. Mechanism of iron removal in estuaries. Geochim. Cosmochim. Acta **41:** 1313-1324.

Bristow, G., and M. Taillefert. 2008. VOLTINT: A Matlab (R)-based program for semi-automated processing of geochemical data acquired by voltammetry. Computers & Geosciences **34:** 153-162.

Bruland, K. W., J. R. Donat, and D. A. Hutchins. 1991. Interactive influences of bioactive trace-metals on biological production in oceanic waters. Limnol. Oceanogr. **36:** 1555-1577.

Bruland, K. W., E. L. Rue, and G. J. Smith. 2001. Iron and macronutrients in California coastal upwelling regimes: Implications for diatom blooms. Limnol. Oceanogr. **46:** 1661-1674.

Buck, K. N., M. C. Lohan, C. J. M. Berger, and K. W. Bruland. 2007. Dissolved iron speciation in two distinct river plumes and an estuary: Implications for riverine iron supply. Limnol. Oceanogr. **52:** 843-855.

Buffle, J., P. Deladoey, J. Zumstein, and W. Haerdi. 1982. Analysis and characterization of natural organic matters in freshwaters. Aquatic Sciences - Research Across Boundaries **44:** 325-362.

Burdige, D. J., M. J. Alperin, J. Homstead, and C. S. Martens. 1992. The role of benthic fluxes of dissolved organic-carbon in oceanic and sedimentary carbon cycling. Geophys. Res. Lett. **19:** 1851-1854.

Burnes, B. S., M. J. Mulberry, and T. J. DiChristina. 1998. Design and application of two rapid screening techniques for isolation of Mn(IV) reduction-deficient mutants of *Shewanella putrefaciens*. Appl. Environ. Microbiol. 64: 2716-2720.

Carey, E., and M. Taillefert. 2005. The role of soluble Fe(III) in the cycling of iron and sulfur in coastal marine sediments. Limnol. Oceanogr. 50: 1129-1141.

Caldwell, C. D., and A. L. Crumbliss. 1998. Molecular recognition of ferrioxamine B by host-guest complex formation with lasalocid A in chloroform. Inorganic Chemistry **37:** 1906-1912.

Ceretti, H., D. Vullo, A. Zalts, and S. Ramirez. 2010. Effect of bacterial growth in the complexing capacity of a culture medium supplemented with cadmium(II). World Journal of Microbiology & Biotechnology **26:** 847-853.

Childress, J. J., and C. R. Fisher. 1992. The Biology of hydrothermal vent animals - phyiology, biochemistry, and autotrophic symbioses. Oceanography and Marine Biology **30:** 337-441.

Coates, J. D., D. J. Ellis, E. L. Blunt-Harris, C. V. Gaw, E. E. Roden, and D. R. Lovley. 1998. Recovery of humic-reducing bacteria from a diversity of environments. Appl. Environ. Microbiol. **64:** 1504-1509.

Cornel, P. K., R. S. Summers, and P. V. Roberts. 1986. Diffusion of humic-acid in dilute aqueous-solution. J. Colloid Interface Sci. **110:** 149-164.

Covington, E. D., C. B. Gelbmann, N. J. Kotloski, and J. A. Gralnick. 2010. An essential role for UshA in processing of extracellular flavin electron shuttles by *Shewanella oneidensis*. Mol. Microbiol. **78:** 519-532.

Crosa, J. H., and C. T. Walsh. 2002. Genetics and assembly line enzymology of siderophore biosynthesis in bacteria. Microbiology and Molecular Biology Reviews **66:** 223-+.

Crowe, S. A., J. A. Roberts, C. G. Weisener, and D. A. Fowle. 2007. Alteration of iron-rich lacustrine sediments by dissimilatory iron-reducing bacteria. Geobiology 5: 63-73.

Dai, M. H., and J. M. Martin. 1995. First data on trace-metal level and behavior in 2 major arctic river-estuary systems (Ob and Yenisey) and in the adjacent Kara Sea, Russia. Earth Planet. Sci. Lett. **131:** 127-141.

Davison, W., J. Buffle, and R. Devitre. 1988. Interpretation of Speciation Measurements - A Case Study - Direct polarographic determination of O2, Fe(II), Mn(II), S(-II) and related species in anoxic waters. Pure and Applied Chemistry **60:** 1535-1548.

Davison, W. 1993. Iron and manganese in lakes. Earth-Science Reviews **34:** 119-163.

Demina, L. L., S. V. Galkin, A. Y. Lein, and A. P. Lisitsyn. 2007. First data on microelemental composition of benthic organisms from the 9 degrees 50 ' N hydrothermal field, East Pacific Rise. Doklady Earth Sciences **415:** 905-907.

DiChristina, T. J., and E. F. Delong. 1994. Isolation of anaerobic respiratory mutants of *Shewanella Putrefaciens* and genetic analysis of mutants deficient in anaerobic growth on Fe3+. J. Bacteriol. 176: 1468-1474.

DiChristina, T. J., C. M. Moore, and C. A. Haller. 2002. Dissimilatory Fe(III) and Mn(IV) reduction by *Shewanella putrefaciens* requires ferE, a homolog of the pulE (gspE) type II protein secretion gene. J. Bacteriol. **184:** 142-151.

DiChristina, T. J., J. K. Fredrickson, and J. M. Zachara. 2005. Enzymology of electron transport: Energy generation with geochemical consequences, p. 27-52. In J. F. Banfield, J. Cervini-Silva and K. H. Nealson [eds.], Molecular Geomicrobiology. Reviews in Mineralogy & Geochemistry. Mineralogical Soc America.

Dollhopf, M. E., K. H. Nealson, D. M. Simon, and G. W. Luther. 2000. Kinetics of Fe(III) and Mn(IV) reduction by the Black Sea strain of *Shewanella putrefaciens* using in situ solid state voltammetric Au/Hg electrodes. Mar. Chem. 70: 171-180.

Doong, R. A., and B. Schink. 2002. Cysteine-mediated reductive dissolution of poorly crystalline iron(III) oxides by *Geobacter sulfurreducens*. Environ. Sci. Technol. **36:** 2939-2945.

Dubilier, N., C. Bergin, and C. Lott. 2008. Symbiotic diversity in marine animals: the art of harnessing chemosynthesis. Nature Reviews Microbiology **6:** 725-740.

Duce, R. A., and N. W. Tindale. 1991. Atmospheric transport of iron and its deposition in the ocean. Limnol. Oceanogr. **36:** 1715-1726.

Duckworth, O. W., and S. T. Martin. 2001. Surface complexation and dissolution of hematite by C-1-C-6 dicarboxylic acids at pH=5.0. Geochim. Cosmochim. Acta 65: 4289-4301.

El-Naggar, M. Y. and others 2010. Electrical transport along bacterial nanowires from *Shewanella oneidensis* MR-1. Proc. Natl. Acad. Sci. U. S. A. **107:** 18127-18131.

Elrod, V. A., W. M. Berelson, K. H. Coale, and K. S. Johnson. 2004. The flux of iron from continental shelf sediments: A missing source for global budgets. Geophys. Res. Lett. **31:** L12307.

Faure, G. 1998. Principles and Applications of Geochemistry: A comprehensive textbook for geology students. 2nd edition. McConnin, R.A. [ed] Prentice-Hall, Inc Upper Saddle River, New Jersey, USA.

Fennessey, C. M., M. E. Jones, M. Taillefert, and T. J. DiChristina. 2010. Siderophores are not involved in Fe(III) solubilization during anaerobic Fe(III) respiration by *Shewanella oneidensis* MR-1. Appl. Environ. Microbiol. **76:** 2425-2432.

Fredrickson, J. K., and J. M. Zachara. 2008. Electron transfer at the microbe-mineral interface: a grand challenge in biogeochemistry. Geobiology 6: 245-253.

Froelich, P. N. and others 1979. Early oxidation of organic-matter in pelagic sediments of the Eastern Equatorial Atlantic - Suboxic digenesis. Geochim. Cosmochim. Acta **43:** 1075-1090.

Fung, I. Y., S. K. Meyn, I. Tegen, S. C. Doney, J. G. John, and J. K. B. Bishop. 2000. Iron supply and demand in the upper ocean. Glob. Biogeochem. Cycle **14:** 281-295.

Furrer, G., and W. Stumm. 1986. The coordination chemistry of weathering .1. Dissolution kinetics of delta-Al2O3 and beo. Geochim. Cosmochim. Acta 50: 1847-1860.

Gerringa, L. J. A., M. J. A. Rijkenberg, H. T. Wolterbeek, T. G. Verburg, M. Boye, and H. J. W. De Baar. 2007. Kinetic study reveals weak Fe-binding ligand, which affects the solubility of Fe in the Scheldt estuary. Mar. Chem. **103:** 30-45.

Gerringa, L. J. A., S. Blain, P. Laan, G. Sarthou, M. J. W. Veldhuis, C. P. D. Brussaard, E. Viollier, and K. R. Timmermans. 2008. Fe-binding dissolved organic ligands near the Kerguelen Archipelago in the Southern Ocean (Indian sector). Deep-Sea Res. II **55:** 606-621.

Gorby, Y. A. and others 2006. Electrically conductive bacterial nanowires produced by *Shewanella oneidensis* strain MR-1 and other microorganisms. Proc. Natl. Acad. Sci. U. S. A. **103:** 11358-11363.

Gralnick, J. A., and D. K. Newman. 2007. Extracellular respiration. Mol. Microbiol. 65: 1-11.

Graybeal, A. L., and G. R. Heath. 1984. Remobilization of transition-metals in surficial pelagic sediments form the eastern pacific. Geochim. Cosmochim. Acta **48:** 965-975.

Gustafson, J.P., 2005. Visual MINTEQ, ver 2.32. Royal Institute of Technology, Stockholm, Sweden, Department of Land and Water Resources Engineering /http://hem.bredband.net/ b108693S.

Haas, J. R., and T. J. Dichristina. 2002. Effects of Fe(III) chemical speciation on dissimilatory Fe(III) reduction by *Shewanella putrefaciens*. Environ. Sci. Technol. **36:** 373-380.

Hassler, C. S., and V. Schoemann. 2009. Bioavailability of organically bound Fe to model phytoplankton of the Southern Ocean. Biogeosciences **6:** 2281-2296.

Hedges, J. I., R. G. Keil, and R. Benner. 1997. What happens to terrestrial organic matter in the ocean? Organic Geochemistry **27:** 195-212.

Hernandez, M. E., and D. K. Newman. 2001. Extracellular electron transfer. Cellular and Molecular Life Sciences **58:** 1562-1571.

Hines, M. E., S. L. Knollmeyer, and J. B. Tugel. 1989. Sulfate reduction and other sedimentary biogeochemistry in a northern New England salt-marsh. Limnol. Oceanogr. **34:** 578-590.

Howarth, R. W., and J. M. Teal. 1979. Sulfate reduction in a New England salt-marsh. Limnol. Oceanogr. **24:** 999-1013.

Huettel, M., W. Ziebis, S. Forster, and G. W. Luther. 1998. Advective transport affecting metal and nutrient distributions and interfacial fluxes in permeable sediments. Geochim. Cosmochim. Acta **62:** 613-631.

Hunter, K. A., and P. W. Boyd. 2007. Iron-binding ligands and their role in the ocean biogeochemistry of iron. Environmental Chemistry **4:** 221-232.

Hutchins, D. A., A. E. Witter, A. Butler, and G. W. Luther. 1999. Competition among marine phytoplankton for different chelated iron species. Nature **400:** 858-861.

Ingledew, W. J., and R. K. Poole. 1984. The respiratory chains of *Escherichia coli*. Microbiological Reviews **48:** 222-271.

Jahnke, R. A., C. R. Alexander, and J. E. Kostka. 2003. Advective pore water input of nutrients to the Satilla River Estuary, Georgia, USA. Estuar. Coast. Shelf Sci. **56:** 641-653.

Jin, Q. S., and C. M. Bethke. 2002. Kinetics of electron transfer through the respiratory chain. Biophysical Journal **83:** 1797-1808.

Jones, M. E., C. M. Fennessey, T. J. DiChristina, and M. Taillefert. 2010. *Shewanella oneidensis* MR-1 mutants selected for inability to produce soluble organic-Fe(III) complexes are unable to respire Fe(III) as anaerobic electron acceptor. Environmental Microbiology **12:** 938-950.

Kaden, J., A. S. Galushko, and B. Schink. 2002. Cysteine-mediated electron transfer in syntrophic acetate oxidation by cocultures of *Geobacter sulfurreducens* and *Wolinella succinogenes*. Archives of Microbiology **178:** 53-58.

Kappler, A., M. Benz, B. Schink, and A. Brune. 2004. Electron shuttling via humic acids in microbial iron(III) reduction in a freshwater sediment. Fems Microbiology Ecology **47:** 85-92.

Koretsky, C. M., C. M. Moore, K. L. Lowe, C. Meile, T. J. DiChristina, and P. Van Cappellen. 2003. Seasonal oscillation of microbial iron and sulfate reduction in saltmarsh sediments (Sapelo Island, GA, USA). Biogeochemistry 64: 179-203.

Kostka, J. E., B. Gribsholt, E. Petrie, D. Dalton, H. Skelton, and E. Kristensen. 2002. The rates and pathways of carbon oxidation in bioturbated saltmarsh sediments. Limnol. Oceanogr. 47: 230-240.

Krachler, R., R. F. Krachler, F. Von Der Kammer, A. Suephandag, F. Jirsa, S. Ayromlou, T. Hofmann, and B. K. Keppler. 2010. Relevance of peat-draining rivers for the riverine input of dissolved iron into the ocean. Sci. Total Environ. **408:** 2402-2408.

Laglera, L. M., and C. M. G. Van Den Berg. 2009. Evidence for geochemical control of iron by humic substances in seawater. Limnol. Oceanogr. **54:** 610-619.

Lam, P. J., and J. K. B. Bishop. 2008. The continental margin is a key source of iron to the HNLC North Pacific Ocean. Geophys. Res. Lett. **35:** L07608.

Leys, D., A. S. Tsapin, K. H. Nealson, T. E. Meyer, M. A. Cusanovich, and J. J. Van Beeumen. 1999. Structure and mechanism of the flavocytochrome c fumarate reductase of *Shewanella putrefaciens* MR-1. Nature Structural Biology **6:** 1113-1117.

Lies, D. P., M. E. Hernandez, A. Kappler, R. E. Mielke, J. A. Gralnick, and D. K. Newman. 2005. *Shewanella oneidensis* MR-1 uses overlapping pathways for iron reduction at a distance and by direct contact under conditions relevant for biofilms. Appl. Environ. Microbiol. **71:** 4414-4426.

Link, T. A. 1999. The structures of Rieske and Rieske-type proteins. Advances in Inorganic Chemistry, Vol 47 **47:** 83-157.

Liu, X. W., and F. J. Millero. 2002. The solubility of iron in seawater. Mar. Chem. **77:** 43-54.

Logan, B. E. and others 2006. Microbial fuel cells: Methodology and technology. Environ. Sci. Technol. 40: 5181-5192.

Lovley, D. R. 1991. Dissimilatory Fe(III) and Mn(IV) Reduction. Microbiological Reviews **55:** 259-287.

Lovley, D. R., E. J. P. Phillips, Y. A. Gorby, and E. R. Landa. 1991. Microbial reduction of uranium. Nature **350:** 413-416.

Lovley, D. R. 1997. Microbial Fe(III) reduction in subsurface environments. Fems Microbiology Reviews **20:** 305-313.

Lovley, D. R., M. J. Baedecker, D. J. Lonergan, I. M. Cozzarelli, E. J. P. Phillips, and D. I. Siegel. 1989. Oxidation of aromatic contaminants coupled to microbial iron reduction. Nature 339: 297-300.

Lovley, D. R., and E. J. P. Phillips. 1986. Organic-matter mineralization with reduction of ferric iron in anaerobic sediments. Appl. Environ. Microbiol. 51: 683-689.

Lovley, D. R., and J. C. Woodward. 1996. Mechanisms for chelator stimulation of microbial Fe(III)-oxide reduction. Chem. Geol. 132: 19-24.

Lovley, D. R., D. E. Holmes, and K. P. Nevin. 2004. Dissimilatory Fe(III) and Mn(IV) reduction, p. 219-286. In R. K. Poole [ed.], Advances in Microbial Physiology, Vol. 49. Advances in Microbial Physiology. Academic Press Ltd.

Luther, G. W. 1987. Pyrite oxidation and reduction - moecular-orbital theory considerations. Geochim. Cosmochim. Acta **51:** 3193-3199.

Luther, G. W., J. E. Kostka, T. M. Church, B. Sulzberger, and W. Stumm. 1992. Seasonal iron cycling in the salt-marsh sedimentary environment - The importance of ligand complexes with Fe(II) and Fe(III) in the dissolution of Fe(III) minerals and pyrite, respectively. Mar. Chem. **40:** 81-103.

Luther, G. W. 2005. Manganese(II) oxidation and Mn(IV) reduction in the environment - Two one-electron transfer steps versus a single two-electron step. Geomicrobiology Journal **22:** 195-203.

Luther, G. W. and others 2001. Chemical speciation drives hydrothermal vent ecology. Nature **410:** 813-816.

Madigan, M.T., and J. M. Martinko. 2006. Brock Biology of Microorganisms Prentice Hall, Upper Saddle River, NJ

Marcotte, N., and A. M. Brouwer. 2005. Carboxy SNARF-4F as a fluorescent pH probe for ensemble and fluorescence correlation spectroscopies. Journal of Physical Chemistry B **109:** 11819-11828.

Marschner, B., and K. Kalbitz. 2003. Controls of bioavailability and biodegradability of dissolved organic matter in soils. Geoderma **113:** 211-235.

Marsili, E., D. B. Baron, I. D. Shikhare, D. Coursolle, J. A. Gralnick, and D. R. Bond. 2008. *Shewanella* Secretes flavins that mediate extracellular electron transfer. Proc. Natl. Acad. Sci. U. S. A. 105: 3968-3973.

Martin, J. M., and M. Meybeck. 1979. Elemental mass-balance of material carried by major World Rivers. Mar. Chem. **7:** 173-206.

Martin, J. H., R. M. Gordon, and S. E. Fitzwater. 1990. Iron in Antarctic Waters. Nature **345:** 156-158.

Martinez, J. S., and A. Butler. 2007. Marine amphiphilic siderophores: Marinobactin structure, uptake, and microbial partitioning. Journal of Inorganic Biochemistry **101:** 1692-1698.

Meiggs, D., and Taillefert, M. In Press. The effect of riverine discharge on biogeochemical processes in estuarine sediments. Limnol. Oceanogr.

Michalski, R. 2006. Ion chromatography as a reference method for determination of inorganic ions in water and wastewater. Critical Reviews in Analytical Chemistry **36:** 107-127.

Miller, L. A., and K. W. Bruland. 1997. Competitive equilibration techniques for determining transition metal speciation in natural waters: Evaluation using model data. Anal. Chim. Acta **343:** 161-181.

Millero, F. J., W. S. Yao, and J. Aicher. 1995. The speciation of Fe(II) and Fe(III) in Natural-waters. Mar. Chem. **50:** 21-39.

Millero, F. J. 1998. Solubility of Fe(III) in seawater. Earth Planet. Sci. Lett. **154:** 323-329.

Mitchell, P. 1961. Coupling of phosphorylation to electron and hydrogen transfer by a chemi-osmotic type mechanism Nature **191:** 144-&.

Morse, J. W., and G. W. Luther. 1999. Chemical influences on trace metal-sulfide interactions in anoxic sediments. Geochim. Cosmochim. Acta **63:** 3373-3378.

Moore, R. M., J. D. Burton, P. J. L. Williams, and M. L. Young. 1979. Behavior of dissolved organic material, iron and manganese in estuarine mixing. Geochim. Cosmochim. Acta **43:** 919-926.

Moore, J. K., and O. Braucher. 2008. Sedimentary and mineral dust sources of dissolved iron to the world ocean. Biogeosciences **5:** 631-656.

Montgomery, H., and J. F. Dymock. 1962. The rapid determination of nitrite in fresh and saline waters. Analyst: 374-378.

Moore, W. S. 1996. Large groundwater inputs to coastal waters revealed by Ra-226 enrichments. Nature **380:** 612-614.

Moore, J. K., S. C. Doney, D. M. Glover, and I. Y. Fung. 2002. Iron cycling and nutrient-limitation patterns in surface waters of the World Ocean. Deep-Sea Res. II **49:** 463-507.

Myers, C. R., and J. M. Myers. 1992. Localization of cytochromes to the outer-membrane of anaerobically grown *Shewanella Putrifaciens* MR-1. J. Bacteriol. **174:** 3429-3438.

Myers, C. R., and K. H. Nealson. 1988. Bacterial manganese reduction and growth with manganese oxide as the sole electron-acceptor. Science 240: 1319-1321.

Nealson, K. H., and D. Saffarini. 1994. Iron and manganese in anaerobic respiration - Environmental significance, physiology, and regulation. Annu. Rev. Microbiol. 48: 311-343.

Nees, H. A. and others 2008. Hydrothermal vent mussel habitat chemistry, pre- and post-eruption at 9 degrees 50 ' North on the East Pacific Rise. Journal of Shellfish Research **27:** 169-175.

Nevin, K. P., and D. R. Lovley. 2002. Mechanisms for accessing insoluble Fe(III) oxide during dissimilatory Fe(III) reduction by *Geothrix fermentans*. Appl. Environ. Microbiol. 68: 2294-2299.

Newman, D. K., and R. Kolter. 2000. A role for excreted quinones in extracellular electron transfer. Nature **405:** 94-97.

Nuester, J., and C. M. G. Van Den Berg. 2005. Determination of metal speciation by reverse titrations. Anal. Chem. **77:** 11-19.

Obrien, J., and R. D. Vetter. 1990. Production of thiosulfate during sulfide oxidation by mitochondria of the symbiont-containing bivalve *Solemya Redi*. Journal of Experimental Biology **149:** 133-148.

Osteryoung, J. G., and R. A. Osteryoung. 1985. Square-wave voltammetry. Anal. Chem. **57:** A101-A110.

Payne, A. N., and T. J. DiChristina. 2006. A rapid mutant screening technique for detection of technetium [Tc(VII)] reduction-deficient mutants of *Shewanella oneidensis* MR-1. FEMS Microbiol. Lett. 259: 282-287.

Peck, H. D., J. Legall, and J. Vanbeeumen. 1982. Biochemistry of dissimilatory sulfate reduction Philosophical Transactions of the Royal Society of London Series B-Biological Sciences **298:** 443-466.

Perdue, E. M., K. C. Beck, and J. H. Reuter. 1976. Organic Complexes of Iron and Aluminum in Natural-Waters. Nature **260:** 418-420.

Petersen, J. M. and others Hydrogen is an energy source for hydrothermal vent symbioses. Nature **476:** 176-180.

Pitts, K. E., P. S. Dobbin, F. Reyes-Ramirez, A. J. Thomson, D. J. Richardson, and H. E. Seward. 2003. Characterization of the *Shewanella oneidensis* MR-1 decaheme cytochrome MtrA. Journal of Biological Chemistry **278:** 27758-27765.

Postma, D. 1985. Concentration of Mn and separation from Fe in sediments. 1.Kinetics and stoichiometry of the reaction between Birnessite and dissolved Fe(II) at 10-degrees-C. Geochim. Cosmochim. Acta **49:** 1023-1033.

Poulton, S. W., and R. Raiswell. 2002. The low-temperature geochemical cycle of iron: From continental fluxes to marine sediment deposition. American Journal of Science **302:** 774-805.

Pyzik, A. J., and S. E. Sommer. 1981. Sedimentary iron monsulfides: Kinetics and mechanism of formation. Geochim. Cosmochim. Acta **45:** 687-698.

Raiswell, R., M. Tranter, L. G. Benning, M. Siegert, R. De'ath, P. Huybrechts, and T. Payne. 2006. Contributions from glacially derived sediment to the global iron (oxyhydr)oxide cycle: Implications for iron delivery to the oceans. Geochim. Cosmochim. Acta **70:** 2765-2780.

Raiswell, R., L. G. Benning, M. Tranter, and S. Tulaczyk. 2008. Bioavailable iron in the Southern Ocean: the significance of the iceberg conveyor belt. Geochemical Transactions **9:** 1-7. doi: 7 10.1186/1467-4866-9-7

Reguera, G., K. D. Mccarthy, T. Mehta, J. S. Nicoll, M. T. Tuominen, and D. R. Lovley. 2005. Extracellular electron transfer via microbial nanowires. Nature **435:** 1098-1101.

Roden, E. E., and J. M. Zachara. 1996. Microbial reduction of crystalline iron(III) oxides: Influence of oxide surface area and potential for cell growth. Environ. Sci. Technol. **30:** 1618-1628.

Roden, E. E., D. Sobolev, B. Glazer, and G. W. Luther. 2004. Potential for microscale bacterial Fe redox cycling at the aerobic-anaerobic interface. Geomicrobiology Journal **21:** 379-391. Roden, E. E. 2006. Geochemical and microbiological controls on dissimilatory iron reduction. C. R. Geosci. 338: 456-467.

Roden, E. E. 2006. Geochemical and microbiological controls on dissimilatory iron reduction. C. R. Geosci. **338:** 456-467.

Ross, D. E. and others 2007. Characterization of protein-protein interactions involved in iron reduction by *Shewanella oneidensis* MR-1. Appl. Environ. Microbiol. **73:** 5797-5808.

Rosso, K. M., J. M. Zachara, J. K. Fredrickson, Y. A. Gorby, and S. C. Smith. 2003. Nonlocal bacterial electron transfer to hematite surfaces. Geochim. Cosmochim. Acta **67:** 1081-1087

Royer, R. A., B. A. Dempsey, B. H. Jeon, and W. D. Burgos. 2004. Inhibition of biological reductive dissolution of hematite by ferrous iron. Environ. Sci. Technol. 38: 187-193.

Rue, E. L., and K. W. Bruland. 1995. Complexation of iron(III) by natural organic ligands in the Central North Pacific as determined by a competitive ligand equilibration adsorptive cathodic stripping voltammetry method. Mar. Chem. **50:** 117-138.

Russell, M. J., and A. J. Hall. 1997. The emergence of life from iron monosulphide bubbles at a submarine hydrothermal redox and pH front. Journal of the Geological Society **154:** 377-402.

Ruzic, I. 1982. Theoretical aspects of the direct titration of natural-waters and its information yield for trace-metal speciation. Anal. Chim. Acta **140:** 99-113.

Saffarini, D. A., T. J. DiChristina, D. Bermudes, and K. H. Nealson. 1994. Anaerobic respiration of *Shewanella Putrefaciens* requires both chromosomal and plasmid-borne genes. FEMS Microbiol. Lett. 119: 271-277.

Salmon, T. P., A. L. Rose, B. A. Neilan, and T. D. Waite. 2006. The FeL model of iron acquisition: Nondissociative reduction of ferric complexes in the marine environment. Limnol. Oceanogr. **51:** 1744-1754.

Sander, S. G., and A. Koschinsky. Metal flux from hydrothermal vents increased by organic complexation. Nature Geoscience **4:** 145-150.

Santos-Echeandia, J., L. M. Laglera, R. Prego, and C. M. G. Van Den Berg. 2008. Copper speciation in estuarine waters by forward and reverse titrations. Mar. Chem. **108:** 148-158.

Schink, B. 1997. Energetics of syntrophic cooperation in methanogenic degradation. Microbiology and Molecular Biology Reviews **61:** 262-&.

Schulze-Makuch, D., L. N. Irwin, J. H. Lipps, D. Lemone, J. M. Dohm, and A. G. Fairen. 2005. Scenarios for the evolution of life on Mars. Journal of Geophysical Research-Planets 110: 12.

Schwertmann, U., and R. M. Cornell. 2000. Iron oxides in the laboratory: Preparation and characterization. Wiley-VCH.

Schwyn, B., and J. B. Neilands. 1987. Universal chemical assay for the detection and determination of siderophores. Analytical Biochemistry 160: 47-56.

Seyfried, W. E., and J. L. Bischoff. 1979. Low-temperature basalt alteration by seawater - Experimental-study at 70 degrees C and 150 degrees C. Geochim. Cosmochim. Acta **43:** 1937-1947.

Shaked, Y., A. B. Kustka, and F. M. M. Morel. 2005. A general kinetic model for iron acquisition by eukaryotic phytoplankton. Limnol. Oceanogr. **50:** 872-882.

Shi, L. and others 2006. Isolation of a high-affinity functional protein complex between OmcA and MtrC: Two outer membrane decaheme *c*-type cytochromes of *Shewanella oneidensis* MR-1. J. Bacteriol. **188:** 4705-4714.

Statham, P. J., M. Skidmore, and M. Tranter. 2008. Inputs of glacially derived dissolved and colloidal iron to the coastal ocean and implications for primary productivity. Glob. Biogeochem. Cycle **22:** 11.

Strong, A. L., J. J. Cullen, and S. W. Chisholm. 2009. Ocean Fertilization Science, Policy, and Commerce. Oceanography **22:** 236-261.

Stookey, L. L. 1970. Ferrozine - A new spectrophotometric reagent for iron. Anal. Chem. **42:** 779-781.

Sung, W., and J. J. Morgan. 1981. Oxidative removal of Mn(II) from solution catalyzed by the γ-FeOOH (Lepidocrocite) surface. Geochim. Cosmochim. Acta **45:** 2377-2383.

Tagliabue, A., L. Bopp, and O. Aumont. 2009. Evaluating the importance of atmospheric and sedimentary iron sources to Southern Ocean biogeochemistry. Geophys. Res. Lett. **36**.

Tagliabue, A., L. Bopp, J. C. Dutay, A. R. Bowie, F. Chever, P. Jean-Baptiste, E. Bucciarelli, D. Lannuzel, T. Remenyi, G. Sarthou, O. Aumont, M. Gehlen, and C. Jeandel. 2010. Hydrothermal contribution to the oceanic dissolved iron inventory. Nature Geoscience **3:** 252-256.

Takai, K. and others 2005. Enzymatic and genetic characterization of carbon and energy metabolisms by deep-sea hydrothermal chemolithoautotrophic isolates of Epsilonproteobacteria. Appl. Environ. Microbiol. **71:** 7310-7320.

Taillefert, M., J. S. Beckler, E. Carey, J. L. Burns, C. M. Fennessey, and T. J. DiChristina. 2007. *Shewanella putrefaciens* produces an Fe(III)-solubilizing

organic ligand during anaerobic respiration on insoluble Fe(III) oxides. Journal of Inorganic Biochemistry 101: 1760-1767.

Taillefert, M., A. B. Bono, and G. W. Luther. 2000a. Reactivity of freshly formed Fe(III) in synthetic solutions and (pore)waters: Voltammetric evidence of an aging process. Environ. Sci. Technol. 34: 2169-2177.

Taillefert, M., G. W. Luther, and D. B. Nuzzio. 2000b. The application of electrochemical tools for in situ measurements in aquatic systems. Electroanalysis 12: 401-412.

Taillefert, M., V. C. Hover, T. F. Rozan, S. M. Theberge, and G. W. Luther. 2002. The influence of sulfides on soluble organic-Fe(III) in anoxic sediment porewaters. Estuaries 25: 1088-1096.

Taratus, E. M., S. G. Eubanks, and T. J. DiChristina. 2000. Design and application of a rapid screening technique for isolation of selenite reduction-deficient mutants of *Shewanella putrefaciens.* Microbiol. Res. 155: 79-85.

Tercier-Waeber, M. L., and M. Taillefert. 2008. Remote in situ voltammetric techniques to characterize the biogeochemical cycling of trace metals in aquatic systems. Journal of Environmental Monitoring **10:** 30-54.

Tessier, A., F. Rapin, and R. Carignan. 1985. Trace-metals in oxic lake sediments-possible adsorption onto iron oxyhydroxides Geochim. Cosmochim. Acta **49:** 183-194.

Thamdrup, B. 2000. Bacterial manganese and iron reduction in aquatic sediments, p. 41-84. Advances in Microbial Ecology, Vol 16. Advances in Microbial Ecology.

Toner, B. M. and others 2009. Preservation of iron(II) by carbon-rich matrices in a hydrothermal plume. Nature Geoscience **2:** 197-201.

Tortell, P. D., M. T. Maldonado, J. Granger, and N. M. Price. 1999. Marine bacteria and biogeochemical cycling of iron in the oceans. Fems Microbiology Ecology **29:** 1-11.

Van Dover, C.L. 2000. The Ecology of Deep-Sea Hydrothermal Vents – Chemical and Physical Properties of Vent Fluids 76-98. Princeton University Press. Princeton, New Jersey, USA.

Vargas, M., K. Kashefi, E. L. Blunt-Harris, and D. R. Lovley. 1998. Microbiological evidence for Fe(III) reduction on early Earth. Nature 395: 65-67.

Venkateswaran, K. and others 1999. Polyphasic taxonomy of the genus *Shewanella* and description of *Shewanella oneidensis* sp. nov. Int. J. Syst. Bacteriol. 49: 705-724.

Von Damm, K. L. 1990. Seafloor hydrothermal activity - Black smoker chemistry and chimneys Annual Review of Earth and Planetary Sciences **18:** 173-204.

Von Damm, K. L. 2000. Chemistry of hydrothermal vent fluids from 9 degrees-10 degrees N, East Pacific Rise: "Time zero," the immediate posteruptive period. Journal of Geophysical Research-Solid Earth **105:** 11203-11222.

Vraspir, J. M., and A. Butler. 2009. Chemistry of Marine Ligands and Siderophores. Annu. Rev. Mar. Sci. **1:** 43-63.

Wade, R., and T. J. DiChristina. 2000. Isolation of U(VI) reduction-deficient mutants of *Shewanella putrefaciens*. FEMS Microbiol. Lett. 184: 143-148.

Wandersman, C., and P. Delepelaire. 2004. Bacterial iron sources: From siderophores to hemophores. Annu. Rev. Microbiol. 58: 611-647.

Wang, Z. M. and others 2008. Kinetics of reduction of Fe(III) complexes by outer membrane cytochromes MtrC and OmcA of *Shewanella oneidensis* MR-1. Appl. Environ. Microbiol. 74: 6746-6755.

Watson, I. A., S. E. Oswald, S. A. Banwart, R. S. Crouch, and S. F. Thornton. 2005. Modeling the dynamics of fermentation and respiratory processes in a groundwater plume of phenolic contaminants interpreted from laboratory- to field-scale. Environ. Sci. Technol. 39: 8829-8839.

Weber, K. A., L. A. Achenbach, and J. D. Coates. 2006. Microorganisms pumping iron: anaerobic microbial iron oxidation and reduction. Nature Reviews Microbiology 4: 752-764.

Wehrli, B., B. Sulzberger, and W. Stumm. 1989. Redox processes catalyzed by hydrous oxide surfaces Chem. Geol. **78:** 167-179.

Weir, S. I., E. C. V. Butler, and P. R. Haddad. 1994. Ion chromatography with UV detection for the determination of thiosulfate and polythionates in saline waters. Journal of Chromatography A **671:** 197-203.

Windom, H. L., W. J. Neal, and K. C. Beck. 1971. Mineralogy of sediments in 3 Georgia estuaries. J. Sediment Petrol. **41:** 497-504.

Wu, J. F., and G. W. Luther. 1995. Complexation of Fe(III) by natural organic-ligands in the Northwest Atlantic-Ocean by a competitive ligand equilibration method and a kinetic approach. Mar. Chem. **50:** 159-177.

Yao, W. S., and F. H. Millero. 1995. Oxidation of hydrogen sulfide by Mn(IV) and Fe(III) (hydr)oxides in seawater. Geochemical Transformations of Sedimentary Sulfur **612:** 260-279.

Yucel, M., A. Gartman, C. S. Chan, and G. Luther. 2011. Hydrothermal vents as a kinetically stable source of iron-sulphide-bearing nanoparticles to the ocean. Nature Geoscience **4:** 367-371.

Zachara, J. M., J. K. Fredrickson, S. M. Li, D. W. Kennedy, S. C. Smith, and P. L. Gassman. 1998. Bacterial reduction of crystalline Fe3+ oxides in single phase suspensions and subsurface materials. American Mineralogist 83: 1426-1443.

Zinder, B., G. Furrer, and W. Stumm. 1986. Coordination chemistry of weathering kinetics of the surface .2. Dissolution of Fe(III) oxides. Geochim. Cosmochim. Acta 50: 1861-1869.